

Molecular Pathology of Birt-Hogg-Dubé Syndrome

Janine Carryl Fenton

Part time M.Phil in the Division of Reproductive and Child Health (6931)

University of Birmingham

College of Medical and Dental Sciences,

Medical Molecular Genetics

Student Number: 1059608

UNIVERSITY OF
BIRMINGHAM

University of Birmingham Research Archive

e-theses repository

This unpublished thesis/dissertation is copyright of the author and/or third parties. The intellectual property rights of the author or third parties in respect of this work are as defined by The Copyright Designs and Patents Act 1988 or as modified by any successor legislation.

Any use made of information contained in this thesis/dissertation must be in accordance with that legislation and must be properly acknowledged. Further distribution or reproduction in any format is prohibited without the permission of the copyright holder.

Date of first registration for this degree: 01/09/2009

Submission and end of maximum registration date: 31/08/2013

Lead Supervisor: Professor E Maher

Co-supervisor: Professor F Latif

Abstract

Autosomal dominantly inherited mutations in the folliculin (FLCN) gene lead to Birt-Hogg-Dubé syndrome (BHD), which is associated with increased risk of kidney cancer. With the aim of better understanding and treating BHD and its associated renal cell carcinoma (RCC) this study analyzes the potential use of tumour growth inhibitors selective for FLCN-defective cells. Fifteen compounds have been initially selected using the COMPARE algorithm from the chemotherapeutic compounds tested in the NCI-60 cell lines panel based on the highest toxicity in the cell lines with low level of FLCN expression. Growth inhibition assays performed in a paired RCC cell lines with and without active FLCN confirmed that seven compounds decreased growth in FLCN-null cells compared with FLCN-wt cells. The greatest inhibitory selectivity was induced by mithramycin in which a 10-fold difference between GI50 values in FLCN negative and positive UOK257 cells. Mithramycin was also shown to be more cytotoxic to FLCN negative cells than to FLCN-positive UOK257 cells by 10 fold (at 200nM), in clonogenic survival assays. Low doses of rapamycin (1 nM) further increased mithramycin's inhibitory selectivity for FLCN mutant UOK cells, encouraging further investigation of mithramycin as a molecularly-targeted therapy for RCC in BHD.

Investigation into potential synthetic-lethal targets for FLCN found that SSH2 (a Slingshot family member implicated in actin reorganization) represents a potential therapeutic target for the development of agents to treat BHD as cell death in FLCN-null cells can be triggered by SSH2 knockdown. SSH2 siRNA knockdown in FLCN-null cells was associated with dysregulated cofilin de/phosphorylation pathways and a reduction in clonogenic survival.

Acknowledgments

Thanks to Eamonn R. Maher, Farida Latif, Xiaohong Lu, Anne Reiman, Laurence Seabra Uncaar Boora, Malgorzata Wiench and everyone in the lab, as well as the Myrovlytis Trust for financial support.

Thanks to my parents Robert and Gillian Round, My husband Martin Fenton and my Friend Anna Anastasi, for support advice and patience.

Contents

Chapter 1: Introduction.....	2
Kidney Cancer	2
Fig 1:1993-2009 European Age-Standardised Incidence Rates of Kidney Cancer in the UK.....	3
Fig 2: Ten-Year Relative Survival Rates for Kidney Cancer for England 1996 to 2003 & England and Wales 1971-1995 and Predicted 2007	4
Fig 3: Diagram of the kidney anatomy	10
Fig 4: Stained tissue sections showing differences in morphology between tumour types (Linehan <i>et al.</i> , 2004)	11
Birt-Hogg-Dubé Syndrome	13
Fig 5: Non-renal manifestations of BHD: Multiple fibrofolliculomas. (Cartwright <i>et al.</i> , 2008). 13	
Fig 6: Non-renal manifestations of BHD: multiple pulmonary cysts. (Cartwright <i>et al.</i> , 2008)... 14	
Fig 7: A shows the multiple white to skin-coloured, dome-shaped, smooth papules on the face of a BHD patient; B shows the family pedigree of an Asian family with a BHD germ-line mutation; C shows the histopathology of one of the papules in the 67-year-old proband, a Japanese woman, showing the features of fibrofolliculoma. (Noriyuki Misago <i>et al.</i> , 2008)	15
Table 1: Estimaed percentage of BHD patients affected by cancers.....	17
Fig 8: A Chromophobe renal carcinoma (top), hybrid-oncocytic neoplasms showing features of both tumor types with stained and non stained areas (centre) and oncocytoma (bottom). Taken from $\times 20$ (top and centre) and $\times 40$ (bottom). From Birt Hogg Dubé-associated bilateral, multifocal renal tumours (Linehan <i>et al.</i> 2004)	18
Fig 9: Birt Hogg Dubé-associated bilateral, multifocal renal tumours: (Linehan <i>et al.</i> , 2004).....	19
Molecular Biology	20
Fig 10: Diagram showing the positions and nature of documented mutations that have been found within the BHD gene (taken from <i>Toro et al.</i> , 2008).	22
mTOR-pathway	23
Fig 11: The mammalian target of rapamycin mTOR signalling pathways (Linehan <i>et al.</i> , 2010).24	
Animal models.....	25
Aims	26

Chapter 2: Materials and methods	28
Cell Lines and Cell Culture.	28
Table 2: Media used in cell cultures.....	28
Table 3: Cell culture media for FTC-133. (FTC-133 cells were purchased from ECACC (Salisbury, United Kingdom).	29
Small interfering Ribonucleic acid (SiRNA) treatment for reverse transfection with INTERFERin®.....	30
Table 4: Experimental cell seeding densities	31
Sulforhodamine B (SRB) Growth Inhibition Assay.....	32
Table 5: Drug concentrations	33
Clonogenic Cell Survival Assay.....	35
Table 6: Mithramycin concentrations and cell numbers used in clonogenic assay with the UOK cell line	35
Table 7: Mithramycin concentrations and cell numbers used in clonogenic assays with the UOK-FLCN cell line.....	35
SSH2 Clonogenic Cell Survival Assay	36
Table 8: SSH2-siRNA treatment condition used for each cell line.....	37
Western Blot Analysis	38
Immunofluorescence	40
Transient Transfection for the expression of over-expression of full-length FLCN or FLCN mutants.	42
Chapter 3: Results of investigations into the effect of FLCN expression on the effect of selected drugs	43
Selection of compounds with the highest therapeutic potential.	43
Table 9: List of compounds selected for further testing by the COMPARE algorithm.	45
Fig 12: Individual dose response curves for the 6 compounds illustrating the dose dependant inhibition of growth.....	51

Table 10: GI ₅₀ for luciferase and FLCN siRNA treated SKRC47 cells.	52
Drug-induced cytotoxicity in CaKi cells	53
Table 11: GI ₅₀ values for compounds in CaKi-1 Cells with and without FLCN siRNA knock down.	54
Fig 12: Graphs and table showing the comparative dose response curves for a selection of compounds in CaKi- 1 Cells treated with luciferase SiRNA (FLCN+ve cells) and CaKi1 cells treated with FLCN SiRNA to knock down the expression of the protein.	55
Establishing GI ₅₀ values for 16 compounds in CaKi-2 cells with and without FLCN siRNA knock down.	56
Table 12: Table of GI ₅₀ values for 16 compounds in CaKi-2 cells with and without FLCN siRNA knock-down.	57
Fig 13: Graphs showing the comparative dose response curves for a selection of compounds in CaKi- 2 Cells treated with luciferase SiRNA (FLCN+ve cells) and CaKi2 cells treated with FLCN SiRNA.	60
Fig 14: Graphs showing the comparative dose response curves for a selection of compounds in CaKi- 2 Cells FLCN+ve and FTC133 FLCN-ve cells.	64
Table 13; GI ₅₀ values for compounds in CaKi-2 Cells and FTC 133 cells taken from the mean of 5 replicates on the same day.	66
Compound Screen in FLCN negative UOK-257 Cells and FLCN+ UOK257-2 cells.	67
Fig 15: Screen in UOK-257 cells and UOK FLCN+ cells	68
Table 14: Compound screen in UOK-257 cells and UOK FLCN+ cells	69
Chapter 4: Results of Further Assessment of Mithramycin	71
Mithramycin-induced cytotoxicity in UOK257 cells and UOK257 cells with FLCN expression restored.	71
Fig 16: Clonogenic assays measured mithramycin cytotoxicity in UOK-257FLCN+ cells and UOK-257. (Data obtained from 3 experiments and the range of values shown by Error bar). (Figure by Xiaohong Lu using my data. Reported in Lu et al., 2011)	72
Mithramycin-induced cytotoxicity in SKRC47cells	73
Fig 17: Mithramycin-induced cytotoxicity in SKRC47cells.....	74
Mithramycin-sensitivity in FLCN Negative Cells originating from tumour of non-renal origin. Mithramycin-induced Cytotoxicity in FTC133 cells	75

Fig 18 Mithramycin-induced cytotoxicity in FTC133 cells	75
Table 15: Mithramycin-induced cytotoxicity in FTC133 cells.	76
Mithramycin sensitivity in VHL positive and negative RCC cell line pairs	76
Fig 19: Mithramycin-induced cytotoxicity in VHL positive(WT) and negative(VI) cells	77
Effectiveness of mithramycin in combination with rapamycin.....	77
Fig 20: Dose response curve for rapamycin in CaKi-2 SiRNA-treated cells	78
Western Blot Analyses	79
Fig 21: Western blotting showing levels of protein expression in UOK257 cells with and without FLCN expression.....	79
Comparison of mithramycin in combination with rapamycin and mithramycin alone, in UOK 257 Cells and UOK 257 FLCN+ cells	80
Fig 22: Comparison of mithramycin alone and in combination with rapamycin in FLCN+ and FLCN- cells.....	81
Fig 23: FLCN+ and UOK257 cell growth inhibition in response to exposure of mithramycin in combination with 1nM rapamycin and mithramycin alone. Figure by Xiaohong Lu using my data (Lu et al., 2011).....	81
Rapamycin's effect on the effectiveness of mithramycin in cells with and without VHL...	83
Fig 24: VHL+(wt) and VHL-(ev) SKRC39 cell growth inhibition in response to exposure of Mithramycin in combination with 1nM rapamycin and Mithramycin alone.	84
Fig 25: VHL+(wt) and VHL- 786-0 cell growth inhibition in response to exposure of Mithramycin in combination with 1nM rapamycin and Mithramycin alone.	85
Chapter 5: Results of Further Assessment of The Effectiveness of vincristine	86
Vincristine with FTC133 cells.....	86
Fig 26: Vincristine-induced cytotoxicity in FTC133 cells	86
Table 15: Vincristine-induced cytotoxicity in FTC133 cells	87
Comparison of vincristine in combination with rapamycin and vincristine alone, in UOK 257 Cells and UOK 257 FLCN+ cells.....	87
Fig 27: UOK FLCN+ and UOK257 cell growth inhibition in response to exposure of Vincristine in combination with 1nM rapamycin and Vincristine alone.	88

Table 16: UOK FLCN+ and UOK257 cell growth inhibition GI50 values in response to exposure of Vincristine in combination with 1nM rapamycin and Vincristine alone.	88
Vincristine sensitivity in VHL positive and negative RCC cell line pairs	89
Fig 28: VHL WT+ and VHL- cell growth inhibition in response to exposure of vincristine alone	89
Investigation of the mTOR involvement in vincristine sensitivity in VHL +&- RCCs.	90
Fig 29: 786-O VHL + and 786-O VHL- cell growth inhibition in response to exposure of vincristine in combination with 1nM rapamycin and with vincristine alone.	90
Fig 30: 786-O VHL + and 786-O VHL- cell growth inhibition in response to exposure to vincristine in combination with 1nM rapamycin and vincristine alone.	90
Chapter 6: Results of Investigations into The Effects of Compound C	92
Fig 31: Inhibition of growth, shown by the SRB assay, in UOK-257 cells with and without FLCN expression by Compound C. Cells were continuously exposed to the concentrations to the chemical for 72 hours.	92
Fig 32: Cell growth inhibition in response to exposure of Mithramycin in combination with 1 nM Compound C and Mithramycin alone, for 72 hours, was determined using the SRB assay	94
Chapter 7: Slingshot 2 as a synthetic lethal target of FLCN.	95
Sling shot (ssh) SiRNA and confocal work,	95
Fig 33: Cell death induced by Sling shot 2 SiRNA treatment of FTC12 cells and FLCN positive FTC22cells, as measured by the clonagenic assay.	96
Fig 34: SSH family phosphatase known pathways (Teng <i>et al.</i> 2011).	98
Effects SSH2 knockdown cofilin phosphorylation and actin.	99
Fig 34: Confocal images showing the effect of treatment with SiRNA to luciferase on Cofilin and F-actin in UOK-257 cells.	100
Fig 35: Confocal images showing the effect of treatment with SiRNA to SSH2 on Cofilin and F-actin in UOK-257 cells.	101
Fig 36: Confocal images showing the effect of treatment with SiRNA to Cofilin on Cofilin and F-actin in UOK-257 cells.	102
Fig 37: Confocal images showing the effect of treatment with SiRNA to luciferase on P-Cofilin and F-actin in UOK-257 cells.	103
Fig 38: Confocal images showing the effect of treatment with SiRNA to Sling shot 2 on P-Cofilin and F-actin in UOK-257 cells.	104
Fig 39: Confocal images showing the effect of treatment with SiRNA to Cofilin on P-Cofilin and F-actin in UOK-257 cells.	105

Fig 40: comparison of the effects of SSH2 and Cofilin SiRNA treatment on Cofilin, phospho-Cofilin and actin structure in FLCN negative UOK cells (a compilation of the merged panes of figures 34 to 39 for comparison.	106
Fig 41: Comparison of the effects of SSH2 treatment on Cofilin, phospho-Cofilin and actin structure in UOK-257 cells.	108
Fig 42: Top UOK-257 treated with SiRNA to luciferase. Bottom UOK-257 treated with SiRNA to SSH2 (phalloidine F-Actin Staining in green and DAPI nuclear staining in blue).....	110
Chapter 8: Confocal microscopy to show the distribution of Miz 1 and Myc proteins in cells with absent mutated and normal FLCN.....	112
Fig 43: Immunofluoresence staining showing FLCN interaction with MIZ-1	114
Fig 44: Top: FTC12 cells stained with anti-MIZ alexa 488 in green and DAPI nuclear stain in blue; Bottom: FTC22 cells stained with anti-MIZ alexa 488 in green and DAPI nuclear stain in blue.....	116
MIZ FLCN Interaction in ACHN (ATCC® CRL-1611™) cells.....	117
Fig 45: ACHN3 FLCN positive cells stained with anti-MIZ and anti-FLCN to show possible colocalization.	118
Fig 46 graphical analysis of fig 45 confocal image of ACHN3 FLCN positive cells stained with anti-MIZ and anti-FLCN to show possible colocalization.	120
Fig 47: Confocal image of ACHN3 FLCN positive cells were stained with anti-MIZ alexa 633 and anti-FLCN alexa488 as well as DAPI nuclear stain to show possible colocalization.	121
Fig 48: Graphical analysis of the confocal image of ACHN3 FLCN positive cells were stained with anti-MIZ alexa 633 and anti-FLCN alexa488 as well as DAPI nuclear stain to show possible colocalization.	122
Fig 49: FTC 12 cells transiently transfected with construct 82. The cells were later stained with anti-Flag alexa 488 and anti-MIZ alexa633 as well as DAPI nuclear stain	124
Fig 50: FTC 12 cells transiently transfected with constructs 82. The cells were later stained with anti-Flag alexa 633 and anti-MIZ alexa488 as well as DAPI nuclear stain.	125
Fig 51: FTC 12 cells which were transiently transfected with constructs 82. The cells were later stained with anti-Flag alexa 633 and anti-MIZ alexa488 as well as DAPI nuclear stain.....	126
Fig 52: Top: FTC12 cells stained with anti -MYC alexa 594 in red and DAPI nuclear stain in blue.	128
Fig 52: Bottom: FTC22 cells stained with anti -MYC alexa 594 in red and DAPI nuclear stain in blue. Myc is present in the nucleus and in small amounts in the cytoplasm in both FLCN positive and negative FTC cells with little difference to be seen between the two states.	128
Fig 53: Merged image of FLCN positive cells stained with anti-FLCN alexa 488 and anti-MYC alexa 594	129
Chapter 9: Discussion.....	131

References	143
APENDIX 1.....	160
NCI60 compounds' FLCN expression Data	160
APENDIX 2.....	161
FNIP3: Evidence that the Folliculin tumour suppressor interacts with Miz-1	161
Fig.A FLCN interacts with Miz-1 in vitro and in vivo.	162
APENDIX 3.....	163

Abbreviations

Akt	proto-oncogene c-Akt;
AMPK	5'-AMP-activated protein kinase
FH	fumarate hydratase;
FLCN	folliculin;
FNIP	folliculin interacting protein;
GLUT1	glucose transporter type 1
HGF	hepatocyte growth factor
HIF	hypoxia-inducible factor
IL-2	Interleukin-2
LKB1	serine–threonine protein kinase 11
MET	hepatocyte growth factor receptor
mTOR	serine–threonine protein kinase mammalian target of rapamycin
PDGF	platelet-derived growth factor
PHD	HIF prolyl hydroxylase
PI3K	phosphatidylinositol 3-kinase
PTEN	phosphatase and tensin homolog
Rheb	GTP-binding protein Rheb
RCC	Renal Cell Carcinoma
SDH	succinate dehydrogenase
TGF	transforming growth factor
TSC	tuberous sclerosis complex
VEGF	vascular endothelial growth factor;
VHL	von Hippel–Lindau disease tumor suppressor
c-Kit	c-Kit protein
VEGFR	vascular endothelial growth factor receptors 1, 2, and 3
Flt-3	FMS-like tyrosine kinase 3
PDGFR β	platelet-derived growth factor receptor β
RET	receptor tyrosine kinases

Chapter 1: Introduction

Kidney Cancer

Cancer is defined by the Oxford English Dictionary as a malignant growth or tumour resulting from an uncontrolled division of cells. The in balance of cell proliferation, differentiation and cell death is disturbed by failure of cells to die, failure of cells to stop dividing, or abnormally increased cell division. It is not one disease, but a group of diseases sharing characteristics of uncontrolled growth and invasion to other tissues (metastasis) threatening the life of the sufferer. It is a common cause of death throughout the world. In the United States of America, cancer is responsible for 22% of deaths (R. J. B. King, 2000). Data from the Vital Statistics of Japan showed that total years of life lost due to all cancers were 1,818,960.4 years in 1995 and 2,160,706.5 years in 2005, corresponding to average years of life lost for all cancer combined of 17.6 and 16.7 years (Pham *et al.* 2010). Increasing understanding of the disease, its causes, progression, behaviour and characteristics can have a great benefit to a large number of people.

Kidney cancer caused the deaths of 12,890 people and affected 51,190 people in the USA in 2007, accounting for about 3.5% of all cancer diagnoses (Jemal *et al.* 2006) and Kidney cancer accounts for almost 40% of deaths from metastases (Murakami *et al.* 2007).

In the UK, 9286 new cases of kidney cancer were diagnosed in 2009 for the UK alone. 39% (3580) of these were in women and 61% (5706) in men, adding up to approximately 3% of the new diagnoses for this year and making it the eighth most frequent cancer in the UK. It was the ninth most frequent cancer among British females and the sixth most frequent cancer in British males at that time (Cancer Research UK, 2013) and it is still a significant cause of death.

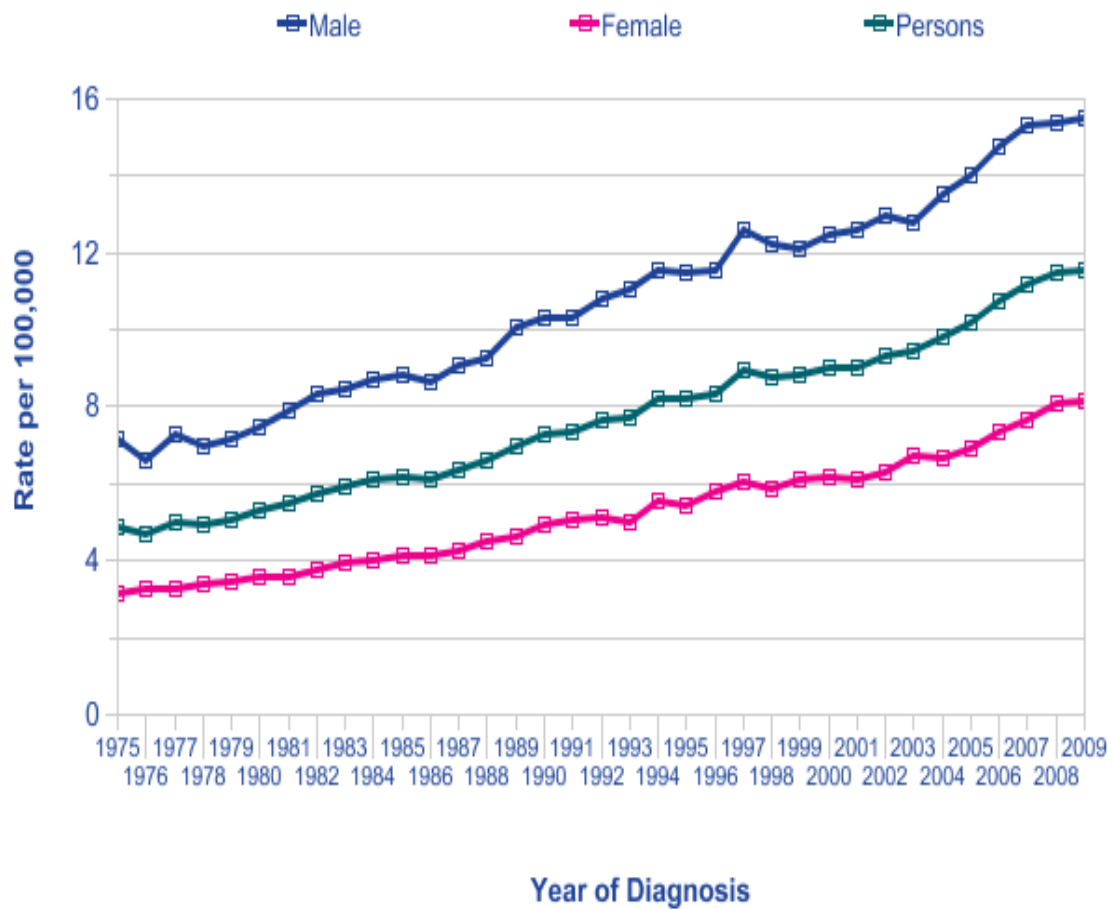


Fig 1:1993-2009 European Age-Standardised Incidence Rates of Kidney Cancer in the UK.

European kidney cancer occurrences had increased to more than double the 1975-1977 rates by 2007-2009 (Fig 1) and correspondingly, in the UK rates of kidney cancer occurrence have gradually grown since the mid-1970s. By 2010 the lifetime risk of developing kidney cancer for British females was 1 in 90 and for British males was 1 in 56. This is believed to be due to an increased occurrence of risk factors such as obesity and smoking. (Cancer Research UK, 2013)

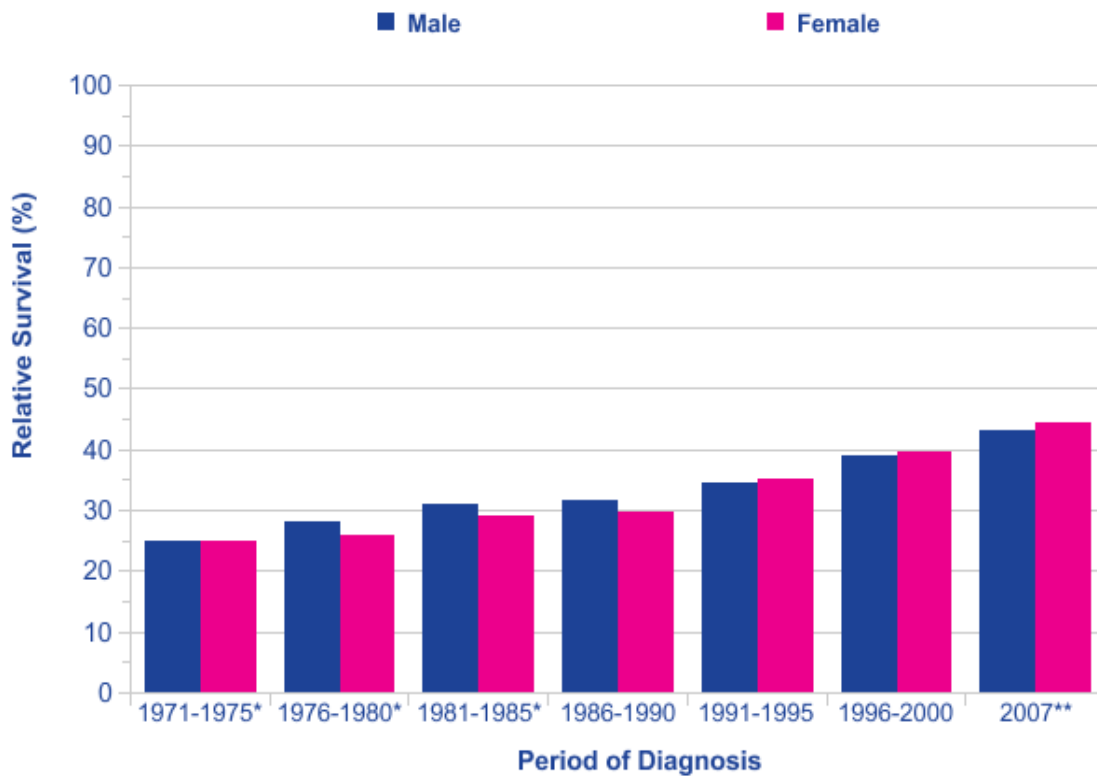


Fig 2: Ten-Year Relative Survival Rates for Kidney Cancer for England 1996 to 2003 & England and Wales 1971-1995 and Predicted 2007

Fig 2 shows the relative increase in rates of survival for ten-years from diagnosis, in both males and females diagnosed with kidney cancer. In England it was thought to be about 43% for 2007, increased from 25% in England and Wales during 1971-1975. Kidney cancer treatment, as with most cancers, has a higher efficacy if it is diagnosed at an early stage but for kidney cancer 24% of cases are emergency presentations (Cancer Research UK, 2013).

Advanced renal cell carcinoma is highly variable in its course, ranging from disease progression with chemotherapy resistance to spontaneous remission. Renal cell cancer is rarely curable if it has undergone metastasis at the time of diagnosis and is known to be resistant to conventional chemotherapy (Coppin *et al.* 2005). Distant metastases develop in

about one third of patients (Hudes *et al.* 2007). For patients with metastatic renal-cell carcinoma less than 10% 5-year survival rate has been seen (Escudier *et al.* 2007). As only 10–15% of such patients respond to currently available single chemotherapy drugs with a reduction in tumor growth, conventional systemic chemotherapy agents have not been deemed effective in these cases, (Cancer connect). For this reason such conventional systemic chemotherapy agents have not played a large role in the treatment of advanced kidney cancers.

As there are few effective chemotherapeutic options for metastasised kidney cancer, many patients die from the disease within 5 years of the diagnosis of metastasised disease. The survival has a median of about 10 months (Motzer *et al.* 1999) and there is only a 10% five year survival rate (Cancer Research UK, 2013). (Newer targeted therapies and immunotherapy offer better outcomes, but it is obvious that there is a need for improved understanding of the disease and better novel treatments to improve the survival rate.

Hopes have been held for improved outcomes from immunotherapy for some time based on the observation that these renal cell carcinoma tumours can occasionally shrink without therapy, especially when spread to the lungs, suggesting that immune system-based approaches to drug development and treatment might be useful. Immunotherapy works by stimulating the immune system to fight the cancer. The two most frequently used types of immunotherapy are interleukin-2 (IL-2) and interferon-alfa. In 2008, IL-2 and interferon were still the only therapies associated with complete long-term remission. Of the fully validated therapies, nephrectomy, followed by interferon-alfa, was thought to be the best strategy for survival for fit patients with metastases at diagnosis and minimal symptoms, with interferon-alfa being shown to give a small survival benefit compared to other commonly used treatments (Coppin *et al.* 2008).

As the most common treatments for renal-cell carcinoma that has undergone metastasis, interferon-alfa and IL-2, alone or in combination, have been shown to result in a median survival of 12.0 to 17.5 months. As they show substantial toxicity and limited efficacy, these cytokines rarely benefit patients with adverse prognostic factors or an extensive tumour burden. These patients have a lower median survival of 4 to 8 months (Hudes *et al.* 2007).

Interferon is a stimulant of the immune system and is produced by the body naturally. Interferon-alfa is a laboratory produced compound that mimics the mode of action of endogenous interferon. It brings about stimulation to the immune system and recognition and destruction of some types of cancer cells (Cancer connect). However, in advanced renal cell cancer, this treatment has a poor prognosis with anticancer responses (reduction of tumor size or tumor growth) in fewer than 15 % of patients. It can also give rise to severe side effects and, coupled with the lack of evidence for improvement of survival, interferon-alfa use on its own remains controversial for renal cell carcinoma treatment (Cancer connect).

Interleukin-2 (also known as Proleukin) was the standard of care for patients with renal cell cancer before the new targeted therapies gained official approval. It is usually given as an inpatient treatment at high doses and has historically been linked with side effects that were quite severe. The safety of interleukin-2 at high-dose has improved significantly over the past ten years however (Cancer connect).

Unfortunately, the results of long-term clinical trials have given indications of low response rates to this treatment. Only about 15% of advanced renal cell carcinoma patients showed an anticancer response after high-dose interleukin-2 treatments (Fyfe *et al.* 1995). This is the reason why the combination of interleukin-2 plus targeted therapy is now being studied in clinical trials (Cancer connect). It has been shown that high dose interleukin-2 can give

equivalent survival to a combination of low dose interleukin-2 plus interferon-alfa, a combination known to have greater toxicity than interferon-alfa alone (Coppin *et al.* 2008).

As interferon alfa only gives a modest increase in survival, and treatment with high-dose interleukin-2 infrequently brings about a complete and lasting response, the need for novel treatments is clear. Until recently, there have been no other treatments for RCC patients who cannot tolerate these cytokines or are ineligible for these treatments (Escudier, 2007).

A targeted therapy is one that is specifically designed to minimize damage to healthy, normal cells, killing just the cancerous cells. Cancer treatments that “target” cancer cells may have advantages including improved outcomes for patients and fewer side effects from the treatment.

Sorafenib (also known as Nexavar) is a multi-kinase inhibitor that is orally active. It has tumor angiogenesis and tumour-cell proliferation effects. Identified in the first instance as an inhibitor of Raf kinase, sorafenib was shown to inhibit c-Kit protein (c-Kit); vascular endothelial growth factor receptors (VEGFR) 1, 2, and 3; FMS-like tyrosine kinase 3 (Flt-3); platelet-derived growth factor receptor β (PDGFR β); and RET receptor tyrosine kinases as well. A placebo was compared to sorafenib in a Phase III clinical trial in over 900 advanced renal cell cancer patients who had been previously treated. The sorafenib treatment gave significant improvement with regard to progression-free survival. 5.5 months progression-free survival was seen for those given sorafenib treatment compared with a progression-free survival time of 2.8 months for those patients who were given a placebo (Escudier, 2007).

Sunitinib (also known as Sutent) is a multi-targeted oral inhibitor of tyrosine kinase that targets VEGF and PDGF receptors - proteins shown to be responsible for stimulating the growth of cancer cells. As second-line treatment in metastatic RCC anti-tumour activity of

Sunitinib has been shown. This is a setting in which until this point no other systemic therapy had been found effective. About 40% of recurrent renal cell cancer patients in trials were shown to have responded to treatment with Sutent, and for three months after treatment about one in four patients experienced stable disease. RCC genetics and positive clinical trial results such as these indicate that VEGF and PDGF receptor-mediated signalling appears to be an effective target for therapy in RCC (Motzer, 2006).

Temsirolimus (CCI-779, also known as Torisel) is a specific inhibitor of the mammalian target of rapamycin kinase (mTOR kinase), which is an intracellular signalling pathway component involved in the response of cells to hypoxic stress, their proliferation and growth. Temsirolimus forms a complex that inhibits mTOR signaling by binding to FKBP-12 (an abundant intracellular protein). The disruption of the mTOR signaling pathway suppresses protein production for factors that regulate angiogenesis and cell cycle progression. As unregulated angiogenesis is prominent in renal-cell carcinoma, the inhibition of angiogenesis by temsirolimus is clinically relevant and may benefit patients with RCC (Hudes *et al.* 2007).

626 patients with poor prognosis metastatic RCC who had not received prior therapy were treated with either temsirolimus, interferon alfa, or a combination of temsirolimus plus interferon-alfa. The addition of temsirolimus to interferon in combination was not shown to improve survival. Temsirolimus, when compared with interferon-alfa, gave an overall improved survival among patients with metastatic renal-cell carcinoma and a poor prognosis. (Hudes *et al.* 2007)

Pazopanib (also known as Votrient) targets vascular endothelial growth factor receptor, c-Kit, and platelet-derived growth factor receptor working as an oral angiogenesis inhibitor. By blocking angiogenesis, the drug has the effect of depriving the tumour of oxygen and nutrients causing growth inhibition. In clinical trials, 435 patients were treated for advanced

and/or metastatic RCC, 54% (233) had been given no previous treatment and 46% (202) had been previously given cytokine treatments. Pazopanib significantly prolonged the progression-free survival time of these patients compared with placebo in the overall study, with a median progression-free survival time of 9.2 months as compared to 4.2 months for the placebo control group. The objective response rate was 3% with placebo compared to 30% for pazopanib and the duration of response had a median of greater than one year. However, side-effects were recorded including vomiting, diarrhoea, pain, high blood pressure and others (Sternberg *et al.* 2010).

The humanised monoclonal antibody anti-VEGF, bevacizumab (also known as Avastin) is used as targeted therapy that works by inhibition of the vascular endothelial growth factor protein known as VEGF. VEGF has a key role in blood vessels' development. By blocking VEGF, bevacizumab affects angiogenesis, depriving the tumour of oxygen and nutrients and inhibiting its growth. For patients with metastatic kidney cancer, treatment with a combination of bevacizumab and interferon alfa results in a longer time to cancer progression than treatment with interferon alpha alone (Escudier *et al.* 2007).

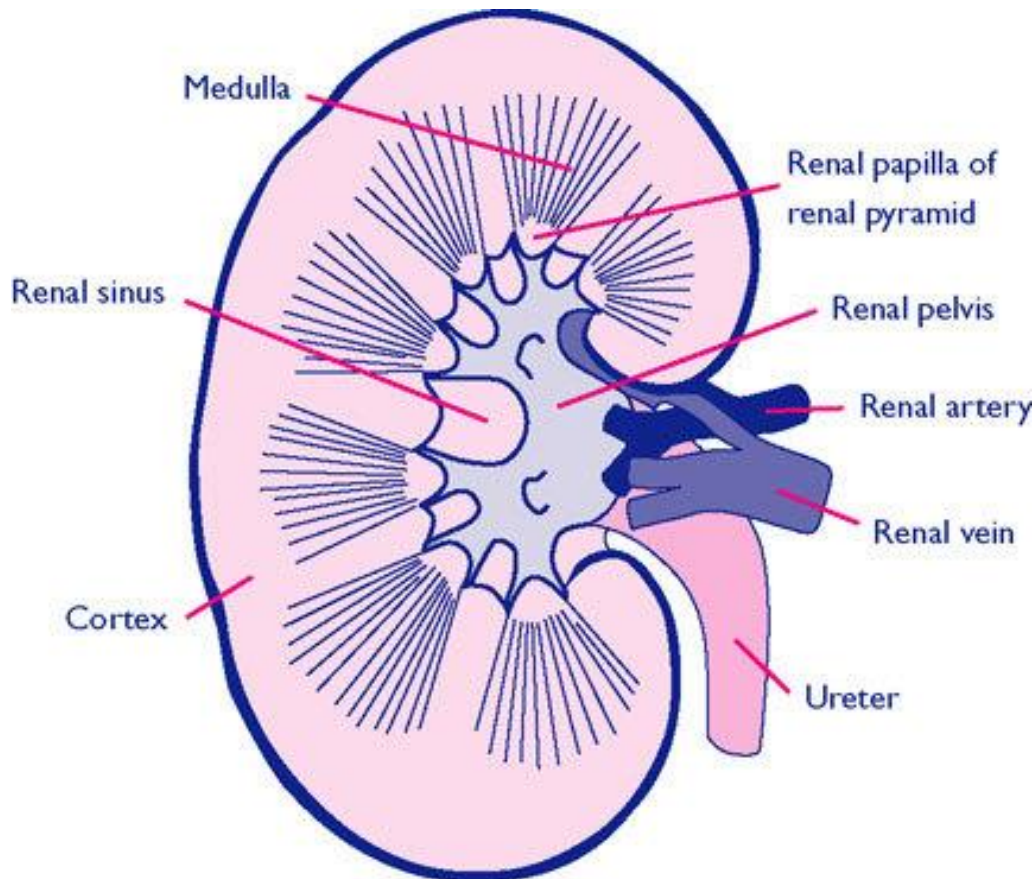
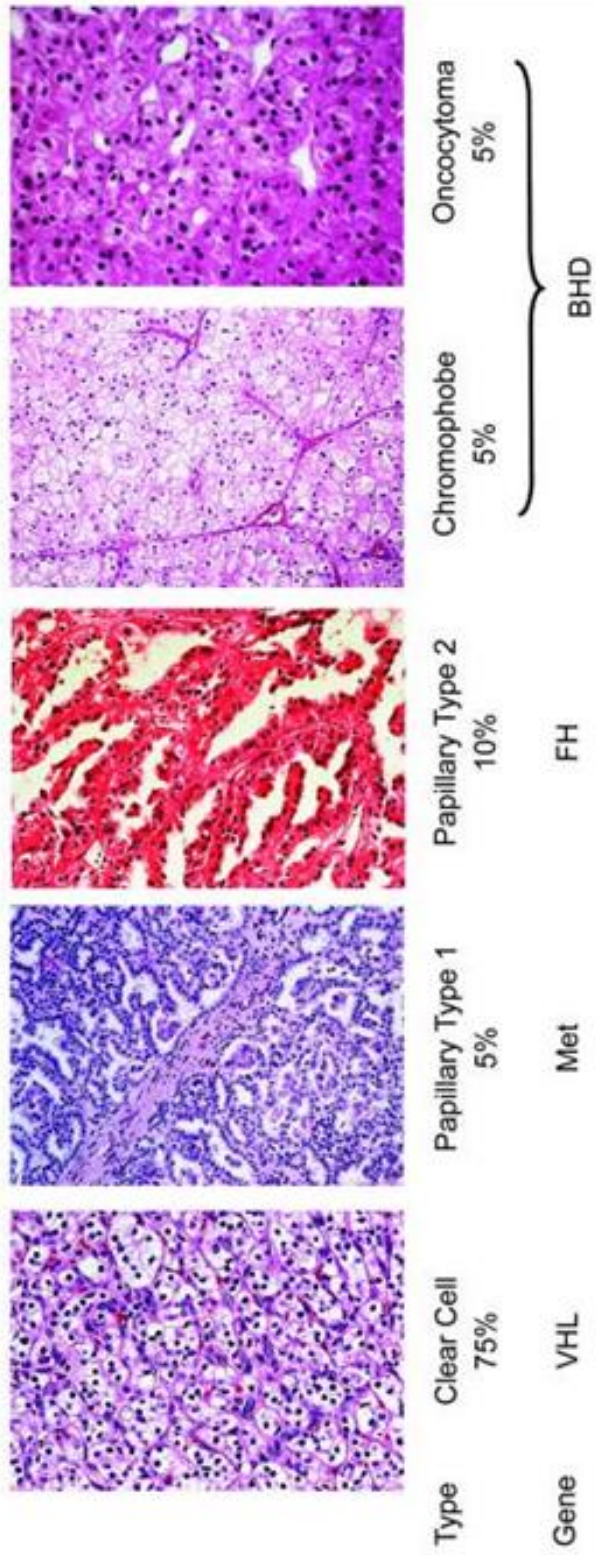


Fig 3: Diagram of the kidney anatomy

Kidney cancer itself is not a single disease. There are a number of different types of kidney cancer with different clinical courses, different responses to treatments, different histologies and different genetic causes. In 2009, it was reported that 5% of kidney cancers occurred in the ureter, 7% in the renal pelvis, and 86% in the rest of the kidney (Cancer Research UK)(see fig 3). Kidney cancers are classified based on molecular genetics findings together with cytomorphological features, into a minimum of five main histological subtypes: medullary-collecting duct carcinoma (1%), chromophobe (5%), oncocytoma (5%) papillary (10%), and clear cell (75–80%),(see Fig 4) (Linehan et al. 2004, Kovacs et al. 1997, Murakami 2007).

Human Renal Epithelial Neoplasms



(VHL= Von-Hipple-Lindau; FH= Fumarate Hydratase)

Fig 4: Stained tissue sections showing differences in morphology between tumour types (Linehan et al., 2004)

The identification of rare familial cancer genes has provided important insights into the pathogenesis of both familial and sporadic cancers. In this way the identification and isolation of the susceptibility genes for von Hippel-Lindau (VHL) disease allowed it to be shown that somatic inactivation of the VHL tumour suppressor genes (TSG) play a critical role in the development of the majority of sporadic clear cell and renal cell carcinoma (Latif *et al.* 1993, Foster *et al.* 1994, Gnarr *et al.* 1994). The identification of the VHL tumour suppressor genes' products and the clarification of its function, as well as the role of the von Hippel Lindau tumour suppressor protein (pVHL) in regulating hypoxia-inducible transcription factors, HIF-1 and HIF-2, by facilitating the oxygen-regulated break down of HIF-alpha, brought about the introduction of tyrosine kinase inhibitors, such as the drugs sunitinib and sorafenib discussed above, for the treatment of advanced sporadic RCC and clinical trials of these agents in VHL disease management (Maxwell *et al.* 1999, Feldman and Motzer 2006). Investigation of the function of rare genetic disorders may allow development of treatments to improve the management of diseases in both patients with the comparatively more common non-familial disorders as well as the familial diseases including Birt-Hogg-Dubè Syndrome.

Birt-Hogg-Dubé Syndrome

Fig 5: Non-renal manifestations of BHD: Multiple fibrofolliculomas. (Cartwright *et al.*, 2008)



Fig 6: Non-renal manifestations of BHD: multiple pulmonary cysts. (Cartwright *et al.*, 2008)

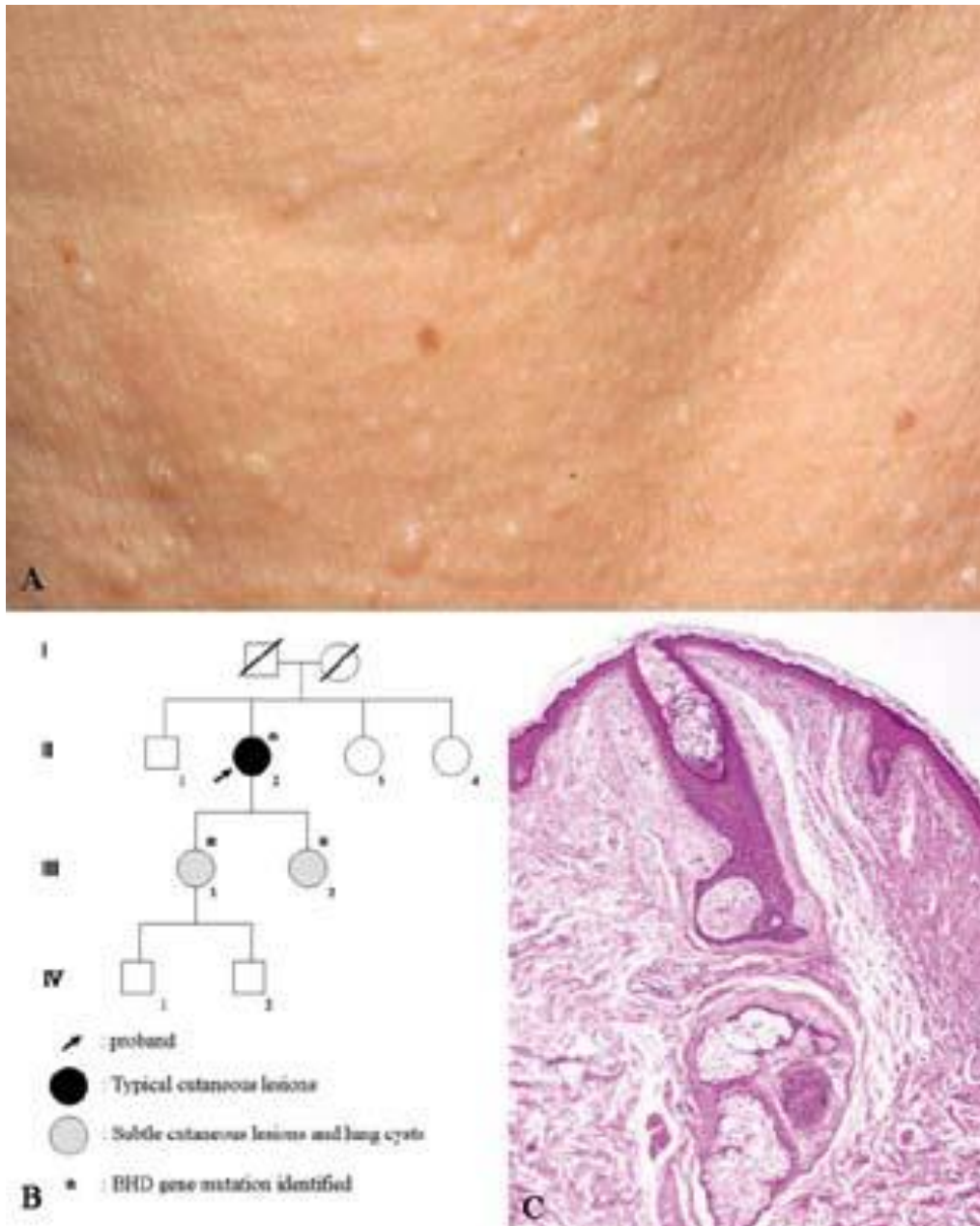


Fig 7: A shows the multiple white to skin-coloured, dome-shaped, smooth papules on the face of a BHD patient; B shows the family pedigree of an Asian family with a BHD germ-line mutation; C shows the histopathology of one of the papules in the 67-year-old proband, a Japanese woman, showing the features of fibrofolliculoma. (Noriyuki Misago *et al.*, 2008)

Birt-Hogg-Dubé (BHD) syndrome is a multisystem, autosomal dominantly inherited disorder characterised by the development of benign skin tumours on the face and upper body in the third decade of life (Birt *et al.* 1977). Histological examination of the tumours reveals them as fibrofolliculomas or trichodiscomas (Fig 5 &7) Fibrofolliculomas are highly penetrant. 85% of patients diagnosed with BHD mutations develop these classical dermatological symptoms which can be a cosmetic problem and cause concern to some patients. Statistics regarding individuals with fibrofolliculoma without identified *FLCN* mutations are unavailable. BHD occurs in about 1/200,000 people (Cartwright *et al.*, 2008), although it may be under-reported due to lack of recognition. BHD is caused by mutations in the folliculin (*FLCN*) gene which is located on the short arm of chromosome 17 (17 p11.2). Additional features of BHD include susceptibility to pulmonary cysts and pneumothorax (Fig 6). Pulmonary cysts develop in over 80% of BHD patients, and almost 25% suffer pneumothorax (Zbar *et al.*, 2002, Toro *et al.* 2007, Toro *et al.* 1999, Linehan *et al.* 2003). The condition also carries an increased risk of kidney cancer and there have been some reports of colorectal polyps and colorectal cancer being observed in association with BHD syndrome (Rongioletti *et al.*, 1989, Zbar *et al.*, 2002). Genetic testing identifies *FLCN* gene mutation in 84 % of clinically diagnosed BHD cases. Renal tumours occur in 25-35% of BHD patients (Zbar *et al.*, 2002, Toro *et al.* 1999, Pavlovich *et al.* 2002) and they are often bilateral and multifocal. Histology is often an oncocytic hybrid (50%). The multifocal hybrid chromophobe-oncocytoma renal carcinoma histological subtype is only seen in BHD patients with chromophobe RCC and oncocytoma features and a combination of individual tumour cell populations within a hybrid tumour (Yang *et al.* 2008). Chromophobe renal cancer histological subtype is also often seen (33%), but tumours could also be of a clear cell renal cancer type (9%), or benign oncocytomas (4%)

(Pavlovich *et al.*, 2002) (% of BHD patients affected is shown in table 1). This is quite a different distribution to the general distribution discussed before.

Table 1: Estimated percentage of BHD patients affected by cancers.

Tumor type	% of BHD patients affected (approximation)
oncocytic hybrid	12
Chromophobe	8
clear cell RCC	2
Oncocytoma benign	1
	Calculated given a 25% cancer incidence rate in BHD patients (see above)

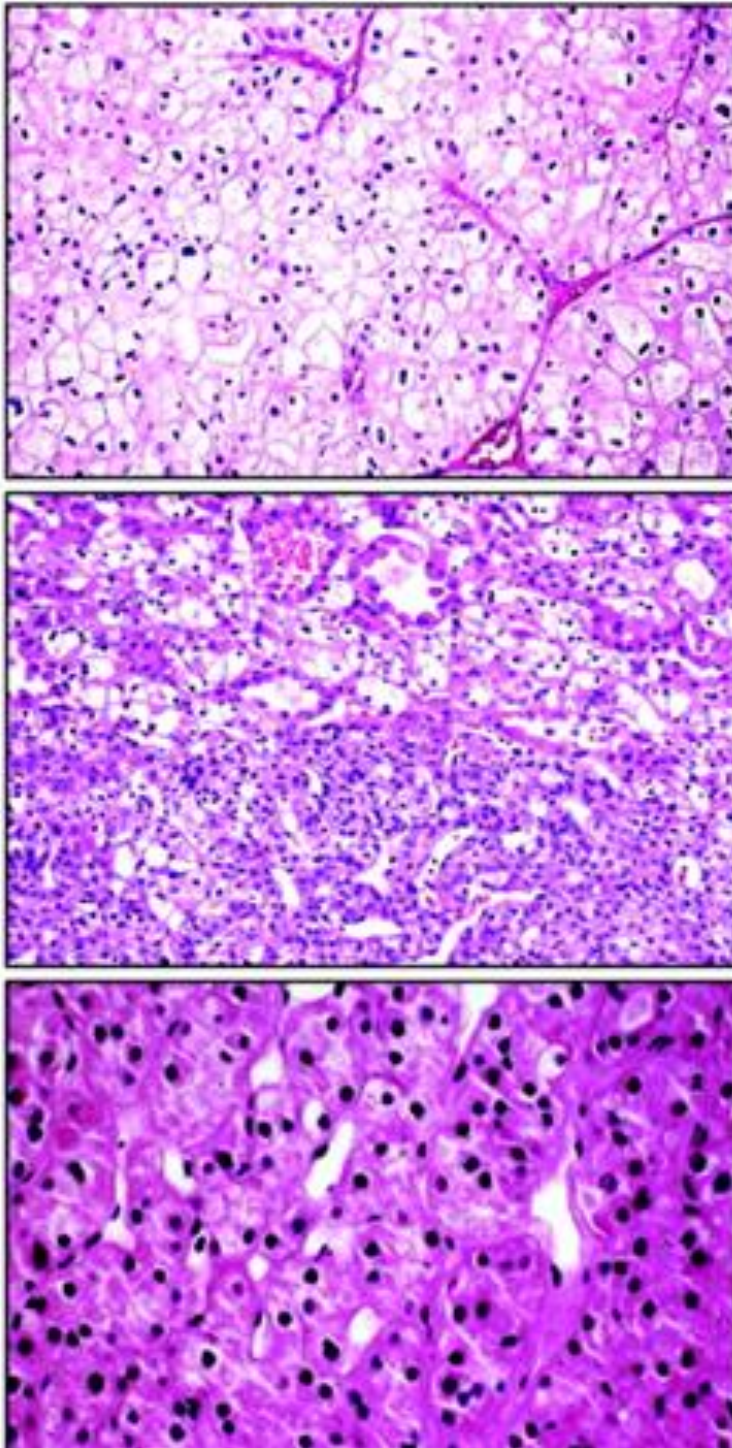


Fig 8: A Chromophobe renal carcinoma (top), hybrid-oncocytic neoplasms showing features of both tumor types with stained and non stained areas (centre) and oncocytoma (bottom). Taken from $\times 20$ (top and centre) and $\times 40$ (bottom). From Birt Hogg Dubé-associated bilateral, multifocal renal tumours (Linehan et al. 2004)

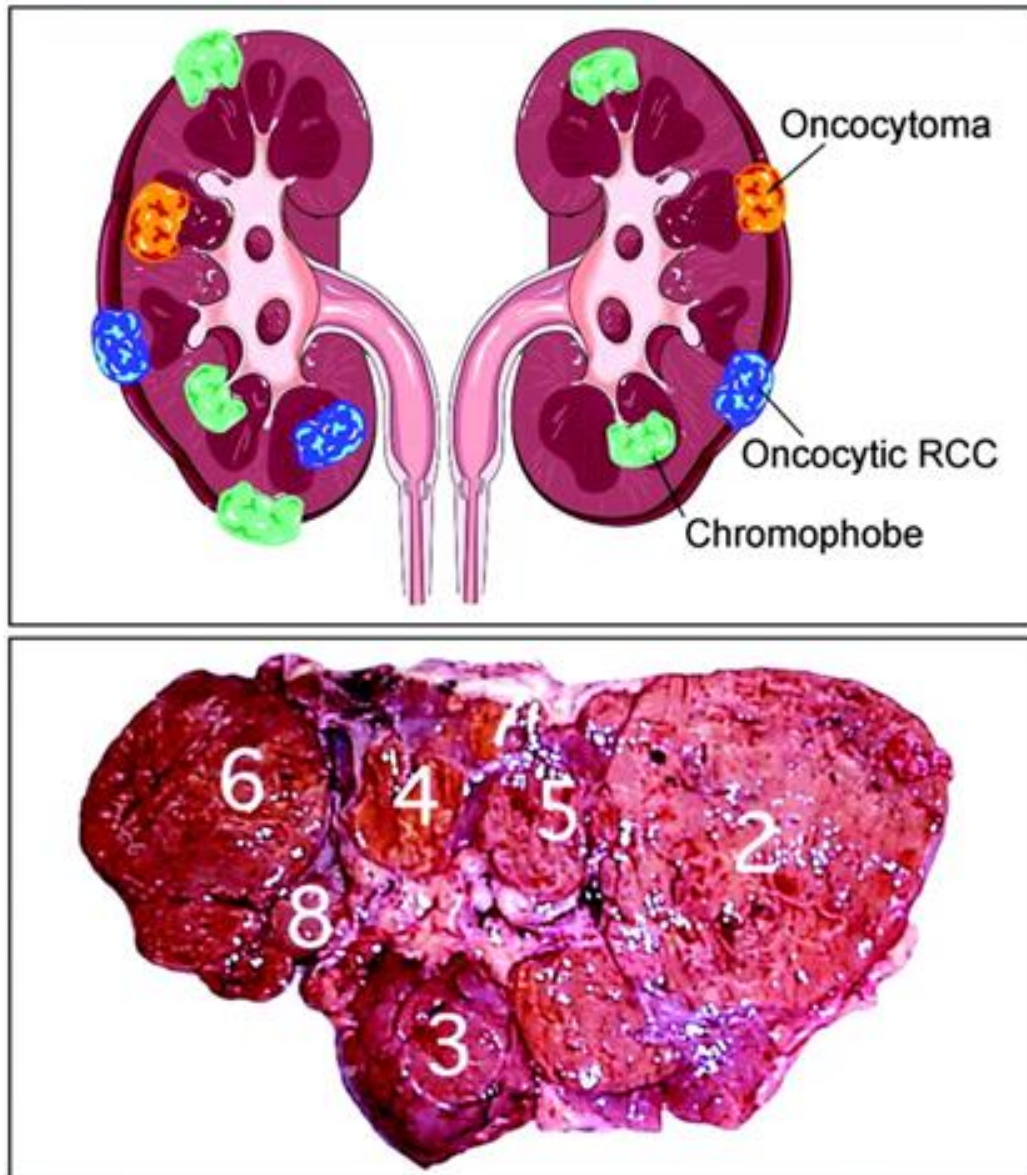


Fig 9: Birt Hogg Dubé-associated bilateral, multifocal renal tumours: (Linehan *et al.*, 2004)

Fig 8 and fig 9 show multiple independent tumours of different sorts with different morphologies and properties that developed following one initial mutation. This may occur in one or often both of the patients' kidneys.

Investigation of a mutation hotspot in genotype/phenotype analysis by Schmidt *et al.* (2005) and Toro *et al.* (1999) showed germ-line deletion of cytosine at exon 11 in the FLCN gene appears as though it may lead to fewer renal tumours in BHD patients than insertion of

cytosine at the same point (c.1733insC, c.1733delC, see fig 10). How, when and where the mutation occurs could all affect the outcome for the individuals affected although no genotype-phenotype correlations have been confirmed to date.

The first reported renal cancer in a BHD patient was in 1993 by Roth *et al.* The occurrence of multiple renal tumours in a BHD patient was reported by Toro *et al.* (1999) and Roth *et al.* (1993). Statistical association of renal tumours and pulmonary problems with BHD was published in 2002 by Zbar *et al.*

The BHD gene *FLCN* encodes a 64 kDa protein, known as folliculin (Nickerson *et al.*, 2002). In kidney tumours, the wild-type allele of *FLCN* has been seen to have undergone somatic mutation and deletion or loss of heterozygosity, which supports the widely held idea that *FLCN* follows the Knudson 2-hit hypothesis and is in fact a classic tumour suppressor gene. No homology to other known proteins could be found for the *FLCN* protein and it has no predicted functional domains identifiable. *FLCN* is a highly conserved protein across many species which gives an indication that it could possibly have an essential role in development. This is supported by the observation that absence of all *FLCN* in mice leads to embryonic lethality from visceral endoderm defects (Baba *et al.*, 2012).

Molecular Biology

Although the protein sequence of folliculin did not contain any obvious functional motifs to indicate a likely function, reports have linked folliculin function to the mTOR pathway, the mammalian target of rapamycin kinase (Baba *et al.*, 2006). Disregulation of the mTOR pathway is common in sporadic RCC and one promising therapy for advanced RCC is the mTOR inhibitor, temsirolimus, (Robb *et al.*, 2007, Hudes *et al.*, 2007). As can be seen in Fig10, nearly all BHD mutations are frame shift or nonsense mutations that are predicted to prematurely truncate the BHD protein *FLCN*. Mutation of *FLCN* in sporadic kidney cancer is

not common but has been seen (Da Silva *et al.*, 2003, Murakami *et al.* 2007), although the exact frequency of such *FLCN* mutations is unknown. Mutation analysis was performed in 35 CRCs and cell lines, and 30 RCC primary tumours and cell lines. A somatic missense mutation with loss of the wild type allele was identified in a primary clear cell RCC (showing consistency with the two hit tumourigenesis mechanism), and a further missense mutation was detected in a clear cell RCC cell line. A somatic missense substitution was detected in a primary CRC, as well as three oncocytoma type RCCs for which matched normal DNAs were not available. A germline missense variant was found in a primary CRC and not detected in 40 control individuals or a further 159 familial and sporadic CRC cases. No evidence of epigenetic silencing of BHD in was found. Da Silva et al (2003) concluded that the findings suggested that BHD inactivation occurred in a subset of clear cell RCC and CRC. Shin et al (2003) also reported BHD frameshift mutations in a subset (~20%) of MSI+ CRCs with micro satellite instability. The most recent data gives the rate of *FLCN* mutation in sporadic clear cell RCC as 0.2% (1 in 418 cases) and 2.8% of 72 cases for CRC (www.cbiportal.org 02/05/2014)

In the case of *FLCN*, mutations occurring 5' in the gene, rendering large parts of the protein absent, might have greater effects than mutations in the 3' coding regions and /or those that affect just a small section of the protein, unless they affect a necessary structural or functional component of the protein produced.

A human FLCN-binding protein (Fnip1) was identified in 2006 (Baba *et al.*, 2006). It is evolutionally conserved, and also interacts with the AMPK complex. Both FLCN and Fnip1 are phosphorylated by AMPK and the phosphorylation of FLCN is regulated directly or indirectly by Mammalian Target of Rapamycin (mTOR). The phosphorylation of S6K1 may also be affected by expression of FLCN (Baba *et al.*, 2006). The interactions with the AMPK and mTOR pathways indicate probable involvement in energy/nutrient sensing. A second FLCN-binding protein, called Fnip2 or FnipL (for Fnip1-Like), which is highly homologous to Fnip1, was reported by two groups (Hasumi *et al.*, 2008, Takagi *et al.* 2008). Fnip2 could positively regulate phosphorylation of FLCN. It binds to phosphorylated FLCN. A role of Fnip2 may be to stop dephosphorylation of FLCN by the formation of a FLCN/Fnip2 complex. Fnip2 is bound and phosphorylated by AMPK. The parts that these phosphorylations, and that of FLCN by AMPK (Baba *et al.*, 2006), play in the functions of Fnip1, Fnip2 and FLCN are not yet known. *FNIP1* knockdown exerted a similar effect as BHD; the FLCN-FnipL and Flcn-Fnip1, complexes may function independently in the mTOR pathway. Suppression of FLCN, their common factor, may give greater effects than suppression of Fnip (Takagi *et al.* 2008, Hasumi *et al.*, 2008). Hasumi *et al.* also found a binding between Fnip1 and Fnip2.

mTOR-pathway

Mammalian Target of Rapamycin (mTOR), a member of the PIKK (Phosphatidylinositol 3-Kinase-related Kinase) family is a serine/threonine protein kinase of 289-kDa in size. The

mTOR pathway is regulated by many cellular signals, including nutrients (amino acids, glucose), mitogenic growth factors, cellular energy levels, hormones such as Insulin, and stress conditions. The PI3K/Akt pathway, involved in the mediation of cell survival and proliferation, acts through mTOR.

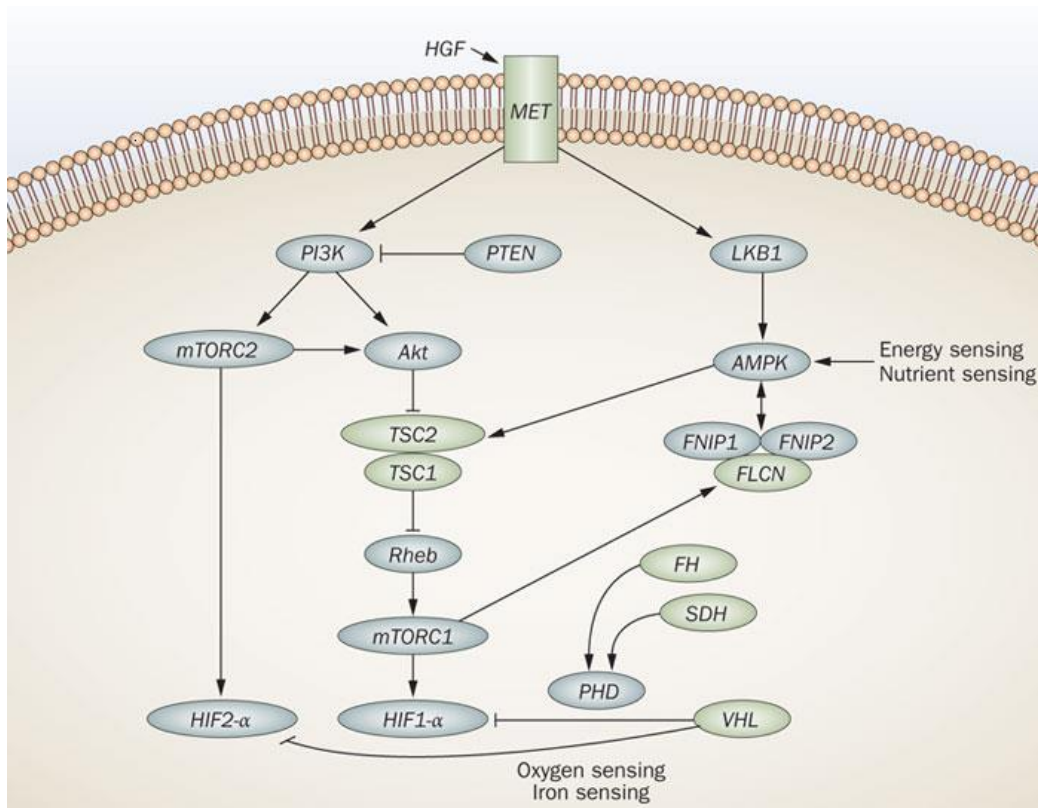


Fig 11: The mammalian target of rapamycin mTOR signalling pathways (Linehan *et al.*, 2010).

Fig 11 shows the basis of FLCN interaction through the mTOR pathway. FLCN loss may lead to disease through actions of mTOR and AMPK signaling.

FLCN, VHL and other genes that have been shown to cause kidney cancer have a feature in common, in that they are all involved in iron, energy, oxygen, or nutrient sensing pathways, indicating that kidney cancer is a metabolic disease. AMPK, the cells' primary energy sensor, is bound by the FLCN–FNIP1–FNIP2 complex and a kinase that is rapamycin-sensitive (e.g. mTORC1) phosphorylates FLCN. The LKB1–AMPK cascade phosphorylates TSC1–TSC2

thus helping mediate the response of the cell to energy and nutrient sensing. (Linehan *et al.*, 2010)

Animal models

Animal models of human cancer are valuable tools for identifying pathways responsible for neoplasia and drug testing prior to any clinical trials. A targeted BHD- kidney-specific mouse model which has a marked polycystic phenotype which develops within the first 3 weeks of life has been developed. In this model, homozygous inactivation of BHD leads to cell proliferation, although BHD-null cells may still require additional genetic or epigenetic events to gain a growth advantage and to facilitate progression to cancer. These BHD-targeted mice develop a recognisable kidney phenotype over a very short time. For this reason this model may be useful for the testing and development of drugs and therapies, even though the mouse model may not precisely mirror BHD syndrome (Baba *et al.* 2008).

The mouse model also indicated that BHD is needed for the proper regulation of cell growth (Baba *et al.* 2008) and proliferation through Akt-mTOR signalling (Fig 11, *vide supra*) during postnatal kidney development (Baba *et al.* 2008). The resulting inappropriate Akt-mTOR signaling could play a part in the observed phenotype of enlarged cystic Kidneys. This is reinforced by the reduced kidney size and tubule/duct dilatation seen with rapamycin treatment, which extended survival of BHD knockout mice (Baba *et al.*, 2008).

Fln mutant Nihon rats are a model of renal cell carcinoma (RCC). They originated from a Sprague-Dawley strain of rats. A germline mutation in the rat homologue of the BHD gene was identified (Okimoto *et al.*, 2004b) in these rats, a single nucleotide insertion on chromosome 10, within exon 3 of *Fln* (c.462_463insC). The mutation results in a frameshift and premature stop codon within the *Fln* gene (Okimoto *et al.*, 2004b). Heterozygous Nihon rats develop RCCs that mainly show clear-cell histology. Homozygous mutants are

embryonic lethal (Okimoto *et al.*, 2004a). Suppression of the Nihon rat phenotype by introduction of a wild-type BHD mini-gene was then shown (Togashi *et al.*, 2006) allowing the Nihon rat to be used as an animal model of BHD.

The German Shepherd dog-model consists of a hereditary multifocal renal cystadenocarcinoma and nodular dermatofibrosis (RCND) associated with a adenine to guanine missense mutation was detected in exon 7 of the canine BHD gene on canine chromosome 5. This nucleotide change gives rise to a histidine-to-arginine mutation in the protein expressed (Lingaas *et al.*, 2003).

It is the intention of the project to investigate the role of FLCN in the cell and in the development and treatment of BHD syndrome, using a variety of techniques including tissue culture, molecular biology and genetics.

Aims

The study will make use of molecular techniques such as cell culture and Western blotting, as well as antibody staining and microscopy (including confocal microscopy). These methods will be employed to study the molecular pathology of BHD.

Treatment of BHD-related tumours (and sporadic tumours with *FLCN* inactivation) could possibly be targeted by developing treatments that target cells without FLCN protein specifically. There are several ways in which possible therapeutic agents could be selected according to a number of criteria. Agents that target signalling pathways linked to FLCN function could be investigated. An approach based in bioinformatics, as described for VHL (Sutphin *et al.*, 2007) could be employed to pick out chemical treatments that are likely to show selective toxicity against FLCN negative cells. To this end the NCI-60 cell lines collection (representing renal, colon, lung, melanoma, leukaemia, central nervous system,

prostate, breast and ovarian tissues), which have been tested for sensitivity to greater than 60,000 chemical compounds, could be ranked using expression levels of the *FLCN* gene in each cell line and correlated with sensitivity to each specific compound so as to allow identification of compounds that could potentially be differentially cytotoxic according to *FLCN* expression levels.

Potential *FLCN*-negative specific agents can then be tested against a panel of cells including UOK257 (Youfeng Yang *et al.* 2008) and cells transfected with wild-type and mutant *FLCN* constructs. Investigation into the effect of chemicals that affect folliculin-associated signalling pathways could be carried out beginning with *in vitro* tumourigenesis assays (e.g. colony formation assays) to pick out chemicals with different results depending on *FLCN* status, and testing cytotoxic compounds in clonogenic survival assays (Sutphin *et al.*, 2007). The effect of chemicals on caspase activity of cells with different *FLCN* levels and mutations will also be of interest, as will other genes that may affect the survival in *FLCN*-deficient cells.

Chapter 2: Materials and methods

Cell Lines and Cell Culture.

Human renal carcinoma of BHD origin cells UOK-257 (UOK-FLCN⁻) and FLCN transfected UOK-257 cells UOK-FLCN⁺ (Yang *et al.*, 2008) were provided by Dr Marston Linehan and Dr. Laura S Schmidt (Urologic Oncology Branch, Centre for Cancer Research, National Cancer Institute, National Institutes of Health, Bethesda, MD 20892, USA) to whom we are grateful. FTC-133 cells were purchased from the European Collection of Cell Cultures (ECACC) (Salisbury, United Kingdom). Transfection of FLCN constructs into FTC cells and selection of stable clones was carried out by Laurence Seabra. Other RCC cell lines, including 786-0, SKRC47, CAKI2 and stable transfectants of 786-0, SKRC39 and RCC4. containing a construct (VHL⁺, or empty vector for control), were obtained from Dean Gentle. All cell lines were cultured in Dulbecco's Modified Eagle Medium (DMEM) with supplement of 10% foetal bovine serum except for FTC-133 cells which were incubated in medium containing DMEM and Ham's F12 nutrient mixture (1:1).

Cells were incubated at a temperature of 37 °C with high humidity levels and elevated CO₂ concentrations (usually 5%) to maintain the proper pH (7.4 ± 0.2) used with bicarbonate buffer medium, and using unsealed dishes and plates or flasks with gas permeable (vented) caps to allow gas exchange. Cell culture media used are shown in Table 2 and Table 3.

Table 2: Media used in cell cultures

DMEM	500 ml	Final conc
Foetal Bovine Serum	50 ml	10%
200mg/ml Glutamine	5 ml	2 mg/ml

(All purchased from Sigma-Aldrich Company Ltd. The Old Brickyard, New Road, Gillingham, Dorset SP8 4XT)

Table 3: Cell culture media for FTC-133. (FTC-133 cells were purchased from ECACC (Salisbury, United Kingdom)).

		Final conc.
DMEM	250ml	
Ham's F12	250ml	
Foetal Bovine Serum	50ml	10%
200mg/ml Glutamine	5ml	2 mg/ml

For stably-transfected clones, G-418-Sulphate-solution (P11-012 from PAA Laboratories Ltd, Termare Close, Houndstone Business Park, Yeovil, Somerset, BA22 8YG, United Kingdom) was added to give selection pressure to keep only the transgenic cells. 1 ml of the G418 solution was added per 100 ml of medium.

Stable expression of an artificially introduced DNA sequence is achieved by integration of the gene of interest into the target cell's chromosome, along with an antibiotic resistance gene to allow the cells containing the construct to be selected and non-transfected cells to be removed so that they do not affect the results of the experiments or overgrow the transfected cells.

Frozen cell vials were taken from the liquid nitrogen tank, the dry ice on which they were shipped, or a -70 °C freezer and the vials were then left at room temperature for 2 minutes. The frozen cells were then melted by immersing the vials in a 37 °C water bath. Working in a class 2 hood, 5ml of medium plus the melted cells (~1 ml) were pipetted into the labelled Universal tubes. Centrifuge down cell pellet at 1000 rpm for 3 minutes. The cell pellet was then re-suspended in 5ml medium and incubated at 37 °C.

Flasks of actively growing cells were prepared, and used at 80 to 90% confluence. 1x Trypsin solution (purchased from Sigma) was used to dissociate cells prior to seeding.

Small interfering Ribonucleic acid (SiRNA) treatment for reverse transfection with INTERFERin®.

A double-stranded RNA molecule is cleaved to give single-stranded RNA (usually from 21 to 25 nucleotides in length) which then binds to complementary sequences in messenger RNA (mRNA) and brings about the cleavage and degradation of the mRNA thus preventing the production of the protein coded by that molecule.

Work was carried out in the Tissue Culture sterile lamina flow hood. Reagents were warmed to room temperature. Appropriate volumes of Opti-MEM® Reduced Serum Medium (11058-021 no Phenol Red, from Invitrogen Life Technologies Ltd, 3 Fountain Drive, Inchinnan Business Park, Paisley, PA4 9RF, UK) and SiRNA for each required treatment were added to separate wells of a 96-well plate. These were mixed well using the plate shaker. This diluted siRNA (folliculin siRNA(h), Santa Cruz Biotechnology 2145 Delaware Avenue Santa Cruz, USA) and SSH2 siRNA (Silencer Select human Phosphatase siRNA Library, Ambion, Warrington, UK) transfection reagent (INTERFERin, Polyplus Transfection, Hampshire, UK) was then added to each of these wells and the plate well mixed for 10 minutes on the plate shaker. These SiRNA treatment mixes were aliquoted into the appropriate wells of the experimental plates at a final volume of 10 µl per well in a 96-well plate with exponentially growing cells for growth inhibition assays (or scaled up for 12 well plates, 6 well plates, or 10 cm dishes for confocal analysis or clonogenic assays). The final siRNA concentration was at 20 nM. After being siRNA transfected, the plates were then mixed gently and incubated at 37 °C for 24 hours. Drug treatments were then added and the plates were incubated for a further 72 hours, after which the cells were fixed and stained. The cells were trypsinised and the cells counted and seeded at 90 µl of cell suspension per well of 96-well plates at a low density. The exact density depended on the cell line used and is shown in Table 4.

Table 4: Experimental cell seeding densities

Cell line	Concentration of cells and Size of well	INFO
UOK257	3-5 x 10 ⁴ cells / ml (3-5 x 10 ³ cells/ 100 µl/well)	<p>HUMAN CLEAR CELL RCC FROM A MALE BHD PATIENT'S KIDNEY TISSUE</p> <p>C.153C>T MUTATION RESULTED IN AN EARLY TRUNCATION OF P53 PROTEIN</p> <p>(WILD TYPE PTEN PRESENT)</p> <p>FLCN FRAMESHIFT MUTATION [C.1285DUPC; PREDICTED, IN THE ABSENCE OF NONSENSE MEDIATED MRNA DECAY, TO LEAD TO PREMATURE PROTEIN TRUNCATION (P.HIS429PROFSX27) (<i>Iu et al</i> 2011)</p>
FTC-133	2.5 x 10 ⁴ cells / ml (2.5 x 10 ³ cells/ 100 µl/well)	<p>SOMATIC FLCN GENE MUTATION (C.1285DELG)</p> <p>PTEN GENE MUTATION RESULTING IN A TRUNCATED PROTEIN</p> <p>POINT MUTATION OF P53 GENE LEADED TO INACTIVATION OF P53 FUNCTION BY ACCUMULATION OF THE PROTEIN. (<i>Iu et al</i>.2011)</p>
CAKI 2	5 x 10 ⁴ cells / ml (5 x 10 ³ cells/ 100 µl/well)	<p>LOSS-OF-FUNCTION SUBSTITUTION - NONSENSE MUTATION IN THE VON HIPPEL-LINDAU (VHL) TUMOR-SUPPRESSOR PROTEIN C.529A>T P.R177*</p> <p>PTEN WILD TYPE</p>
CAKI1	6 x 10 ⁴ cells / ml	<p>VHL WILD TYPE(http://www.medogene.com/My%20Researches/Kidney%20cell%20lines.html)</p> <p>P53 WILD TYPE AND PTEN WILD TYPE</p>
SKRC45	2 x 10 ⁴ cells / ml	VHL MUTATION R82P (<i>Gemmil et al.</i> 2005)
SKRC47	2 x 10 ⁴ cells / ml	VHL MUTATION
SKRC39	10 ⁴ cells / ml	<p>VHL MUTATION <i>Jafri et al.</i> 2012FLCN ALA238VAL (C.1168 C→T) SUBSTITUTION</p> <p>PATHOGENICITY UNCONFIRMED(<i>da Silva et al.</i>2003)</p>
786-0	10 ⁴ cells / ml	<p>NON-FUNCTIONAL VHL (1 BASE DELETION)(<i>Wada et al.</i> 1999)</p> <p>P53 MUTATION C.832C>GPROTINE CHANGE C.560-2A>G (SPLICE JUNCTION)</p> <p>EFFECT INCONCLUSIVE;</p>

Sulforhodamine B (SRB) Growth Inhibition Assay

The Sulforhodamine B assay (SRB) (Skennan *et al.*, 1990) was used to assess the sensitivity of the cell lines to growth inhibition caused by chemical treatment. Exponentially growing adherent cells were seeded into 96-well plates wells B2 – H11 (10 x 6) at a suitable density – see Table 4.

Allowing for 24 hrs settling down and 72 hours growth, 100 µl medium was put into the outside wells to compensate for ‘edge effect’. In another plate 5-wells of cell suspension were seeded in one row for each cell line and these were surrounded by media containing wells to avoid edge effect. This was the Day 0 plate. After 20-24 h incubation at 37 °C, the day 0 plate was fixed by adding an equal volume of Carnoy’s fixative and stored at 4 °C until staining.

Also after 20-24 h incubation, drugs were added to the experimental wells at the appropriate concentrations for each compound tested. One row (five replicates) was treated for each drug concentration. 10x drug final concentrations in 10% dimethyl sulfoxide (DMSO) were prepared (DMSO plus five concentrations were used for each experiment by adding 12.3 µl 100x into 100 µl medium in a 96-well format) see table 5.

10 µl of this 10x solution was then added into the appropriate wells containing 100 µl medium to give the final 1x concentration and 1% DMSO. The drug was mixed with the medium in the wells by placing the plate in a plate shaker for 2 minutes. The plates were then incubated at 37°C for 72 hours.

Table 5: Drug concentrations

Compound	1x Solution Concentration	10x Solution Concentration
Morpholino-ADR	0.01, 0.1, 1, 10, 100 nM	0.1, 1, 10, 100, 1000 nM
Cyanomorpholino-ADR	0.01, 0.1, 1, 10, 100 nM	0.1, 1, 10, 100, 1000 nM
Echinomycin	0.01, 0.1, 1, 10, 100 nM	0.1, 1, 10, 100, 1000 nM
Chromomycin A3	0.1, 1, 10, 100, 1000 nM	0.001, 0.01, 0.1, 1, 10 µM
Bruceantin	0.1, 1, 10, 100, 1000 nM	0.001, 0.01, 0.1, 1, 10 µM
Vincristine sulphate	0.1, 1, 10, 100, 1000 nM	0.001, 0.01, 0.1, 1, 10 µM
DidemninB	0.1, 1, 10, 100, 1000 nM	0.001, 0.01, 0.1, 1, 10 µM
Taxol	0.001, 0.01, 0.1, 1, 10 µM	0.01, 0.1, 1, 10, 100 µM
Mithramycin	0.001, 0.01, 0.1, 1, 10 µM	0.01, 0.1, 1, 10, 100 µM
Phyllanthoside	0.001, 0.01, 0.1, 1, 10 µM	0.01, 0.1, 1, 10, 100 µM
Bisantrene hydrochloride	0.01, 0.1, 1, 10, 100 µM	0.1, 1, 10, 100, 1000 µM
Doxorubicin	0.01, 0.1, 1, 10, 100 µM	0.1, 1, 10, 100, 1000 µM
Rapamycin	0.01, 0.1, 1, 10, 100 µM	0.1, 1, 10, 100, 1000 µM
VM-26	0.01, 0.1, 1, 10, 100 µM	0.1, 1, 10, 100, 1000 µM
Menogaril	0.01, 0.1, 1, 10, 100 µM	0.1, 1, 10, 100, 1000 µM
N,N-dibenzyl-daunomycin	0.01, 0.1, 1, 10, 100 µM	0.1, 1, 10, 100, 1000 µM

After drug treatment for 72 hours, the cells were fixed *in situ* by adding an equal volume of Carnoy's fixative (methanol: acetic acid=3:1) to each well containing cells. This was then placed at 4°C for at least 1 hour and up to one week before SRB staining. The plates were then washed in water and air dried. 100 µl of SRB solution (0.4 % w/v Sulforhodamine B Solution dissolved in 1% w/v acetic acid (Sigma-Aldrich, Poole, United Kingdom)) was

added to each well and left for 30 minutes at room temperature, after which time the plates washed with 1% w/v acetic acid solution to remove all excess stain. The acetic acid solution was then removed and the plates placed in the drying oven until dry. Prior to reading the plates, the protein-bound SRB was solubilised by the addition 10 mM Tris Base (pH 10.5) to each well. Gentle agitation in a plate mixer was used to ensure a completely homogenous solution.

The absorbance for each well was measured at 570 nm on a Victor X3 Multilabel Plate Reader (PerkinElmer, Beaconsfield, United Kingdom).

Carnoy's fixative: methanol: acetic acid=3:1, store at 4 °C.

(Morpholino-ADR (NSC 354646), Cyanomorpholino-ADR (NSC 357704), Echinomycin (NSC 13502), Chromomycin A3 (NSC 58514), Bruceantin (NSC 67574), Vincristine sulfate (NSC 165563), DidemninB B (NSC 325319), Paclitaxel (Taxol, NSC 125973), Mithramycin (NSC 24559), Phyllanthoside (NSC 266492), Bisantrene hydrochloride (NSC 337766), doxorubicin (Adriamycin, NSC 123127), VM-26 (Teniposide, NSC 122819), Menogaril (NSC 269148), N,N-dibenzyl-daunomycin (NSC 268242), and rapamycin (NSC 226080) were kindly provided by the Developmental Therapeutics Program of the National Cancer Institute (NCI)/NIH (<http://dtp.nci.nih.gov>).) Compound C AMPK Inhibitor, 6-[4-(2-Piperidin-1-yl-ethoxy)-phenyl]-3-pyridin-4-yl-pyrazolo[1,5-a]-pyrimidine, Dorsomorphin (171260 -1MG) was obtained from Calbiochem MERCK.

The levels of growth inhibition induced by the various concentrations of agents were measured in all cases, after 72 hours of treatment. GI₅₀ values were calculated by fitting a sigmoidal concentration/inhibition curve to the data obtained from the SRB assays, using non-linear least square regression (Graph Pad PRISM™).

Clonogenic Cell Survival Assay

The ability of Mithramycin to kill cells and the efficiency with which it did it was investigated in UOK-257 cells with (UOK FLCN) and without (UOK257) FLCN expression.

Exponentially growing cells were seeded into 10 cm tissue culture plates at several densities from 250 to 1×10^5 cells per dish. Two seeding densities in duplicate for each seeding density were set for the experiment. The cell seeding density was calculated to give an estimated 10-300 colonies/plate following drug exposure. DMSO controls and five concentrations of Mithramycin treatment were used for each cell line (see tables 6 and 7)

Table 6: Mithramycin concentrations and cell numbers used in clonogenic assay with the UOK cell line.

UOK:						
Mithramycin concentration / nM	0	10	50	100	200	500
Seeding density/plate	150	150	500	1000	5000	5000
	300	300	1000	5000	10000	10000

Table 7: Mithramycin concentrations and cell numbers used in clonogenic assays with the UOK-FLCN cell line.

UOK-FLCN:						
Mithramycin concentration / nM	0	100	200	500	1000	10000
Seeding density/plate	150	150	150	500	1000	5000
	300	300	300	1000	5000	10000

The cells were trypsinised and counted following standard procedures and the cells diluted to the appropriate seeding density in the medium. The maximum volume used in each 10cm plate is 10ml. All plates were then incubated for 24 h at 37°C to allow the cells to attach. Solution was made up and 70µl of 100x Mithramycin (dissolved in DMSO) was added to give the final concentrations given above in the dishes. The final concentration of DMSO in the medium was 1%. At least three experiments were carried out under each set of conditions. All plates were incubated for 72hrs.

At the end of this time the drug-containing medium was removed from all cells and they were washed gently once with 5ml of warm PBS. 10ml fresh medium was added into each of the plates and all plates were incubated for an additional 10 to 15 days. The medium was then carefully removed and the cells were fixed *in situ* by adding Carnoy's fixative mixed with an equal volume of PBS to each plate containing cells; this was then removed after a short incubation at ambient temperature and the plates placed at 4°C for at least 1 hour and up to one week and air-dried before SRB staining. SRB solution (Sigma-Aldrich, Poole, United Kingdom) was added to each of the plates and left for 30 minutes at room temperature. After this time the plates were washed with 1% w/v acetic acid solution to remove all excess stain. The acetic acid solution was then removed and the plates dried in the drying oven. Colonies with over 30 cells were counted. Cloning efficiencies of untreated cells were: UOK257-FLCN⁻ 26% and UOK257-FLCN⁺ 34%. Cell survival following drug exposure was expressed as % control cloning efficiency or survival.

SSH2 Clonogenic Cell Survival Assay

The ability of SSH2 siRNA knock-down to kill cells and the efficiency with which it did it was investigated in FTC133 cells with (FTC133-12) and without (FTC133-22) FLCN expression.

Exponentially growing cells were seeded into 10 cm tissue culture plates at several densities from 100 to 4000 cells per dish. Two sets in duplicate for each treatment concentration were set for the experiment. The cell-seeding density was calculated to give an estimated 10-300 colonies/plate following treatment exposure. Luciferase controls and four concentrations SSH2 siRNA treatment were used for each cell line.

Table 8: SSH2-siRNA treatment conditiond used for each cell line

FTC12:				
SSH2 siRNA concentration / nM	1	5	10	20
Seeding densit cells/plate	900	1200	2000	4000
luci siRNA concentration / nM	1	5	10	20
Seeding density/plate	100	100	100	100
FTC22				
SSH2 siRNA concentration / nM	1	5	10	20
Seeding density/plate	300	300	500	500
luci siRNA concentration / nM	1	5	10	20
Seeding density/plate	600	600	600	600

The cells were trypsinised and counted following standard procedures and the cells diluted to the appropriate seeding density in the medium. The maximum volume used in each 10 cm plate is 10 ml. All plates were then incubated for 24 h at 37°C to allow the cells to attach. SiRNA knock-downs were carried out as described above with the amounts scaled up for the larger plates. All plates were incubated for 72 hours.

Once again at the end of this incubation time the drug-containing medium was removed from all cells and they were washed gently once with 5 ml of warm PBS. 10 ml fresh medium was added into each of the plates and all plates were incubated for an additional 10 to 15 days. The

medium was then carefully removed and the cells were fixed *in situ* by adding Carnoy's fixative mixed with an equal volume of PBS to each plate containing cells. This was then removed after a short incubation at ambient temperature and the plates placed at 4°C for at least 1 hour and up to one week and air dried before SRB staining. SRB solution (Sigma-Aldrich, Poole, United Kingdom) was added to each of the plates and left for 30 minutes at room temperature, after which time the plates were washed with 1% w/v acetic acid solution to remove all excess stain. The acetic acid solution was then removed and the plates dried in the drying oven). Colonies with over 30 cells were counted. Cloning efficiencies of untreated cells were: UOK257-FLCN⁻ 26% and UOK257-FLCN⁺ 34%. Cell survival following drug exposure was expressed as % control cloning efficiency or survival.

Western Blot Analysis

Cellular protein expression in cells with/without FLCN protein were identified from complete cell lysate obtained after 48 h treatment and the changes due to the treatments applied to the cells determined.

Cells were cultured in plates until they reached 80% confluence. They were then washed with 5ml PBS which was aspirated. 5ml PBS was added into each plate and cells detached by a cell scraper (rubber policeman). The cell-containing PBS was transferred into a universal tube and centrifuged down at 1000rpm for 3minutes to give a cell pellet. The supernatant was removed and the pellet re-suspended in 1ml PBS, which was then transferred into an Eppendorf tube and centrifuged down to give a cell pellet at 2000rpm for 1 minute. The supernatant was removed and all tubes stored at -70°C. Lysis buffer (6.25mM Tris HCl pH6.8, 10% glycerol, 2%SDS) was then added to the pellet to disrupt the cells.

DC protein assay kit was used to test the protein concentrations in the lysate samples. The manufacturer's instructions were followed (Bio-Rad Laboratories Ltd, Hertfordshire, United

Kingdom). Electrophoresis was carried out on 20 µg samples of protein on 12.5% (w/v) SDS-PAGE gels (using BIORAD Mini-PROTEAN® Tetra electrophoresis system, following manufacturer's instructions, at 100v for approximately 1 hour) and then electro-blotted (using BIORAD Mini Trans-Blot® Cell system, following manufacturer's instructions, at 100v for 1 hour) on to nitrocellulose membrane (Amersham Pharmacia Biotech UK Ltd., Buckinghamshire, United Kingdom). The membrane was then washed in PBStw (PBS with 0.1% tween 20 added, both obtained from Sigma-Aldrich Company Ltd) in which milk protein had been dissolved at 5% to block non-specific binding. Primary antibodies were then used to probe for the proteins of interest. The antibodies diluted 1:100 to 1:1000 in 5% milk PBStw were applied to the membrane and incubated overnight at 4°C. After the removal of the primary antibody the membrane was washed in PBStw, a secondary antibody appropriate to the primary antibody (anti-mouse IgG-HRP conjugate, or an anti-rabbit IgG-HRP conjugate (DAKO, Ely, United Kingdom)) was used at a concentration of 1:2000 in 5% milk PBStw incubated at room temp for 2 hours to bind the primary antibody. The bound HRP conjugate in conjunction with the enhanced chemiluminescence (ECL+Plus, Amersham) system was used to produce a signal which was detected using Kodak film following the manufacturers recommended method.

Antibodies used were against FLCN (generously provided by Prof. Arnim Pause, Rosalind and Morris Goodman Cancer Centre Montreal, Canada) and a further FLCN antibody, caspase3, pS6 Ribosomal, pAMPK α , p AMPK β , AMPK α and AMPK β all obtained from Cell Signaling Technology, Hertfordshire, United Kingdom. The p53 antibody was DO7, Novacastra, Newcastle upon Tyne, United Kingdom and the Actin antibody was obtained from Sigma-Aldrich Company Ltd., Dorset, United Kingdom.

Immunofluorescence

Solutions

PBS

4% paraformaldehyde: (paraformaldehyde is toxic) (In a fume hood 4g added to 100 ml of PBS which had been warmed to 60 °C the bottle was then sealed, and keep warm to dissolve when dissolved it was left to cool and aliquots were stored at -20°C.)

0.2% TritonX100 in PBS

Invitrogen pro long gold mounting medium with Dapi

Cells were grown on glass cover slips which had been cleaned with ethanol and treated with UV light to reduce risk of bacterial contamination. When the cells had grown sufficiently the medium was carefully removed and discarded and the cells were fixed in 4% paraformaldehyde for 20 minutes at room temperature. The fixative was then removed and disposed of appropriately and the cover slips were washed 3 times in PBS. Cover slips were then stored in PBS at 4°C for up to 5 days. Usually they were used within 24 hours. At this point they were permeabilised in 0.2% TritonX100 for 3 to 5 min at room temperature. Washed and then blocked for 2 hours in 1% BSA dissolved in PBS. They were then washed 3 more times in PBS before the cover slip was drained and inverted onto a 50 µl drop of primary antibody (diluted 1:100, or 1:1000 for mouse anti-tubulin), on parafilm so that it covered all of the cells, throughout the 1 hour incubation. During this time it was kept covered and humid. It was incubated for 1 hour at room temp (or overnight at 4°C).

The cover slips were then washed 3 times in PBS. The cover slips were then each inverted onto a 50ul drop of secondary antibody (diluted 1:250) on parafilm so that it covered all of the

cells, throughout the 1 hour incubation. During this time it was kept in the dark, covered and humid.

A-11005 Alexa Fluor® 594 goat anti-mouse IgG (H+L) *2 mg/ml*

A-11012 Alexa Fluor® 594 goat anti-rabbit IgG (H+L) *2 mg/ml

A-11001 Alexa Fluor® 488 goat anti-mouse IgG (H+L) *2 mg/ml

All from Invitrogen, Life Technologies Ltd, 3 Fountain Drive, Inchinnan Business Park, Paisley PA4 9RF, UK.

After this they were washed 3 times PBS as before, and then once in dH₂O

The cover slip was then inverted onto drop of mounting medium with Dapi (Invitrogen ProLong® Gold ant fade reagent with DAPI P-36931) on labelled slide.

They were then dried in the dark for 15 min, sealed with clear nail varnish and the slides stored at 4 °C until they were visualised and photographed using the Leica confocal microscope.

Primary antibodies used were against FLCN (a gift from Prof. Arnim Pause, Rosalind and Morris Goodman Cancer Centre Montreal, Canada), FLCN (Cell Signaling Technology, Hertfordshire, United Kingdom), Miz (Santa Cruz Biotechnology). (flag) DYKDDDDK Tag, Alpha Tubulin and Actin (Sigma-Aldrich Company Ltd., Dorset, United Kingdom) were used. Bcl-2, SLK, p15, p21(abcam 330Cambridge Science Park, Cambridge, CB4 0FL UK) c-Myc (Life Technologies Ltd, 3Fountain Drive, Inchinnan Business Park, Paisley PA4 9RF, UK).

Transient Transfection for the expression of over-expression of full-length FLCN or FLCN mutants.

Fugene HD transfection reagent was purchased from Roche (Roche Diagnostics Deutschland GmbH, Roche Applied Science, Sandhofer Str. 116, 68305 Mannheim) and used at a 6:2 ratio. 300µl of opti-MEM (*vida supra*) was mixed with 6µg of plasmid. 18µl fugene HD was added directly to the plasmid medium mixture mixed and incubated for 15 min before being added drop-wise to the cells in the 6-well plate. 100µl of transfection mixture per well which contains 2 ml of cell suspension.

The plasmids used were contained flag-tagged full-length normal foliculin, empty vector control, two mutant FLCN plasmids Cys82Ala and Cys85Ala, where Cys in FLCN potential metal binding domain had been mutated to Ala by site-directed mutagenesis by Uncaar Boora who kindly provided the plasmids.

Chapter 3: Results of investigations into the effect of FLCN expression on the effect of selected drugs

Selection of compounds with the highest therapeutic potential.

To determine the most effective drugs to assess, the NCI-60 cell lines database was interrogated using the COMPARE algorithm (Developmental Therapeutics Program) by Xiaohong Lu and Wenbin Wei, to identify cytotoxic compounds which appeared to be least effective against cells with high FLCN protein expression and most effective against cell lines with low FLCN protein expression. In principle, this should help identify those drugs which may be most use in treating tumours with *FLCN* inactivation.

The NCI60 cell line panel was set up from 60 tumour cell lines from nine different tissue types as a tissue-directed anticancer drug screen in 1990 by the NCI to evaluate the compound's antineoplastic activity. The 60 cell lines cover a wide range of molecular defects so that the analysis of drug activity can be made regarding specific molecular alterations (Sutphin *et al.*, 2007). Gene expression for these cell lines was measured using the Gene Logic Inc. U95 array and Affymetrix U133 FLCN expression values were extracted. The results of this are included in appendix 1.

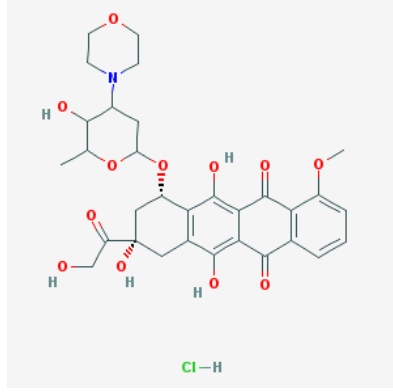
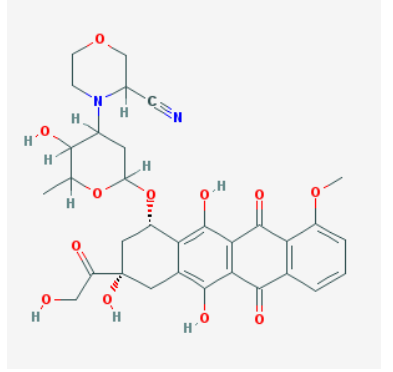
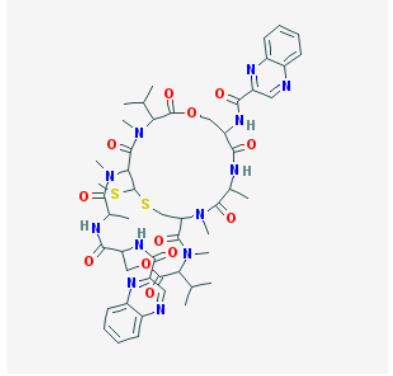
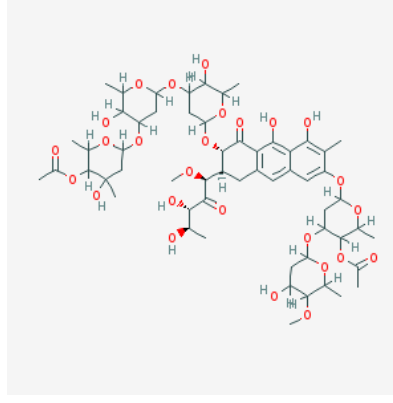
The design for the drug sensitivity seed pattern was developed by Xiaohong Lu and Wenbin Wei and was similar to protocols previously used for identifying anticancer agents that preferentially affect VHL-deficient cell lines by Sutphin *et al.* (2007). The drug sensitivity seed pattern was compared with individual compounds in the DTP database using the COMPARE algorithm (Lu *et al.*, 2011).

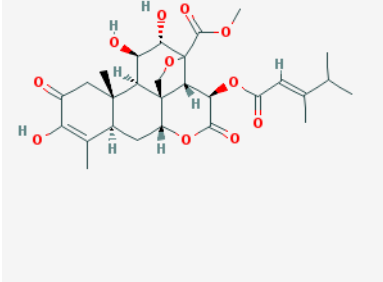
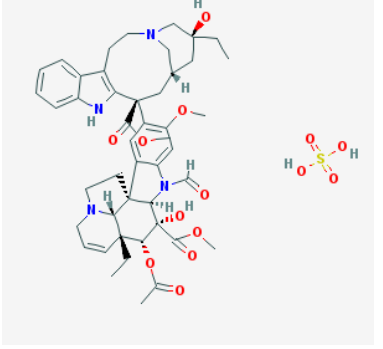
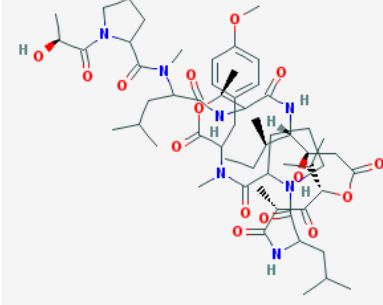
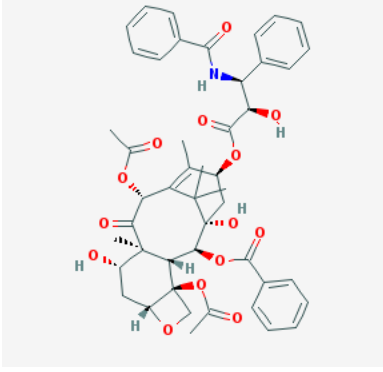
To view the correlation of FLCN expression levels to drug sensitivity, FLCN expression of the cell lines was determined from publicly available data available through the

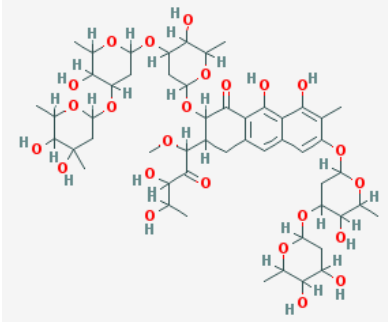
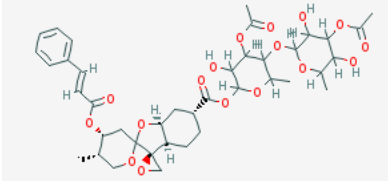
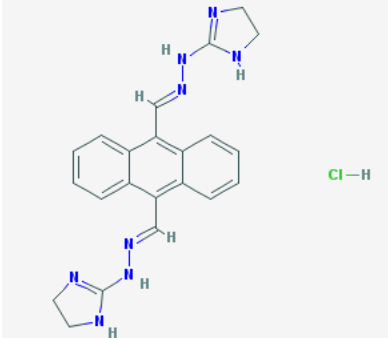
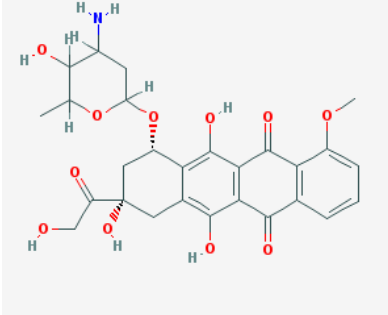
Developmental Therapeutics Program. This was used to sort the NCI60 cells into three groups: those with low FLCN expression, mid FLCN expression, and high FLCN expression. A seed pattern, or theoretical drug activity pattern, that would be representative of the target, i.e. cells with low or no functional FLCN protein, was built from the FLCN expression groupings. The cells known to have high levels of active FLCN were set to have low sensitivity to the compound to be selected, and cells known to have very low levels of active FLCN or none at all were set to have high sensitivity to the compound to be selected. Mid-range expressers were of neutral sensitivity.

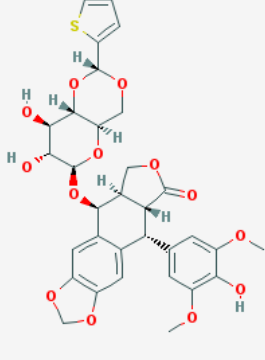
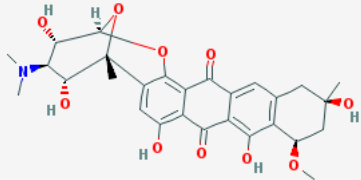
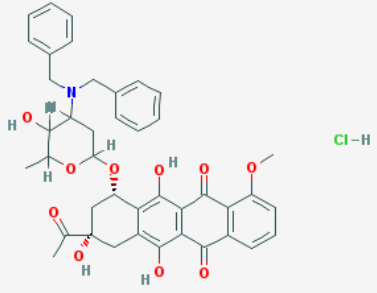
A pattern recognition algorithm known as the COMPARE algorithm was used to make a comparison of the seed pattern of each of the compounds in the DTP's Standard Agent Database, at the NCI, individually. The program output was a list of 15 drugs which most closely matched the seed pattern of expected sensitivities in the system according to GI50 (the concentration of an agent which inhibits cell growth by 50%). The name, structure and selected information for these compounds can be seen in Table 9. More detailed information about each compound is included in the appendix. Additional compounds selected for their known therapeutic activity are also included in Table 9.

Table 9: List of compounds selected for further testing by the COMPARE algorithm.

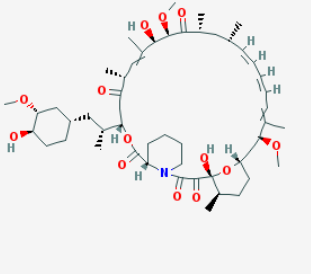
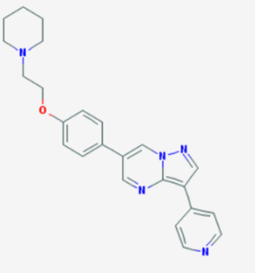
Compound Name	Structure	Further info
(NSC354646) Morpholino-ADR	 <p style="text-align: center;">Cl-H</p>	
(NSC357704) cyanomorpholino-ADR		
(NSC13502) Echinomycin		Binds to DNA and inhibits RNA synthesis
(NSC58514) ChromomycinA3		Used as a fluorescent stain of DNA and as an antineoplastic agent.

<p>(NSC165563) Bruceantin</p>		
<p>(NSC67574) Vincristine sulfate</p>		<p>Antitumour alkaloid isolated from <i>Vinca Rosea</i>.</p>
<p>(NSC325319) Didemnin B</p>		
<p>(NSC125973) Taxol or paclitaxel</p>		<p>A cyclodecane isolated from the bark of the Pacific Yew tree, <i>taxus brevifolia</i>. It stabilizes microtubules in their polymerized form leading to cell death.</p>

<p>(NSC24559) Mithramycin</p>		<p>Inhibits RNA and protein synthesis by adhering to DNA.</p>
<p>(NSC266492) Phyllanthoside</p>		
<p>(NSC337766) Bisantrene hydrochloride</p>	 <p style="text-align: right;">Cl-H</p>	
<p>(NSC123127) Doxorubicin hydrochloride (also known as adriamycin)</p>	 <p style="text-align: center;">Cl-H</p>	<p>Exerts its antitumour effects by interference with the synthesis and function of DNA.</p>

<p>(NSC 122819) VM-26 Teniposide</p>	 <p>The structure shows a complex molecule with a central chromone core. It features a 2,3-dihydro-2H-benzofuran ring system fused to the chromone. A thienyl group is attached to the 2-position of the benzofuran. The chromone core has a 4-methoxyphenyl group at the 6-position and a 3,4-dimethoxyphenyl group at the 7-position. The 4-position of the chromone is substituted with a 2,3-dihydro-2H-benzofuran ring, which is further substituted with a thienyl group.</p>	<p>Has antitumour activity and forms a complex with topoisomerase II and DNA and thereby inhibits DNA synthesis as this complex induces breaks in double stranded DNA and prevents repair by topoisomerase. Accumulated breaks in DNA stop cells from beginning the mitotic phase of the cell cycle, and lead to cell death. Teniposide acts primarily in the G2 and S phases of the cycle.</p>
<p>(NSC269148) Menogaril</p>	 <p>The structure shows a complex molecule with a central chromone core. It features a 2,3-dihydro-2H-benzofuran ring system fused to the chromone. A 2,3-dihydro-2H-benzofuran ring is attached to the 2-position of the benzofuran. The chromone core has a 4-methoxyphenyl group at the 6-position and a 3,4-dimethoxyphenyl group at the 7-position. The 4-position of the chromone is substituted with a 2,3-dihydro-2H-benzofuran ring, which is further substituted with a thienyl group.</p>	<p>Displays a range of antineoplastic activity against a variety of tumours.</p>
<p>(NSC268242), N,N- dibenzyl-daunomycin</p>	 <p>The structure shows a complex molecule with a central chromone core. It features a 2,3-dihydro-2H-benzofuran ring system fused to the chromone. A 2,3-dihydro-2H-benzofuran ring is attached to the 2-position of the benzofuran. The chromone core has a 4-methoxyphenyl group at the 6-position and a 3,4-dimethoxyphenyl group at the 7-position. The 4-position of the chromone is substituted with a 2,3-dihydro-2H-benzofuran ring, which is further substituted with a thienyl group. The structure is shown as a hydrochloride salt, with a Cl-H label.</p>	

Compounds selected separately from the compare algorithm for testing because of their known actions.

<p>(NSC22608) Rapamycin</p>		<p>Selected for its mTOR pathway activity.</p> <p>Selectively blocks the transcriptional activation of cytokines thus inhibiting cytokine production. It is bioactive only when bound to immunophilins.</p>
<p>Compound C</p>		<p>Compound c was selected for its properties as an AMPK inhibitor</p> <p>It has also been shown to promote neural differentiation from human pluripotent stem cell (hPSC) line and to inhibit BMP signals necessary for embryogenesis.</p>

Information on structure and identification of compounds tested obtained from <http://pubchem.ncbi.nlm.nih.gov/> (19/07/2013)

As a proof of concept that the COMPARE algorithm could effectively select active drugs that could differentiate between FLCN⁺ and FLCN⁻ cells, six of those highlighted as possible effective agents and that were easily available were screened. The compounds tested were Echinomycin, Chromomycin A3, Vincristine sulfate, DidemninB, doxorubicin and N,N-dibenzyl-daunomycin.

The initial group of compounds was screened using the SRB growth inhibition assay in SKRC47 cells. The SRB assay was chosen as it was known to be a robust method for determination of cytotoxicity (Skennan *et al.*, 1990). The SRB stains the fixed cells in the plate and excess dye is removed. The dye that is then present in each well is proportional to the cells present in each well. The SRB is then re-dissolved and the absorbance measured in a

plate reader to establish the amount of dye and there for the amount of cell matter present and, from that, the amount of proliferation that has occurred.

The SKRC47 cell line was chosen as it was an established cell line already characterized and in use in the lab for which growth conditions were known. SKRC47 cells are human sporadic renal cell carcinoma-derived FLCN positive cells. To give differential FLCN expression, cells were treated with FLCN siRNA, to lower FLCN protein expression (giving up to a 90% possible reduction according to the data sheet of the transaction reagent). Others were treated with luciferase SiRNA as a control. GI50 values for the compounds were calculated in cells. In both conditions the GI50 values were compared to allow any FLCN-associated changes in sensitivity to these drugs to be identified.

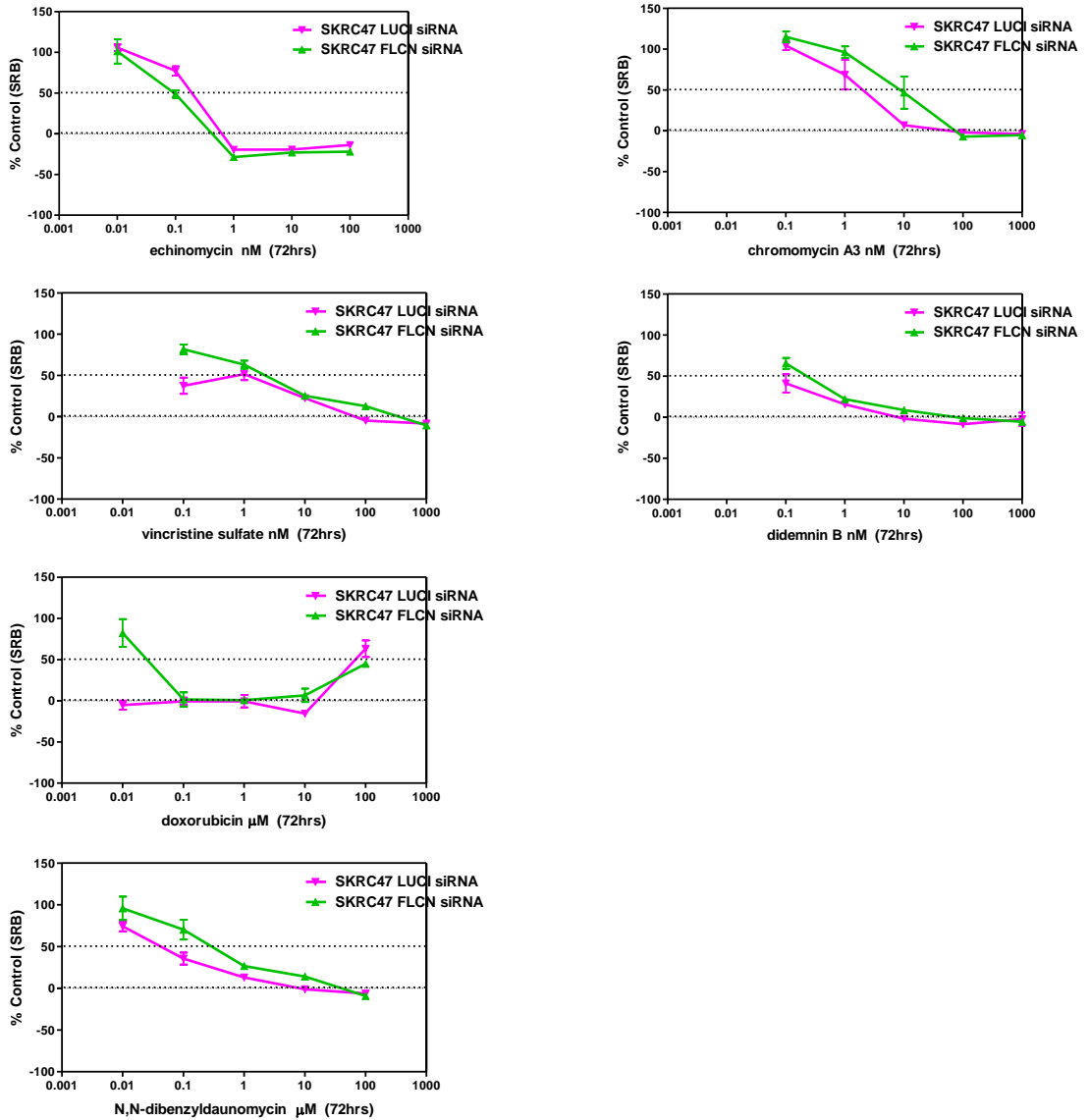


Fig 12: Individual dose response curves for the 6 compounds illustrating the dose dependant inhibition of growth.

The estimated concentration of drug required to give a 50% inhibition of growth (GI50) was calculated from these graphs plotting the observed inhibitions for the doses given and calculating the gradient of the trend line and the value of x (concentration) at which y+50% inhibition (values were calculated in Graph Pad PRISM™ by fitting a sigmoidal

concentration/inhibition curve to the data obtained from the SRB assays using non-linear least square regression).

Table 10: GI₅₀ for luciferase and FLCN siRNA treated SKRC47 cells.

Table of drug concentrations calculated to give a 50% inhibition of growth for cells with normal and reduced levels of FLCN protein, Mean \pm SD shown.

SKRC 47	mean GI50 nM luci SiRNA	SD	meanGI50 nM FLCN SiRNA	SD
Echinomycin	2.3	2.3	2.05675	2.39461
Chromomycin A3	14.0	18.3	7.06925	3.00931
Vincristine sulfate	9.0	4.4	8.69125	6.97942
DidemninB B	6.9	7.6	4.14	2.50397
Doxorubicin	100.0	0.2	186	0.07095
N,N-dibenzyl-daunomycin	2100.0	2.8	700	0.34699

The data (Fig 12) shows small differences in response to the drugs with regard to FLCN expression. These could be indicative of the possibility to identify chemotherapeutic agents with the ability to differentiate between FLCN⁺ and FLCN⁻ cells by this method. The data (Table 10) indicate that all drugs tested, except doxorubicin, have higher GI₅₀ values in cells with normal FLCN expression compared to the FLCN knockdowns (although in most cases this is not statistically significant). The biggest alteration in response due to FLCN knock down was a threefold change sensitivity to N,N-dibenzyl-daunomycin (experimental planning and cell treatment were performed with the kind help of Xiaohong Lu). Building on this evidence, we obtained a greater array of compounds for study from Table 9 as highlighted by the COMPARE algorithm.

The range of concentrations tested was considered with regard to these experiments and lower concentrations of compound were used for some drugs in other experiments.

Drug-induced cytotoxicity in CaKi cells

In order to establish the best assay system for the identification compounds with differential sensitivity with regard to folliculin status, 8 compounds (see table 11) were tested by SRB assay in a CaKi-1 Cell system, both with and without knockdown of FLCN Protein by siRNA treatment for comparison. The CaKi-1 is a well characterized adherent human epithelial kidney clear cell carcinoma cell line originated from a 49-year-old Caucasian male with a metastatic site in the skin and established in 1971 (Fogh and Trempe, 1971). CaKi-1s are aneuploid cells, with triploid range chromosome counts, but an absent Y chromosome. All normal autosomes except chromosome N9 and N19 are represented, often by two or three copies. Normal chromosome N5 is and chromosomes N10 and N16 may be over-represented with when compared to the copy number of other normal chromosomes. Features of CAK11 cell ultrastructural include many microvilli, few filaments, many small mitochondria, well developed Golgi and ER, many lipid droplets and multilaminar bodies, secondary lysosomes, and no virus particles. (<http://www.lgcstandards-atcc.org> 17/08/2013) Graphs of the comparative dose response curves were generated as before in Luciferase and FLCN siRNA treated CaKi-1 cells, after 72 hours of treatment, for the drugs from the mean \pm SD of 5 replicates from the same day and the GI₅₀ values generated. (Planning and cell treatment with the kind help of Xiaohong Lu)

Table 11: GI₅₀ values for compounds in CaKi-1 Cells with and without FLCN siRNA knock down.

CAKI1	GI50 (LUCI siRNA)	GI50 (FLCN siRNA)
doxorubicin (Adriamycin)	0.560 μ M	0.65 μ M
N,N-dibenzyl-daunomycin	8.1 μ M	8.8 μ M
mithramycin	422.0 nM	563.0 nM
phyllanthoside	425.0 nM	771.0 nM
chromomycin A3	44.0 nM	42.7 nM
vincristine sulfate	10.4 nM	65.4 nM
didemnin B	22.8 nM	49.8 nM
echinomycin	5.7 nM	5.9 nM

Fig 12 illustrates the way cells with different FLCN protein levels react to different chemicals. The GI₅₀ values for the compounds are different in these cells compared to the SKRC47 cells (Table 11) and the trend for those compounds that do show a difference appears to be one of decreased sensitivity (higher GI₅₀) in cells with FLCN knockdown (shown in table3). The conclusions that can be drawn from this data are limited due to the incomplete nature of siRNA knock down (INTERFERin® can provide around 90% silencing efficiency at 1 nM siRNA according to the data sheet [<http://www.polyplus-transfection.com>]29/08/2013). Its inclusion adds useful insight as furthers investigation into the diversity within kidney cancers as a group and their reactions to treatment.

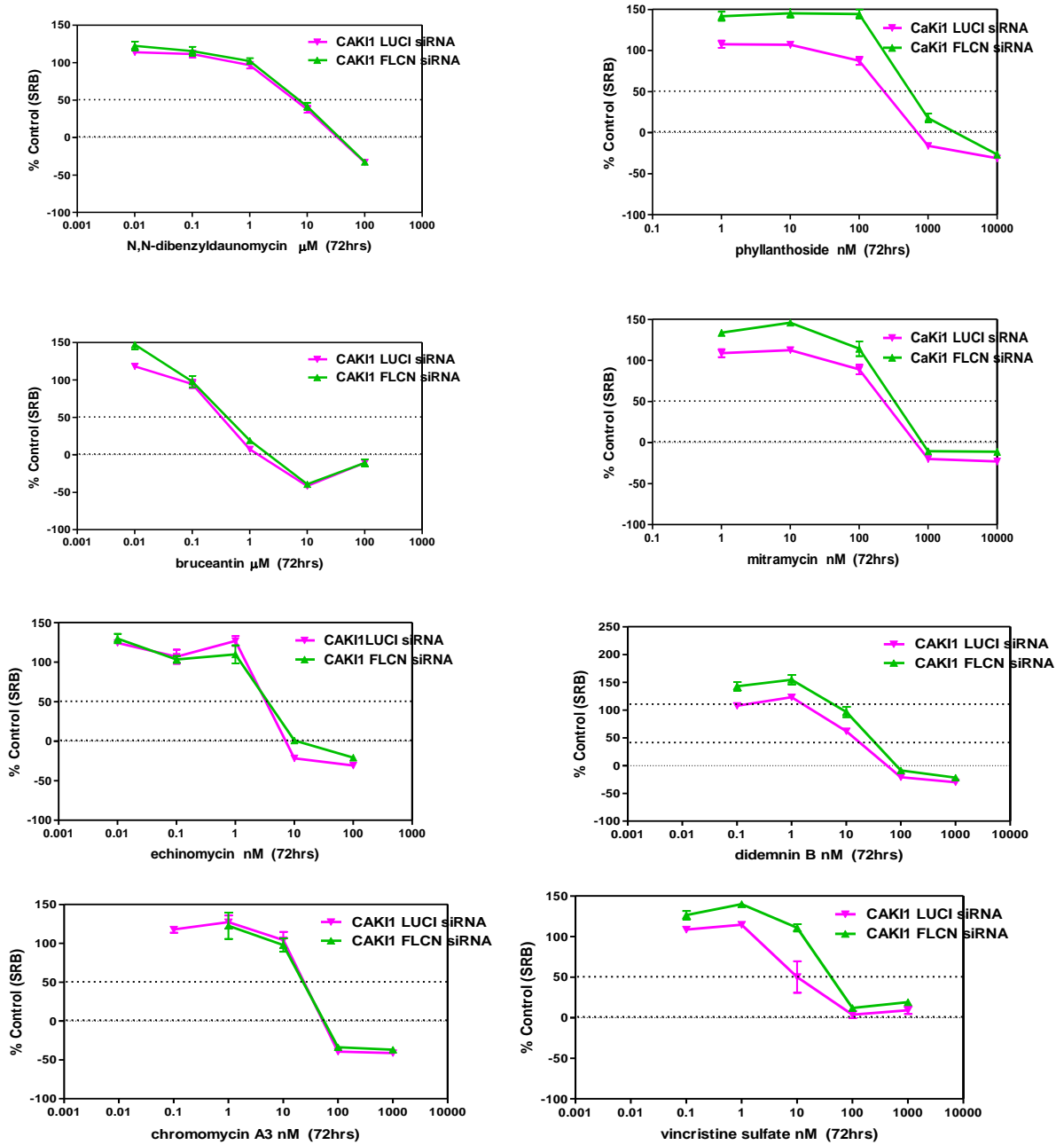


Fig 12: Graphs and table showing the comparative dose response curves for a selection of compounds in CaKi- 1 Cells treated with luciferase SiRNA (FLCN+ve cells) and CaKi1 cells treated with FLCN SiRNA to knock down the expression of the protein.

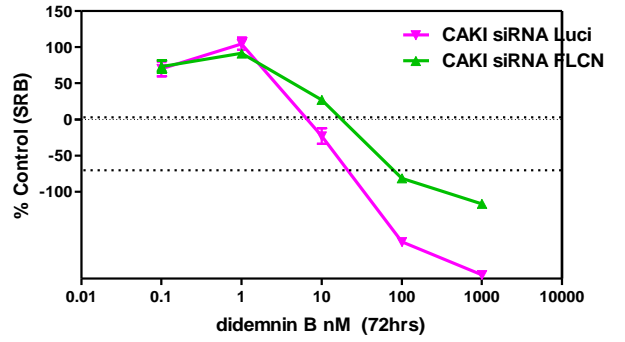
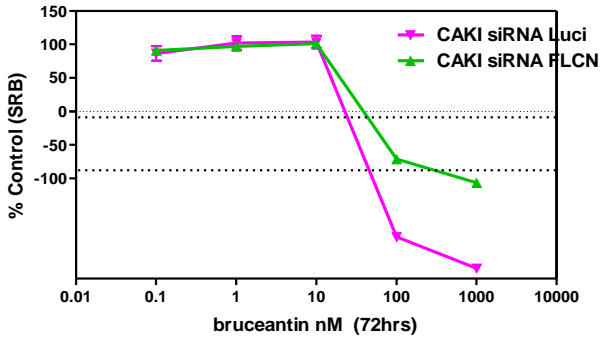
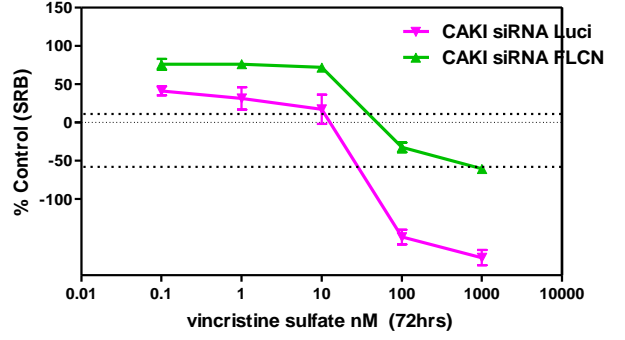
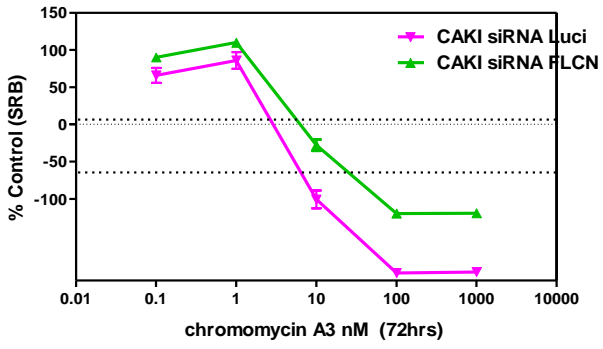
Establishing GI_{50} values for 16 compounds in CaKi-2 cells with and without FLCN siRNA knock down.

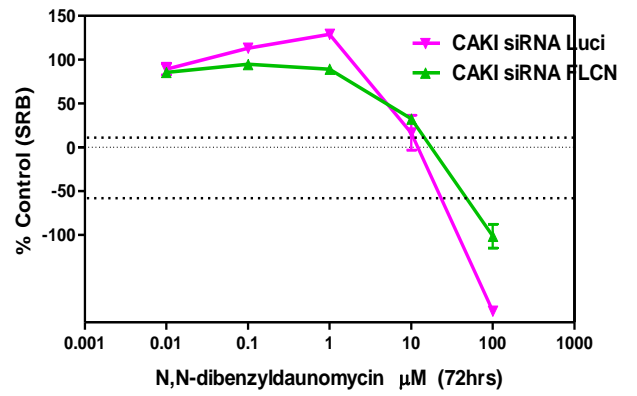
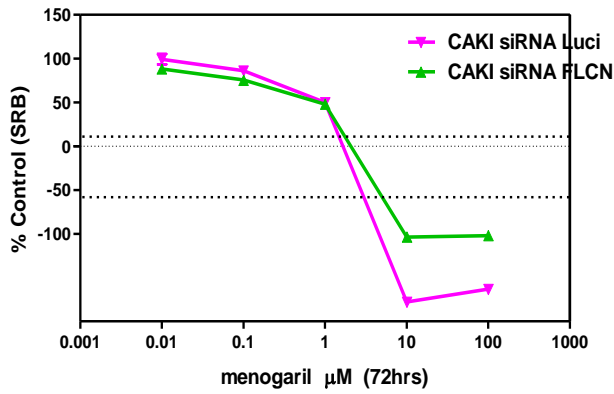
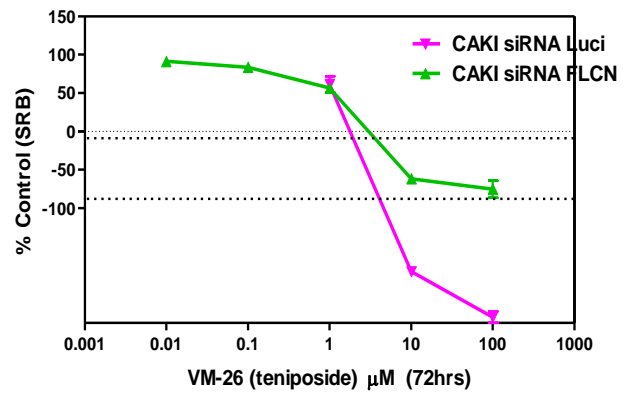
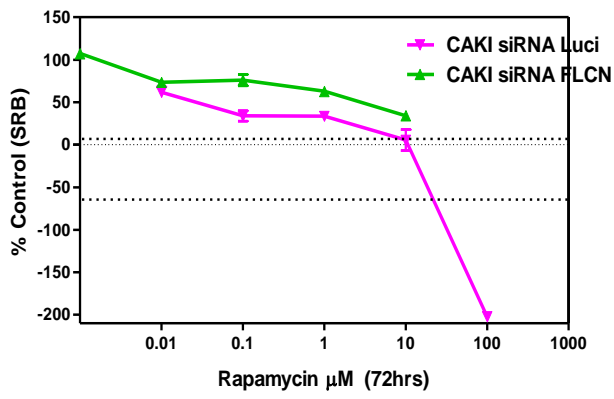
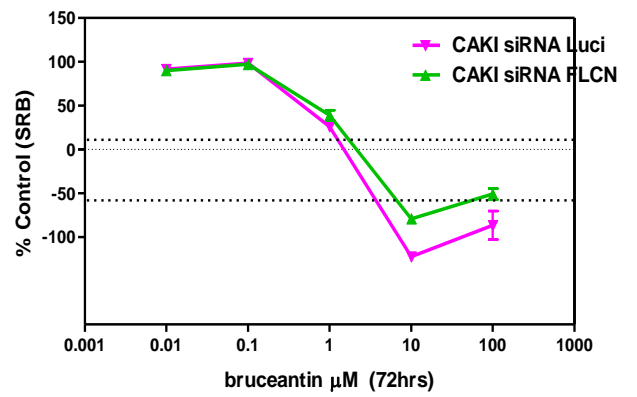
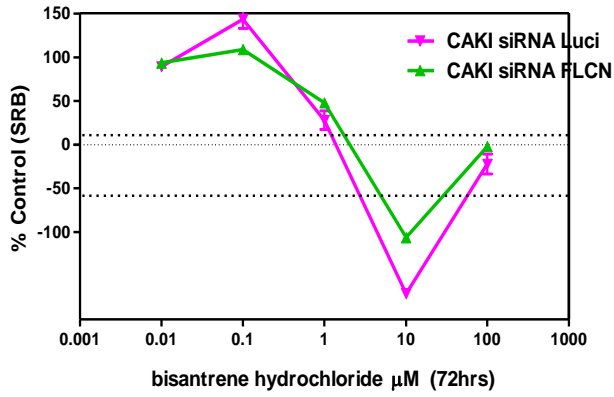
Once all compounds from the COMPARE list were obtained, a larger experiment was carried out for the 16 compounds listed in Table 12 below (with the GI_{50} s obtained) in CaKi-2 cells both with and without knockdown of FLCN Protein by siRNA treatment. It was decided to use a different cell line for this experiment. It was theorized that using a different line may provide a better system and would at least increase the breadth of data for the compounds already tested. CaKi-2 cells were chosen as they were a long established and well characterized line of kidney clear cell carcinoma cells already tested in the lab (unpublished data). Caki-2 cells are derived from a sporadic kidney tumour in a 69-year-old male Caucasian. Levels of growth inhibition induced by various concentrations of agents were measured in both FLCN states, using the sulforhodamine B (SRB) assay, after 72 hours of treatment as before, and dose response curves and GI_{50} values were generated from the mean of 5 replicates on the same day. (Planning and cell treatment with the kind help of Xiaohong Lu)

The results are shown in table 12 and Fig 13 below.

Table 12: Table of GI50 values for 16 compounds in CaKi-2 cells with and without FLCN siRNA knock-down.

CAKI-2	IC₅₀ siRNA Luci	IC₅₀ siRNA FLCN
bisantrene hydrochloride	0.7 μ M	0.97 μ M
doxorubicin	0.70 μ M	0.82 μ M
Rapamycin	0.05 μ M	5.1 μ M
VM-26 (teniposide)	1.4 μ M	1.5 μ M
Menogaril	1.0 μ M	1.0 μ M
N,N-dibenzyl-daunomycin	7.3 μ M	7.2 μ M
paclitaxel (Taxol)	46.5nM	22.1 nM
Mithramycin	202.7nM	93.2 nM
phyllanthoside	223.8nM	268.1 nM
chromomycin A3	2.5nM	3.9 nM
Bruceantin	26.5nM	36.7 nM
vincristine sulfate	6.1nM	28.6 nM
didemnin B	4.1 nM	6.8 nM
morpholino-ADR	21.1 nM	35.4 nM
cyanomorpholino-ADR	0.5 nM	0.8 nM
Echinomycin	3.0 nM	5.7 nM





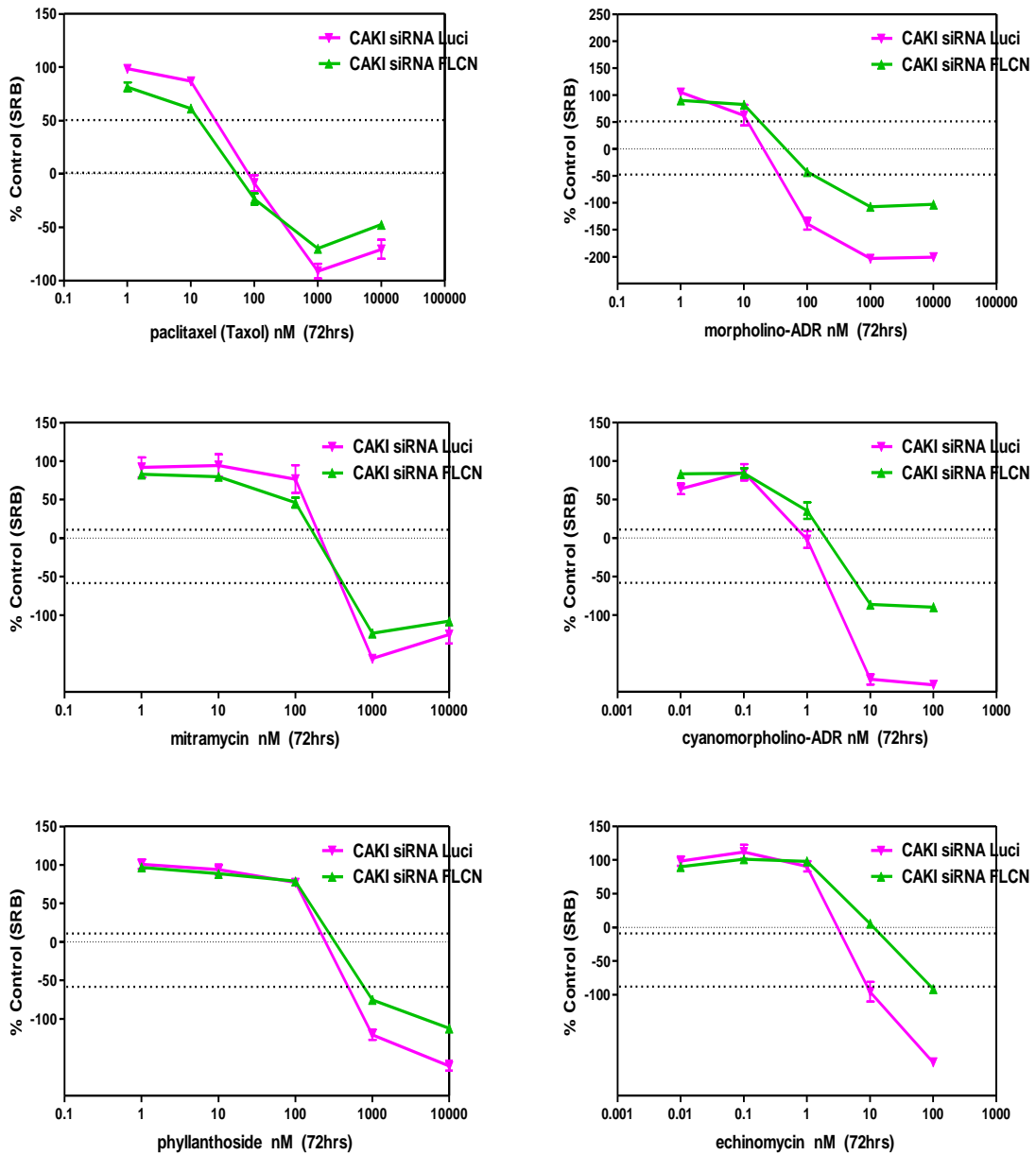


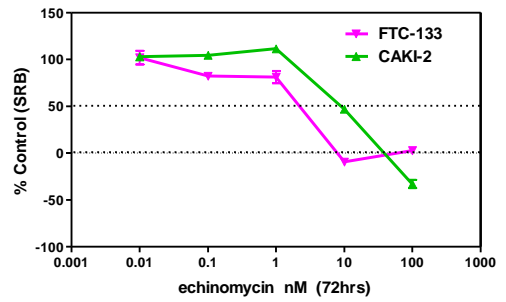
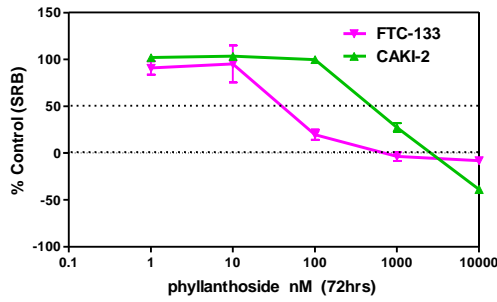
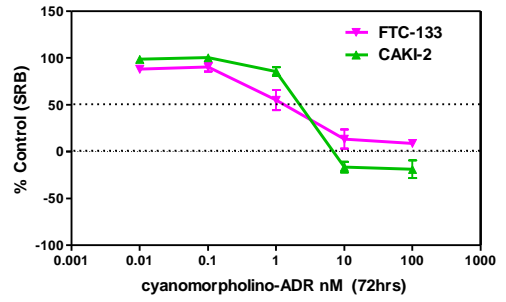
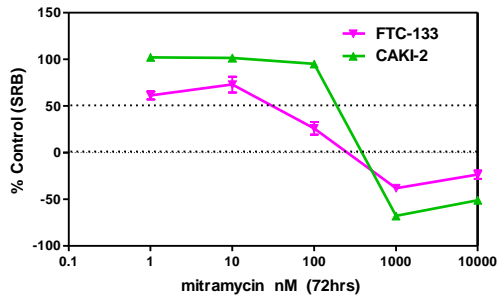
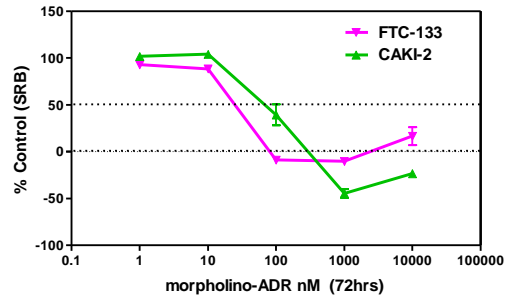
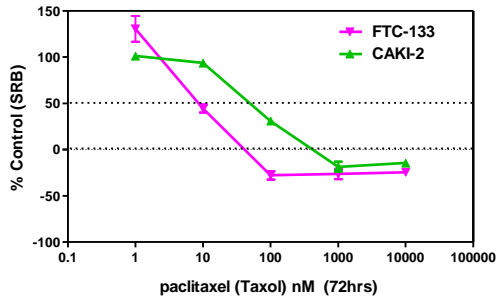
Fig 13: Graphs showing the comparative dose response curves for a selection of compounds in CaKi- 2 Cells treated with luciferase SiRNA (FLCN+ve cells) and CaKi2 cells treated with FLCN SiRNA.

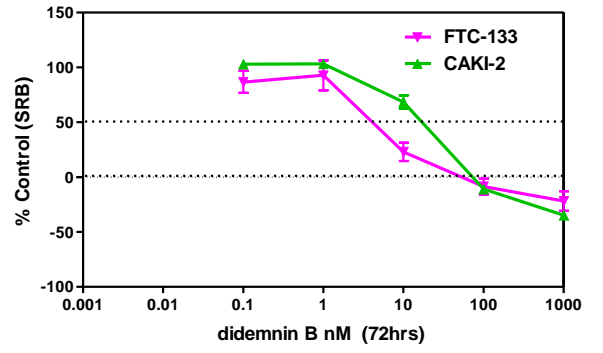
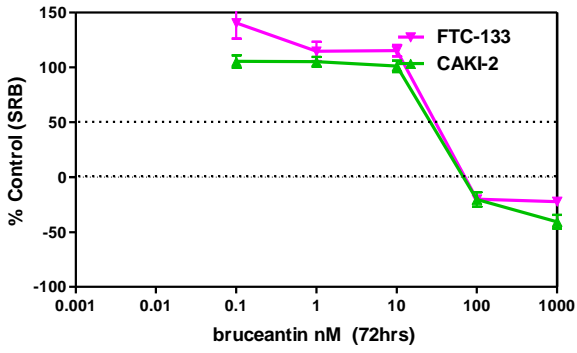
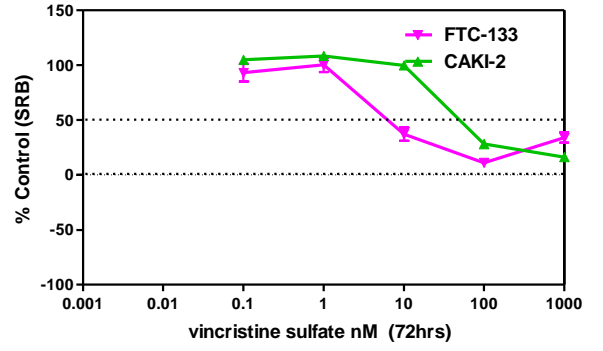
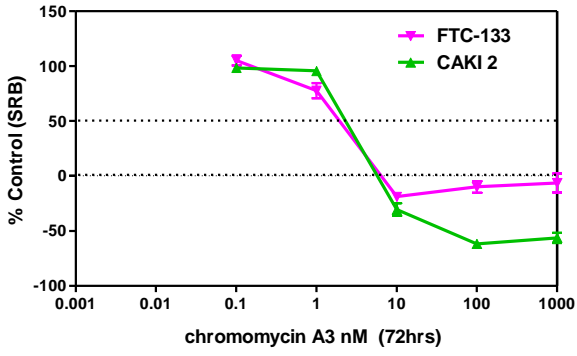
Fig 13 compares the response curves for a selection of compounds with CaKi-2 Cells treated with luciferase SiRNA (FLCN+ve cells) and CaKi2 cells treated with FLCN SiRNA. In

these cells, there was no consistent response to siRNA FLCN knockdown on sensitivity to the different agents. For many of the compounds the results seem to be showing greater sensitivity in the Caki-2 cells with no reduction in FLCN level. This is not what we would expect from the predictions of the COMPARE algorithm. However, it is worth noting that Mithramycin and Taxol still show the expected reduction in GI_{50} in FLCN-reduced cells.

Knockdown of FLCN expression by siRNA in sporadic RCC with wild-type FLCN was incomplete (Lu *et al.* 2011) and so a more suitable model might be to study paired cells in which there was no wild-type FLCN expression in one of the pair. Hence comparisons in a stable cell system would seem to offer the best opportunity to obtain suitable results on which to base sound judgments on the suitability of the drugs as possible treatments for BHD tumours. In order to address this issue, a stable cell system was set up where FLCN negative cell line was identified and the relevant cells (thyroid metastasis FTC133 cells) were obtained. The majority of the final full group of compounds selected after the use of the COMPARE algorithm (listed in Table 1 with the GI_{50} s obtained) was screened using the SRB growth inhibition assay in CaKi- 2 cells (FLCN positive kidney cancer cells described above) and FTC133 cells (FLCN negative thyroid metastasis cells) establishing their comparative sensitivities to 15 drugs selected from the COMPARE analysis by Xiaohong Lu. The levels of growth inhibition induced by various concentrations of agents were measured, using the sulforhodamine B (SRB) assay, after 72 hours of treatment with no siRNA treatments and the GI_{50} values calculated in the usual way. Graphs of the comparative dose response curves for the selection of compounds in this model showing the mean \pm SD of 5 replicates done on the same day are below in Fig 14.

(Planning and cell treatment with the kind help of Xiaohong Lu)





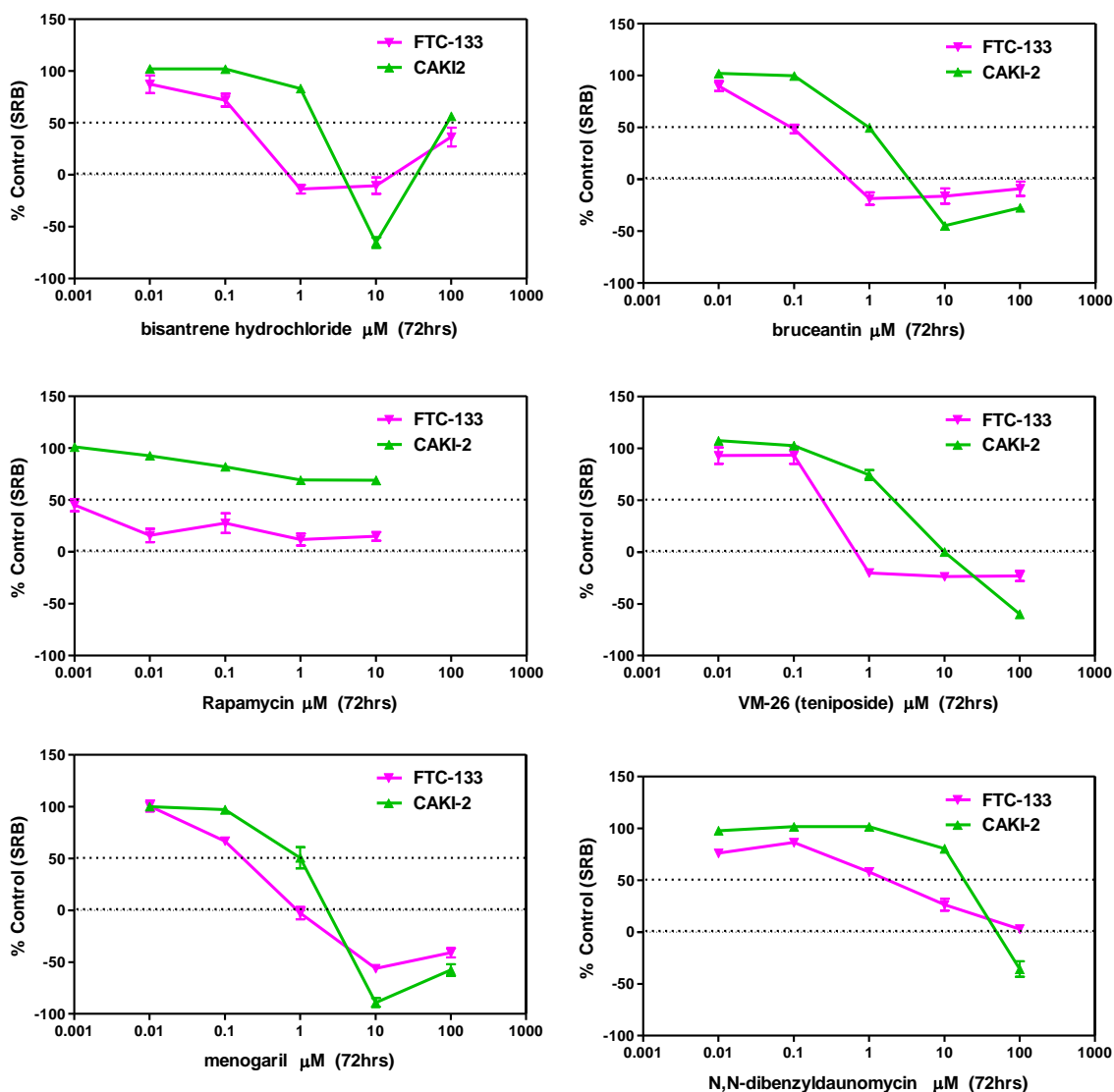


Fig 14: Graphs showing the comparative dose response curves for a selection of compounds in CaKi-2 Cells FLCN+ve and FTC133 FLCN-ve cells.

The promising trend for lower GI_{50} values in FLCN negative cells does seem to be present for the majority of the compounds screened in this experiment, most notably in the case of mithramycin- and vincristine-treated cells. This system appeared to give a good indication for the suitability of the COMPARE algorithm for choosing prospective drugs and the possibility

of identifying a good candidate compound from this selection for further study but it was decided that these cell lines were not strictly comparable due to the differing nature of the cells in many aspects other than FLCN status and that this system was unsuitable for drawing robust conclusions with regard to the effects of FLCN. (Planning and cell treatment with the kind help of Xiaohong Lu)

While not strictly comparable due to the differing nature of the cells and therefore unsuitable for drawing any strong conclusions, I include this experiment as a further investigation and illustration of the way different cells react to different chemicals. The FTC133 cells seem to show a trend to greater sensitivity to the majority of compounds in this experiment seen from comparison of the GI_{50} values to those of the CAKI cells. This can be clearly seen in Table 13 below. This could be due to many differences in the cells as they have different genetic backgrounds and derive from different tissues (Kidney and thyroid).

Table 13; GI₅₀ values for compounds in CaKi-2 Cells and FTC 133 cells taken from the mean of 5 replicates on the same day.

72 hour treatment	GI₅₀ (CAKI2)	GI₅₀ (FTC133)
bisantrene hydrochloride	3.01 μ M	0.44 μ M
doxorubicin	1.004 μ M	0.10 μ M
Rapamycin	>10 μ M	0.0009 μ M
VM-26 (teniposide)	3.95 μ M	0.42 μ M
Menogaril	1.04 μ M	0.49 μ M
N,N-dibenzyl-daunomycin	33.5456 μ M	3.3 μ M
(carboxyphthalato)platinum	>100 μ M	>100 μ M
paclitaxel	72.92575 nM	9.0 nM
mithramycin	348.8 nM	68.1 nM
phyllanthoside	717.4 nM	63.9 nM
chromomycin A3	3.9 nM	4.3 nM
bruceantin	47.9 nM	53.4 nM
vincristine sulfate	72.6 nM	8.0 nM
didemnin B	30.9 nM	6.6 nM
morpholino-ADR	83.2 nM	46.4 nM
cyanomorpholino-ADR	4.1 nM	2.1 nM
echinomycin	9.6 nM	4.1 nM

Compound Screen in FLCN negative UOK-257 Cells and FLCN+ UOK257-2 cells.

Addressing the need for a robust, stable isogenic FLCN positive and negative pair of cell lines to provide a system by which to screen the drugs was a key focus of our initial investigation. UOK-257 cells were identified from the literature (Yang *et al.* 2008, Hong *et al.* 2010) and obtained to form the basis of the main drug screen experiment.

UOK-257 is the only RCC cell line available that has been derived from a BHD patient with a germ line *FLCN* mutation (a frame shift c.1285dupC). It is predicted to lead to premature protein termination, without nonsense-mediated decay (Yang *et al.*, 2008). Growth inhibition assays were performed in both UOK-257 and UOK-257-2 (Hong *et al.* 2010) (an isogenic FLCN positive stably-transfected cell line) in order to establish their comparative sensitivities to the 15 drugs selected from the COMPARE analysis by Xiaohong Lu. The levels of growth inhibition induced by various concentrations of agents were measured, using the sulphorhodamine B (SRB) assay, after 72 hours of treatment as in the other systems and the dose response curves and the GI₅₀ values calculated. The ratio of each UOK-257 GI₅₀ value to the corresponding FLCN-expressing GI₅₀ value was then calculated as it mirrors the difference in sensitivities to the chemical shown by the two cell lines and therefore the selectivity of the drug. These sensitivities are compared in Fig 15 and more detail about the data is shown in Table 14. GI₅₀ values were calculated by fitting a sigmoidal concentration/inhibition curve to the data obtained from the SRB assays using non-linear least square regression (Graph Pad PRISMTM). Mean \pm SE values are shown in Table 14 with the number of the experiments given in brackets. Experiments and analysis were completed with the kind help of Xiaohong Lu who designed the experiment and seeded the plates.

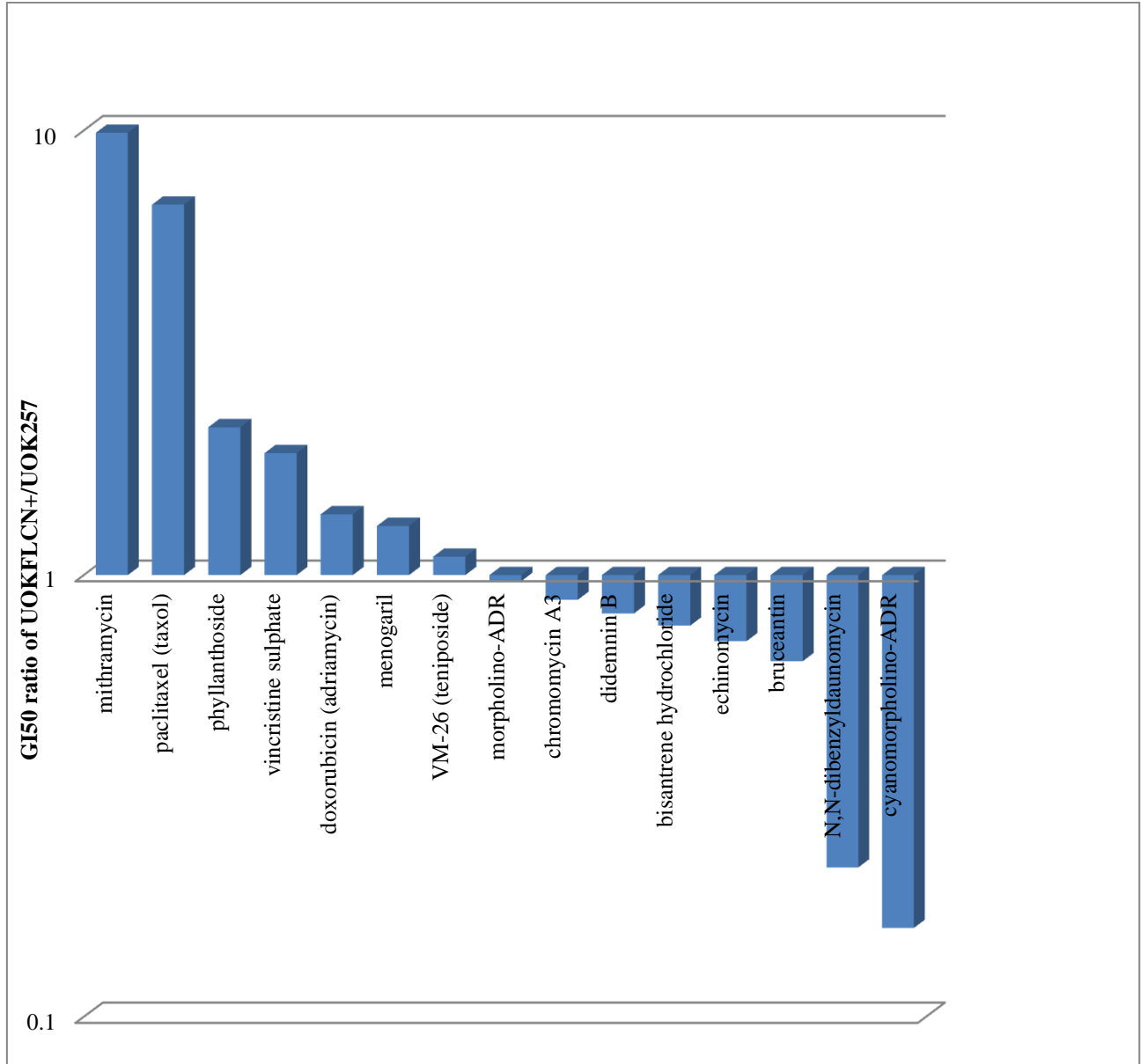


Fig 15: Screen in UOK-257 cells and UOK FLCN+ cells

Table 14: Compound screen in UOK-257 cells and UOK FLCN+ cells

Compounds	GI₅₀ nM in UOK-257	GI₅₀ nM in UOK-FLCN⁺	GI₅₀ Ratio Of UOK-FLCN⁺/ UOK-257
Mithramycin	64.2 ± 7.9 (3)	634 ± 148 (4)	9.88
paclitaxel	75.5 ± 9.2 (5)	514 ± 86 (3)	6.81
Phyllanthoside	199 ± 79 (5)	427 ± 97 (4)	2.15
Vincristine sulphate	30.1 ± 10.3 (5)	56.4 ± 17.5 (5)	1.88
doxorubicin	423 ± 54 (3)	581 ± 109 (4)	1.37
Menogaril	588 ± 57 (4)	757 ± 117 (4)	1.29
VM-26 (Teniposide)	773 ± 162 (3)	849 ± 358 (3)	1.10
Morpholino-ADR	0.45 ± 0.03 (3)	0.44 ± 0.10 (3)	0.97
Chromomycin A3	37.4 ± 6.9 (3)	33.0 ± 5.7 (3)	0.88
DidemninB B	7.94 ± 1.66 (4)	6.53 ± 1.78 (4)	0.82
Bisantrene hydrochloride	1753 ± 288 (6)	1345 ± 602 (5)	0.77
Echinomycin	5.72 ± 0.22 (3)	4.03 ± 0.89 (3)	0.71
Bruceantin	68.4 ± 14.9 (3)	43.6 ± 5.1 (3)	0.64
N,N-dibenzyl-daunomycin	5739 ± 918 (4)	1273 ± 549 (4)	0.22
Cyanomorpholino-ADR	3.79 ± 0.39 (3)	0.62 ± 0.16 (3)	0.16

In Table 14 eight chemicals have a ratio greater than 1 showing that these drugs are selective for the FLCN negative cell state, having a greater inhibitory affect in UOK-257 cells than in UOK-257-FLCN+ cells. The most selective compound was Mithramycin, with an almost 10-fold difference in the GI₅₀ values of UOK-257 cells (64.2 ± 7.9 nM; n=3) and FLCN⁺ cells (634.3 ± 147.9 nM; n=4). Therefore, this compound was selected for further study.

There were seven compounds in Table 14 with a ratio below one showing that the UOK-257 cells were less sensitive to these chemicals than the cells that had FLCN expression restored and that the FLCN mutant state was being selected for. Cyanomorpholino-ADR showed a 6-

fold difference in the GI₅₀ values between FLCN⁺ cells (0.62 ± 0.16 nM; n=3) and UOK257-FLCN⁻ cells (3.79 ± 0.39 nM; n=3) giving the lowest GI₅₀ ratio.

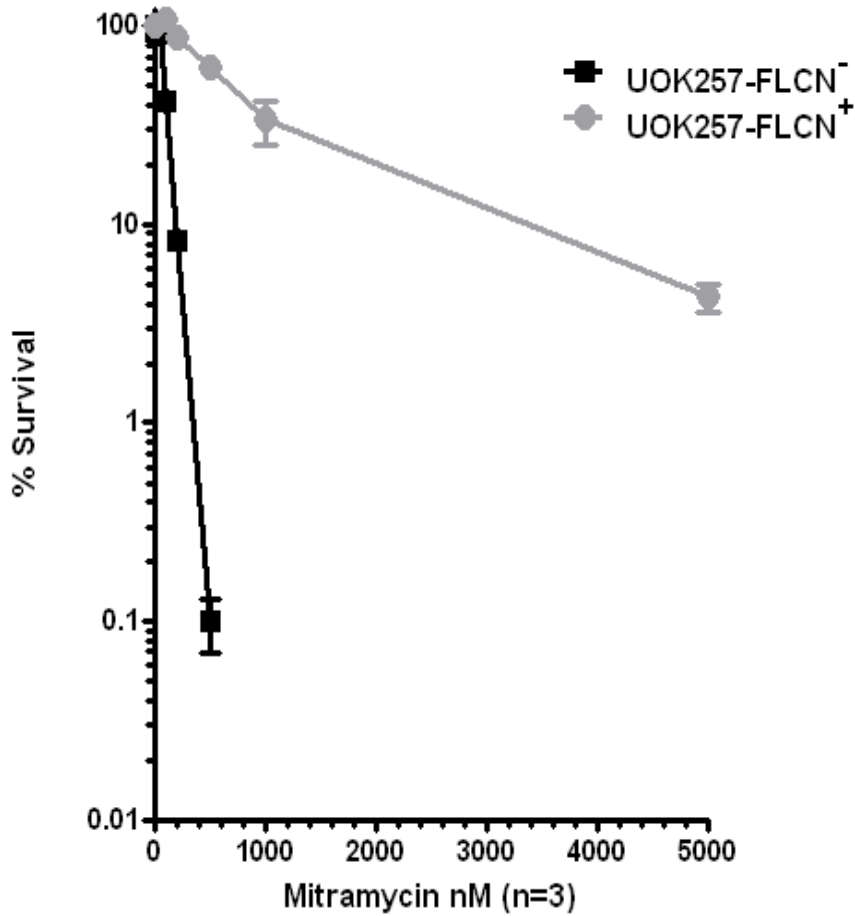
The data showed considerable differences in the selectivity of the chemicals tested for cells with and without FLCN expression, although the compounds were all selected by the COMPARE algorithm using the same criteria.

The data suggest that loss of functional FLCN due to the mutation in UOK-257 cells may lead to a greater mithramycin sensitivity measured by these methods. The hypothesis that mithramycin preferentially cytotoxic to UOK-257 cells without FLCN expression and is less harmful to cells with normal FLCN expression fitted the data obtained.

Chapter 4: Results of Further Assessment of Mithramycin

Mithramycin-induced cytotoxicity in UOK257 cells and UOK257 cells with FLCN expression restored.

Clonogenic assays were carried out to further assess the efficacy of mithramycin with regard to possible clinical use in the future and examine whether differences in sensitivity to mithramycin between cells expressing FLCN and those not expressing it were reflected in differential effects in cell survival and ability to grow, divide and form colonies. After exposure to mithramycin at a range of concentrations for 72 hours, followed by the subsequent removal of the treatment, UOK257 and UOK257-FLCN⁺ cells were then incubated in drug-free medium after the removal of the compound for a further 10 – 15 days until colonies formed. Mithramycin-induced cytotoxicity was then measured by clonogenic cell survival as shown in Fig 16. (Planning and cell treatment with the kind help of Xiaohong Lu)



Survival %	100nM	200nM	500nM
UOK257-FLCN ⁻	42 ± 9 (12)	8 ± 2 (12)	0.1 ± 0.1 (11)
UOK257-FLCN ⁺	106 ± 11 (12)	87 ± 12 (12)	61 ± 17 (12)

Fig 16: Clonogenic assays measured mithramycin cytotoxicity in UOK-257FLCN⁺ cells and UOK-257. (Data obtained from 3 experiments and the range of values shown by Error bar). (Figure by Xiaohong Lu using my data. Reported in Lu et al., 2011)

At a concentration of 500 nM of mithramycin, more than 60% of the UOK-257-2-FLCN⁺ cells survived, while less than 0.1% UOK257-FLCN⁻ cells were able to form colonies. Fewer than 8% of cells were observed to be viable in FLCN negative UOK-257 cells, at a concentration of 200 nM, in comparison to UOK-257-FLCN⁺ cells in which a cell survival

rate of greater than 85% was observed. This is a 10-fold difference between two cell lines. At 5000 nM, the highest concentration examined, there were still more than 4% FLCN⁺ cells surviving and forming colonies.

The data suggest that loss of functional *FLCN* due to the mutation in UOK-257 cells may lead to a greater mithramycin sensitivity measured by these methods. The hypothesis that mithramycin is preferentially cytotoxic to UOK-257 cells without FLCN expression and is less harmful to cells with normal FLCN expression fitted the data obtained.

Such a strong cytotoxic effect and selectivity for the mutant cancer cells over the more normal surrounding cells provides a basis for further studies to investigate its possible clinical uses BHD associated kidney tumours.

Mithramycin-induced cytotoxicity in SKRC47 cells

To try and get a broader view of the usefulness of mithramycin as a putative chemotherapeutic agent for the treatment of kidney cancers, mithramycin was tested using the same protocol as previously discussed for the SRB growth inhibition assay in SKRC47 cells. As before the cells were treated with luciferase SiRNA or FLCN SiRNA to investigate any FLCN associated changes in this cell line sensitivity to mithramycin. (Planning and cell treatment with the kind help of Xiaohong Lu)

The data obtained for mithramycin shown in Fig 17 in comparison to that of phyllanthoside, showed no significant difference between the IG50 for the Luciferase SiRNA treated cells and the FLCN SiRNA treated cells. One possible explanation for this could be because the knock down was not sufficient to lead to a difference in sensitivity or because there is no FLCN-dependent difference in sensitivity to mithramycin in this particular cell line. The

phyllanthoside data appeared to show a trend to increased sensitivity in FLCN positive, Luciferase SiRNA Treated cells.

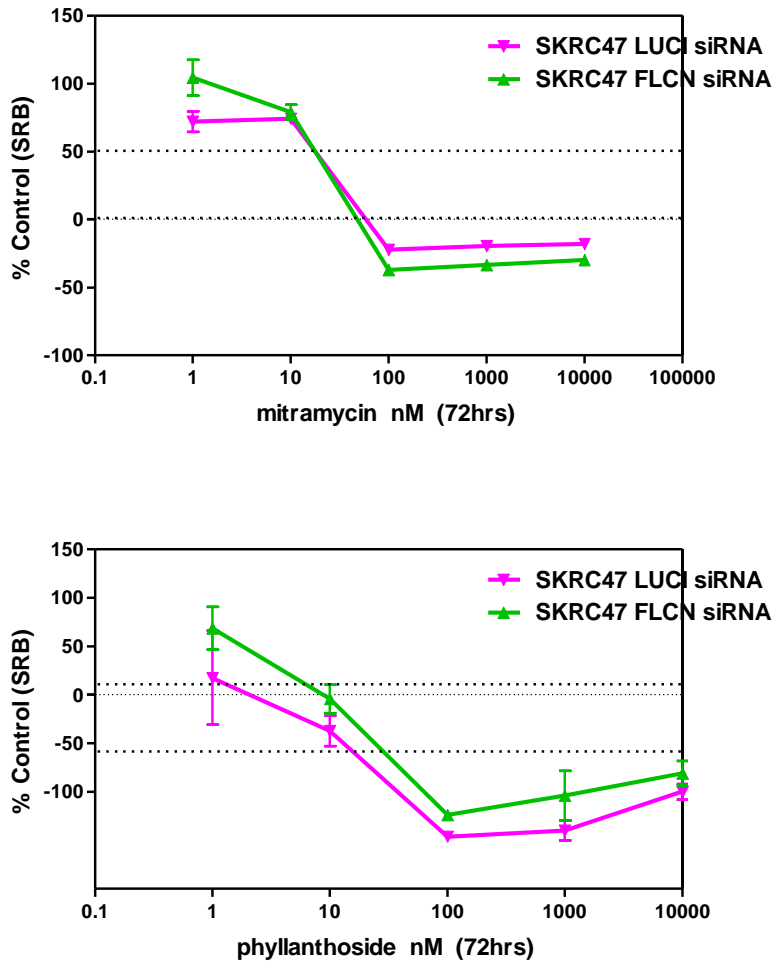


Fig 17: Mitramycin-induced cytotoxicity in SKRC47 cells

Mithramycin-sensitivity in FLCN Negative Cells originating from tumour of non-renal origin. Mithramycin-induced Cytotoxicity in FTC133 cells

To investigate mithramycin-sensitivity in FLCN negative cells originating from cancers of non renal origin, a human thyroid carcinoma line, FTC133, was used and SRB growth-inhibition assays were carried out. The FTC133 cell line is derived from a thyroid metastasis that is FLCN-negative. A FLCN-containing construct was introduced into the FTC133 parental cell line and stably transfected cells were selected. Mithramycin sensitivity was then examined in transfected cells with empty vector and low FLCN and high FLCN expression as well as in cells transfected with empty vector and therefore no FLCN expression. (with the kind help of Xiaohong Lu in planning and preparation) (Transfections were carried out by Laurence Seabra).

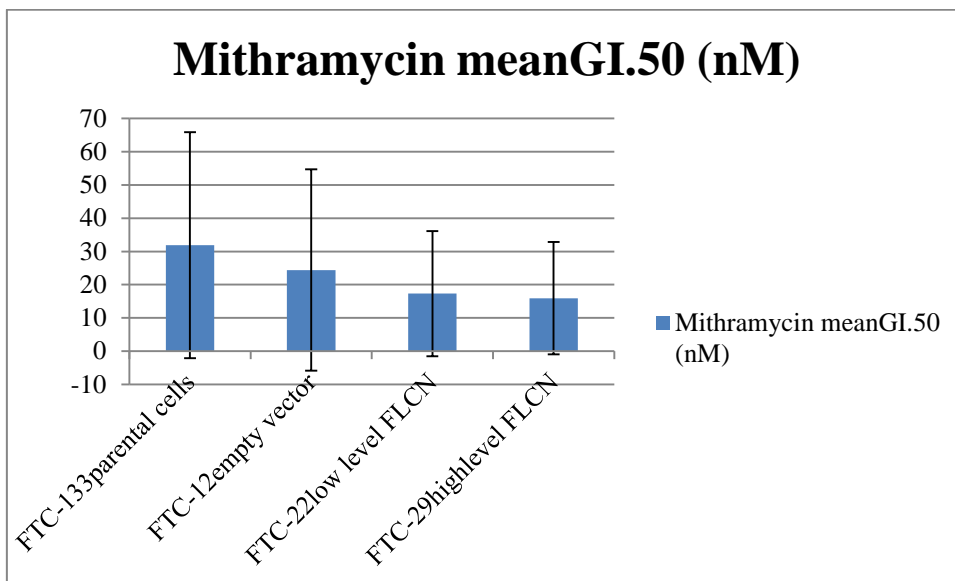


Fig 18 Mithramycin-induced cytotoxicity in FTC133 cells

In Fig 18 we compare the mithramycin response in the parental line with that in stably transfected lines with differing levels of FLCN expression. The trend appears to be the opposite to that in the UOK cells, with the higher levels of FLCN appearing possibly to have a slightly lower GI50, but these differences are not significant.

	Mithramycin meanGI.50 (nM)	Sd	n
FTC-133parental cells	31.9	34.0	3
FTC-12empty vector	24.4	30.3	5
FTC-22low level FLCN	17.3	18.8	3
FTC-29highlevel FLCN	15.9	16.9	5

Table 15: Mithramycin-induced cytotoxicity in FTC133 cells.

Table 15 shows the IG50s of Mithramycin in the 4 differently transfected FTC lines and the standard deviations showing that difference in GI50 are not significant.

Mithramycin sensitivity in VHL positive and negative RCC cell line pairs

We chose *VHL* of another gene that gives rise to an inherited kidney cancer syndrome and also as an example of a gene commonly mutated in sporadic kidney cancers, as another therapeutic target to investigate, to see if the positive indications for the treatment of BHD kidney tumors might be applicable to a wider range of diseases and patients. We chose the cell lines as there were stable isogenic VHL positive and negative cell pairs that were already established and used in the lab. 786-0 cells are a human renal cell adenocarcinoma cell line established from a 58-year-old male Caucasian. SKRC45 cells are a human renal *cell* carcinoma *cell* line. (with the kind help of Xiaohong Lu in planning and preparation)

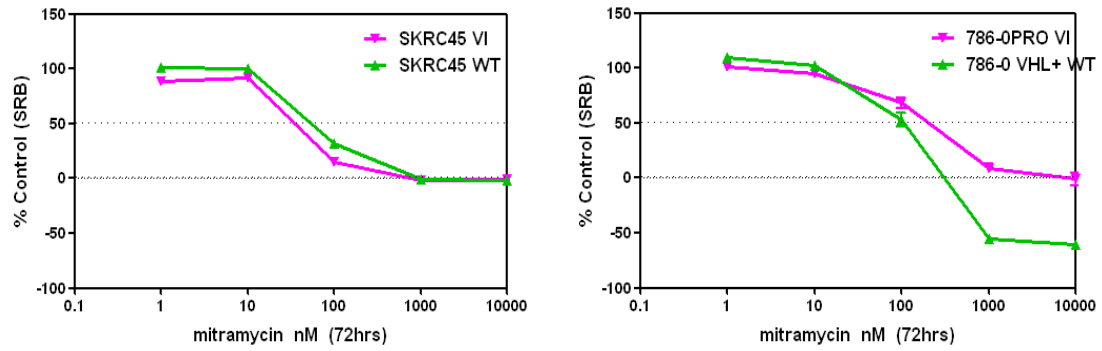


Fig 19: Mithramycin-induced cytotoxicity in VHL positive(WT) and negative(VI) cells

A small difference in the sensitivity to mithramycin was indicated between 786-0 cells with and without VHL but there was no apparent difference in sensitivity to mithramycin seen in SKRC45 cells with regard to *VHL* status (Fig 19).

Effectiveness of mithramycin in combination with rapamycin

Facilitated by the FNIP proteins *FLCN* inactivation in transgenic mice (Hasumi *et al.*, 2008) (Baba *et al.*, 2008) and in human cell lines, has been reported to be associated with changes in mTOR signalling and energy and/or nutrient sensing. The *FLCN*-interacting protein, FNIP1, interacts with a key negative regulator of mTOR and an important energy-sensing molecule 5AMP-activated protein kinase (AMPK). AMPK phosphorylates FNIP1 and AMPK inhibitors reduced this phosphorylation, resulting in reduced expression of FNIP1. *FLCN* phosphorylation was also reduced by AMPK inhibitors. Amino acid starvation and rapamycin treatment also reduced *FLCN* phosphorylation facilitated by FNIP1 over-expression, suggesting that *FLCN* may be regulated by mTOR and AMPK signalling. (Baba *et al.*, 2006)

To investigate the potential involvement of the mTOR (mammalian target of rapamycin) signalling pathway in the differential response of cells with regard to *FLCN* expression a rapamycin dose response assay was performed in CaKi-2 cells both with and without knockdown of *FLCN* protein, produced as before by treating control cells with luciferase

siRNA and test cells with FLCN SiRNA. The levels of growth inhibition induced by various concentrations of rapamycin alone were measured in both cases, using the sulforhodamine B assay after 72 hours of treatment as in previous experiments. Fig 20 shows a graph of the comparative dose response curves for the mean \pm SD of 5 replicates carried out on the same day. The Caki cell/siRNA system, though not ideal, was used for this experiment as it was the best system we had at the time, being carried out before the arrival of the FTC and UOK cells. (with the kind help of Xiaohong Lu in planning and preparation)

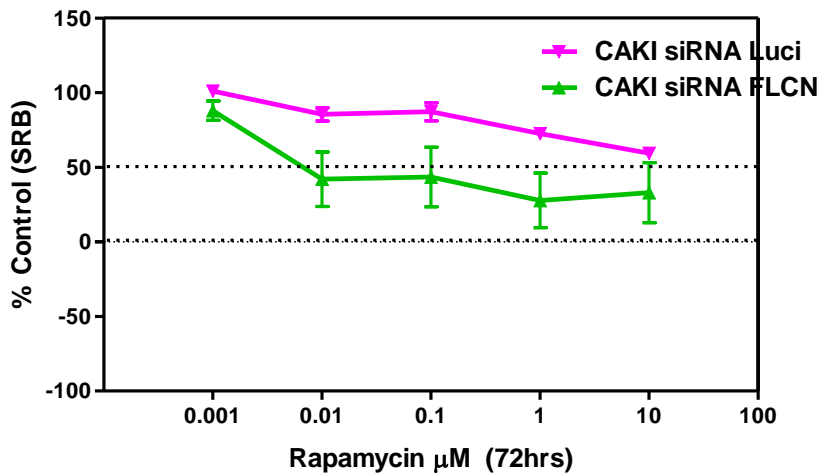


Fig 20: Dose response curve for rapamycin in CaKi-2 SiRNA-treated cells

Fig 20 shows that even at relatively high doses the growth inhibition brought about by rapamycin alone was modest but did appear to show tendencies to selectivity regarding FLCN levels.

While strong conclusions are best avoided due to the limitations of the experimental system, I include this experiment as a further investigation and illustration of the way cells with different FLCN protein levels reacted to rapamycin treatment.

Western Blot Analyses

UOK-257 and FLCN positive cells were cultured with a range of concentrations of rapamycin for 72 hours. The cells were then collected and lysed. The protein content was then extracted and a Western blot analysis was carried out to assess the relative amounts of proteins present. The blots are shown in Fig 21 below.

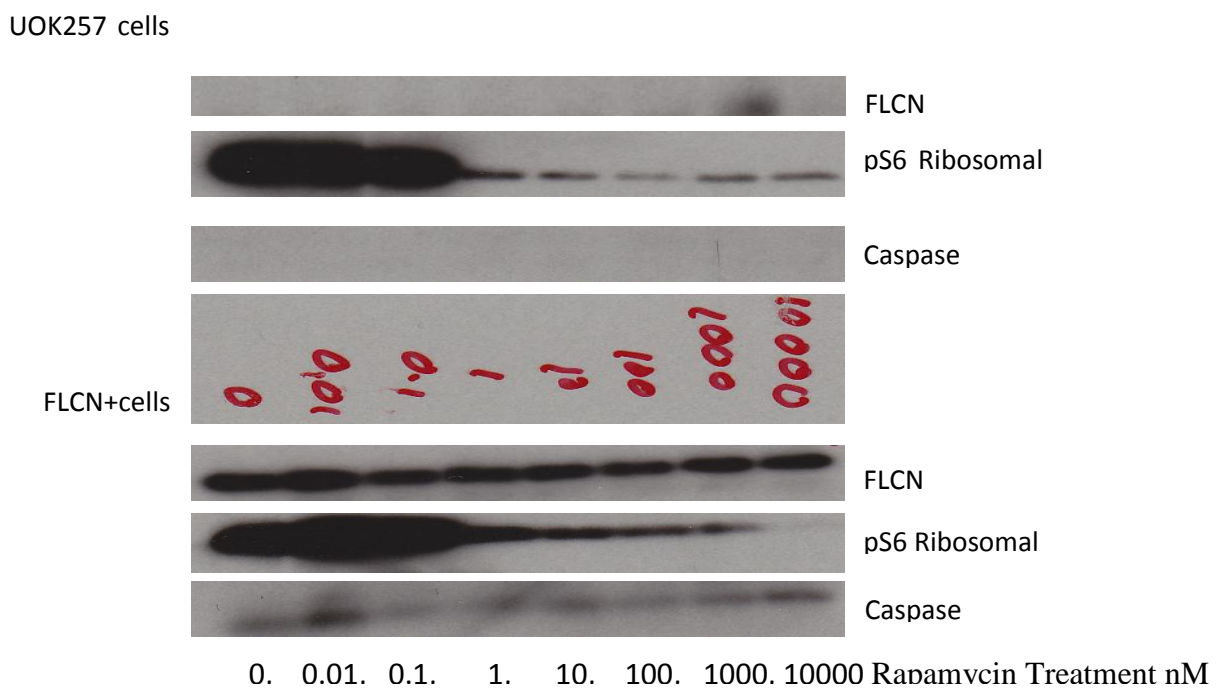


Fig 21: Western blotting showing levels of protein expression in UOK257 cells with and without FLCN expression

At a low concentration of rapamycin (1 nM), mTOR activity was shown to be inhibited (as measured by S6R phosphorylation) However, only a 10-20% reduction in cell proliferation was seen at this concentration (Lu et al 2011) as measured using the sulforhodamine B assay after 72 hours of treatment as in previous experiments.

Further investigation of the potential mechanisms underlying the induced differential proliferation effects between the two cell lines included assessment of caspase3 activation by western analysis also shown in the figure below. There was a markedly higher level of active caspase3 in FLCN⁺ compared to UOK257-FLCN⁻ cells. (with the kind help of Xiaohong Lu in planning and preparation)

Comparison of mithramycin in combination with rapamycin and mithramycin alone, in UOK 257 Cells and UOK 257 FLCN⁺ cells

To investigate whether the differential mithramycin sensitivity found in UOK257 cells and cells with FLCN expression was influenced by inhibition of the mTOR pathway by rapamycin, both UOK-257 and FLCN⁺ cells were incubated overnight, with 1nM rapamycin in the medium or without. Mithramycin was then added at a range of concentrations for 72 hours as was done for the previous experiments. Growth inhibition curves and GI₅₀ values were then calculated and are compared in Fig 22 and Fig 23, below. (with the kind help of Xiaohong Lu in planning and preparation)

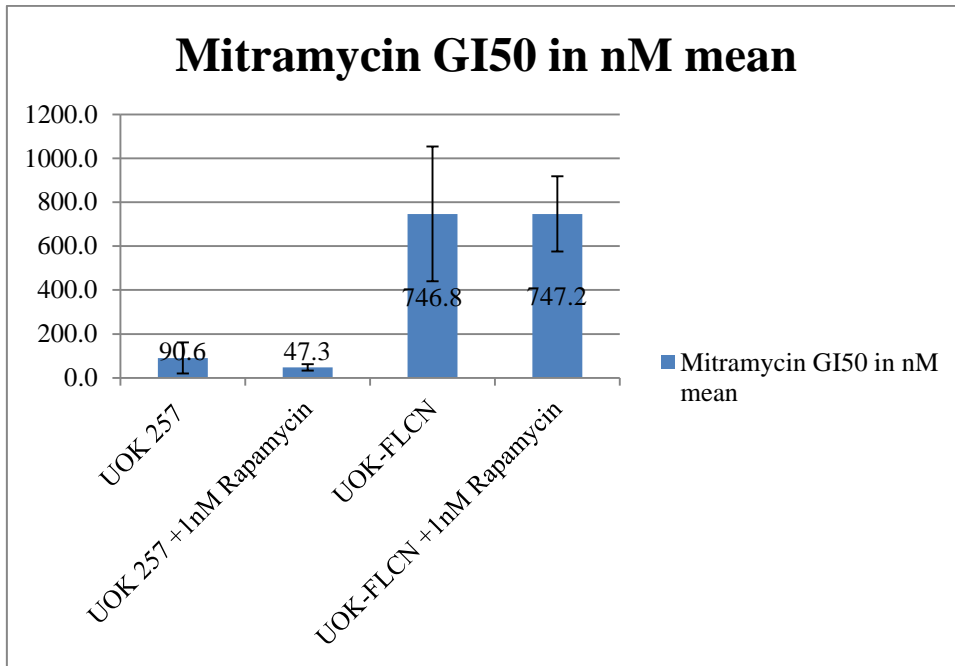


Fig 22: Comparison of mithramycin alone and in combination with rapamycin in FLCN+ and FLCN- cells.

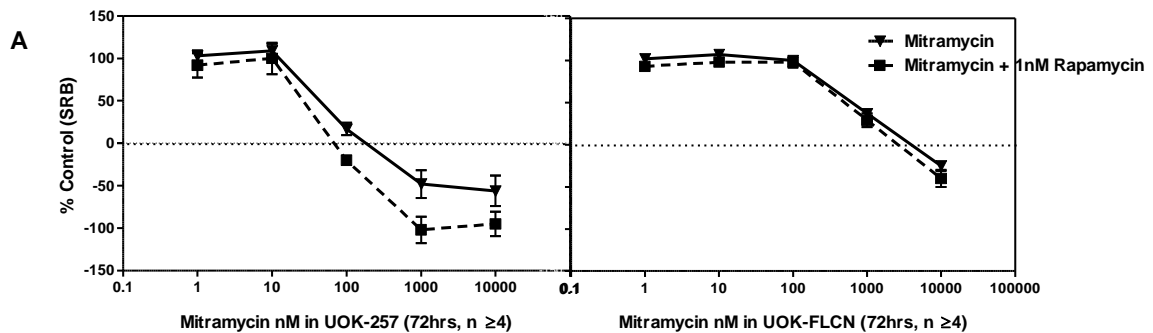


Fig 23: FLCN+ and UOK257 cell growth inhibition in response to exposure of mithramycin in combination with 1nM rapamycin and mithramycin alone. Figure by Xiaohong Lu using my data (Lu et al., 2011)

The addition of 1 nM rapamycin can bring about a one-and-a-half-fold increase in sensitivity to mithramycin in UOK-257 cells (47 ± 14 nM $n=4$ for mithramycin and rapamycin, as compared to 69 ± 10 nM $n=6$ for mithramycin alone). This indicates a synergistic effect of the

two drugs in these cells. There was also a very slight (1.1 fold) difference in UOK-257-2 FLCN⁺ cell growth inhibition induced by the combination of Mithramycin and rapamycin at high concentration, this was not as strong as seen in UOK257-FLCN⁻ cells (shown in the graphs in fig 23) and did not significantly affect the apparent increase in the selective effect against the mutant cancer cells. These results indicate an increased probability that the drug treatment may be useful clinically as a possible treatment for BHD associated tumours at some point in the future. This evidence also fits with the published reports discussed above that show FLCN to be associated with changes in mTOR signaling.

Rapamycin's effect on the effectiveness of mithramycin in cells with and without VHL

We once again chose to investigate VHL as an example of an inherited kidney cancer syndrome and a common change in sporadic kidney cancers, as another possible therapeutic target of interest, to see if the positive indications for the treatment of BHD kidney tumours might possibly be applied to a wider range of patients and diseases.

To investigate whether mithramycin sensitivity in VHL-negative cells and cells with VHL expression was influenced by inhibition of the mTOR pathway by rapamycin-stable isogenic VHL positive and negative cell pairs that were already established and used in the lab were chosen. This time 786-0 and SKRC39 cells, a human sporadic renal clear cell carcinoma cell line from a primary tumour thought by members of the lab to be a suitably representative cell line for this experiment, were chosen.

Both VHL positive and VHL negative 786-0 and SKRC39 cells were incubated overnight. A medium containing 1 nM rapamycin with or without mithramycin was then added at a range of concentrations for 72 hours as was done for the previous experiments. Growth inhibition curves and GI₅₀ values were then calculated and are compared in Fig 24 and Fig25 below. (with the kind help of Xiaohong Lu in planning and preparation) No change in the mithramycin sensitivity of 786-0 cells or SKRC39 cells, with or without VHL expression, in response to rapamycin treatment, could be detected.

As the addition of rapamycin to the mithramycin treatment of VHL tumour cells made little to no difference to the efficacy of the growth inhibition, from these data the indications are that the mTOR pathway is unlikely to be greatly involved in these responses.

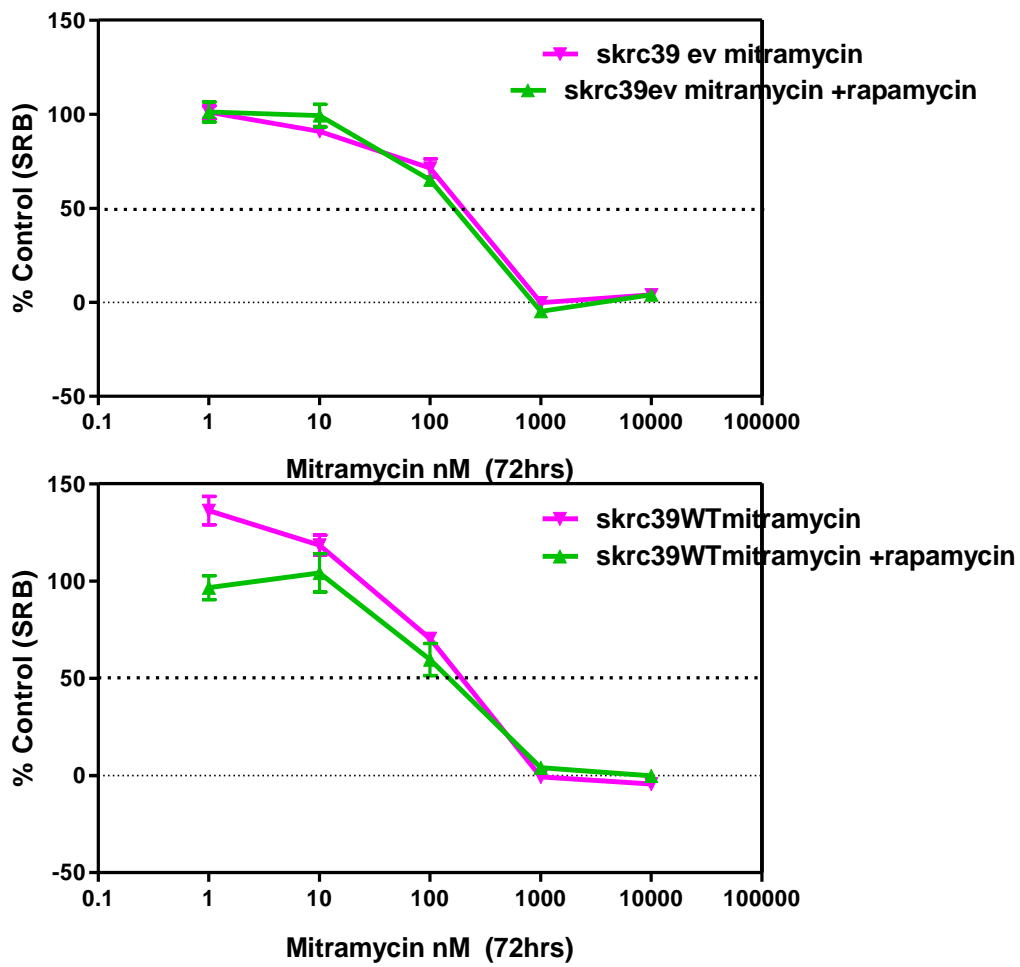


Fig 24: VHL+(wt) and VHL-(ev) SKRC39 cell growth inhibition in response to exposure of Mitramycin in combination with 1nM rapamycin and Mithramycin alone.

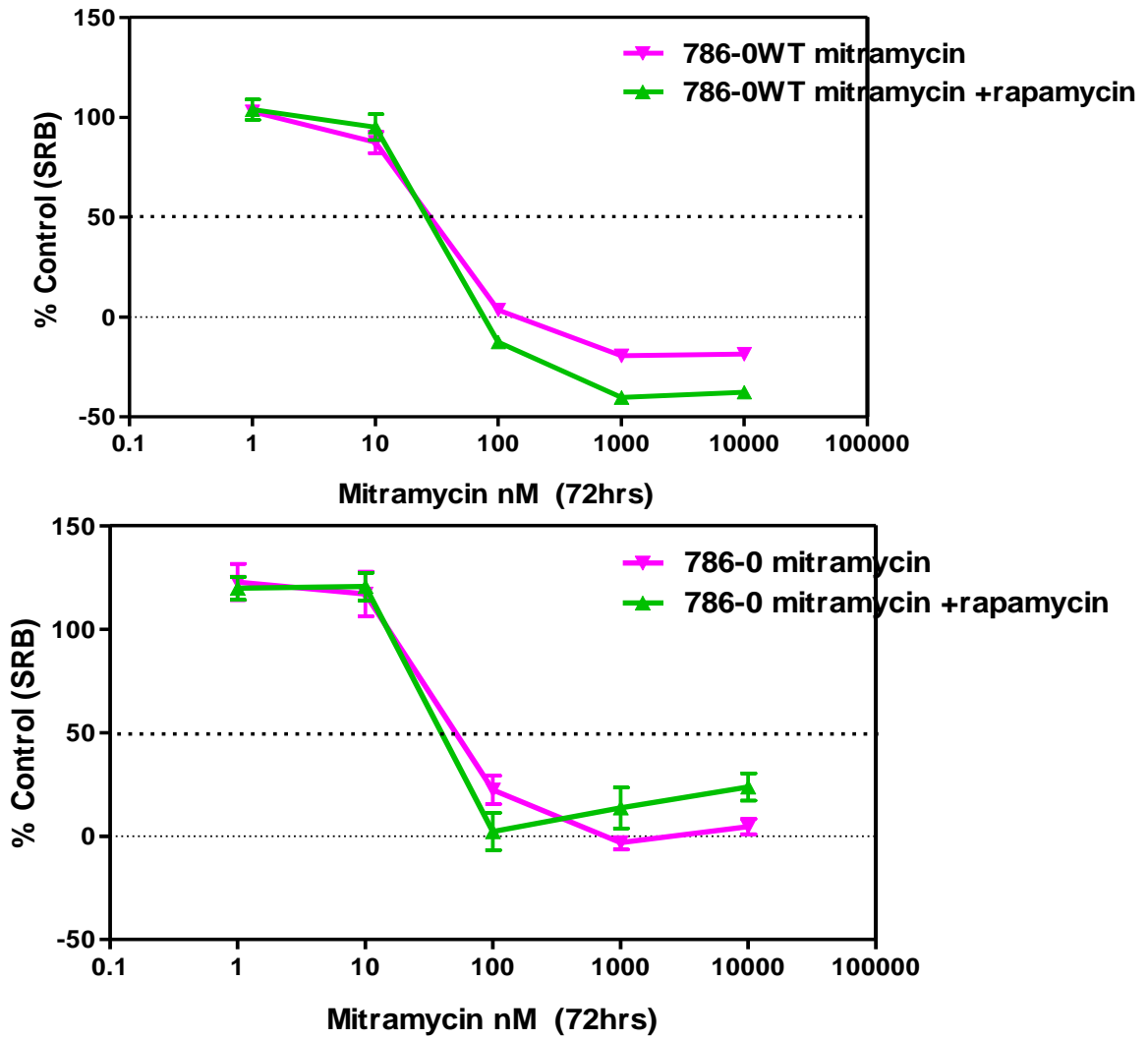


Fig 25: VHL+(wt) and VHL- 786-0 cell growth inhibition in response to exposure of Mitramycin in combination with 1nM rapamycin and Mitramycin alone.

Chapter 5: Results of Further Assessment of The Effectiveness of vincristine

Vincristine also showed a good selectivity in earlier experiments (Fig 15) and of the compounds with selectivity for FLCN positive cells it had the lowest GI₅₀ (See table 14). As a compound already in use as a chemotherapeutic agent for the treatment of some forms of cancer, it's possible usefulness for use in the case of BHD, kidney cancer and other tumours is of considerable interest.

Vincristine with FTC133 cells

To investigate vincristine sensitivity in FLCN negative cells originating from cancers of non-renal origin, the human thyroid carcinoma line FTC133 was used and vincristine sensitivity was then examined in stably transfected cells with low FLCN and high FLCN expression as well as in cells transfected with empty vector and therefore no FLCN expression. SRB growth inhibition assays were carried out as before (Fig 26)

(with the kind help of Xiaohong Lu in planning and preparation)

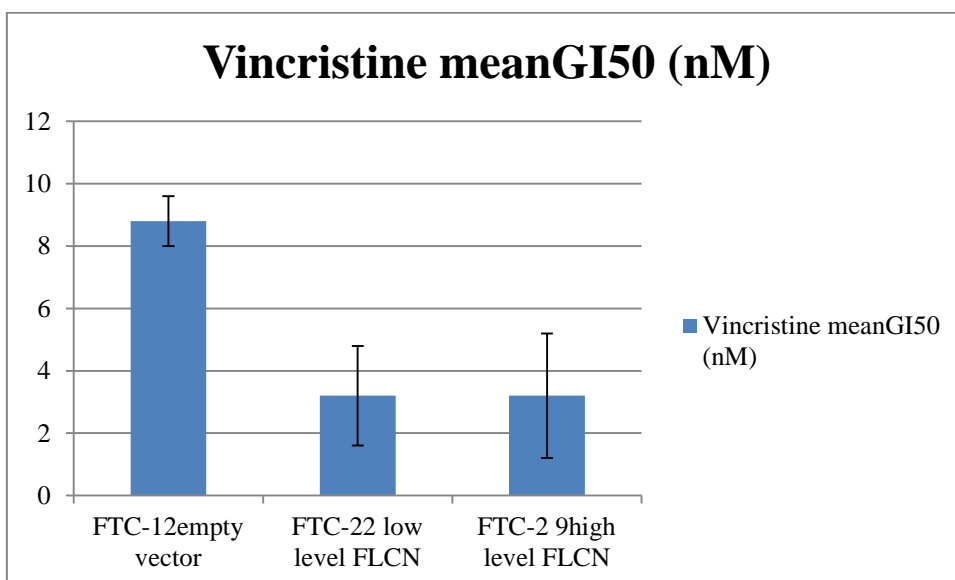


Fig 26: Vincristine-induced cytotoxicity in FTC133 cells

Table 15: Vincristine-induced cytotoxicity in FTC133 cells

	Vincristine meanGI₅₀ (nM)	Sd	n
FTC-12empty vector	8.8	0.8	3
FTC-22 low level FLCN	3.2	1.6	3
FTC-2 9high level FLCN	3.2	2.0	5

A possible trend apparently indicating slightly increased sensitivity in FTC-133 cells with normal to high FLCN levels to the drug vincristine was seen (Fig 26 and table 15above). This trend differs from the result seen in UOK cell lines and indicates that the lack of FLCN in the FTC133 (cells in combination with other factors, unknown, within this cell line) may confer some resistance to the cytotoxic effects of vincristine. This once again shows the differences between cancer cells and the variability of their responses.

Comparison of vincristine in combination with rapamycin and vincristine alone, in UOK 257 Cells and UOK 257 FLCN+ cells.

To investigate whether the differential vincristine sensitivity found in UOK-257 cells and cells with FLCN expression was influenced by inhibition of the mTOR pathway by rapamycin, both UOK-257 and FLCN⁺ cells were incubated overnight, with 1nM rapamycin in the medium or without. Vincristine was then added at a range of concentrations for 72 hours as was done for the previous experiments. (with the kind help of Xiaohong Lu in planning and preparation) Growth inhibition curves and GI₅₀ values were then calculated and are compared in Fig 27 and Table 16. The addition of Rapamycin appeared to have no significant effect on the GI₅₀ of vincristine regardless of the FLCN status of the cells. As no synergistic effect could be detected it therefore seems unlikely that the mTOR pathway is involved in the selective effects of vincristine in UOK cells with regard to FLCN status.

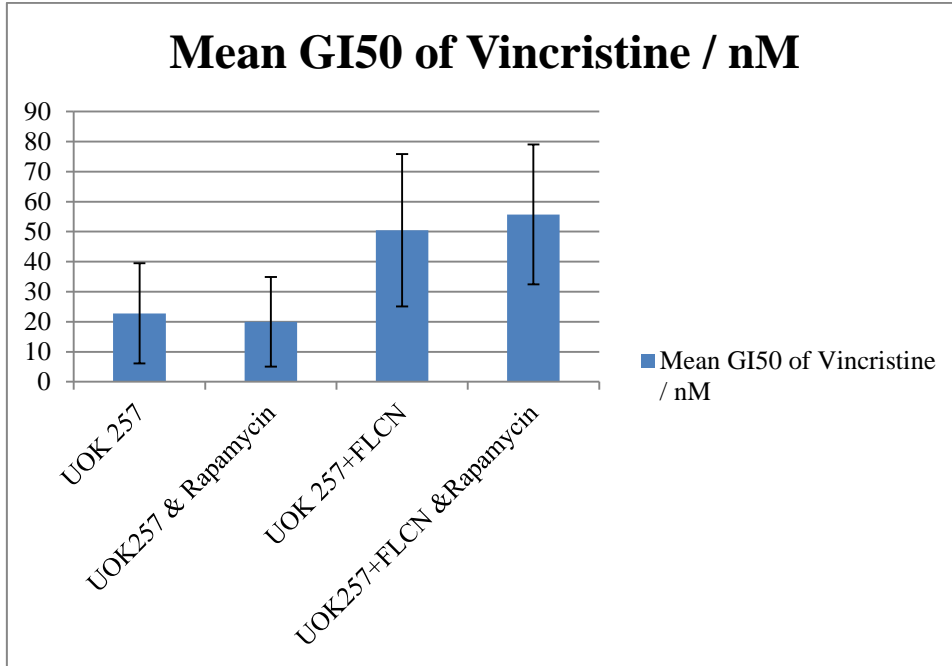


Fig 27: UOK FLCN+ and UOK257 cell growth inhibition in response to exposure of Vincristine in combination with 1nM rapamycin and Vincristine alone.

Table 16: UOK FLCN+ and UOK257 cell growth inhibition GI50 values in response to exposure of Vincristine in combination with 1nM rapamycin and Vincristine alone.

	Mean GI ₅₀ of Vincristine / nM	S.D.
UOK 257	22.8	16.7
UOK257 & Rapamycin	20	14.9
UOK 257+FLCN	50.5	25.4
UOK257+FLCN & Rapamycin	55.7	23.3

Vincristine sensitivity in VHL positive and negative RCC cell line pairs

To complete the data on vincristine it was decided that VHL should be investigated as an example of another inherited kidney cancer syndrome, and also a common change in sporadic kidney cancers, to see if the positive indications for the treatment of BHD kidney tumours might be applicable to a wider range of diseases and patients. There were stable isogenic VHL positive and negative cell pairs used in the lab that were already established. The same lines were used as for the complementary experiments with mithramycin; a 786-0 human renal cell adenocarcinoma cell line established from a 58-year-old male Caucasian; and SKRC45 human renal cell carcinoma cell line pairs used for the SRB growth inhibition assays for vincristine alone (with the kind help of Xiaohong Lu in planning and preparation). Results are shown in Fig 28.

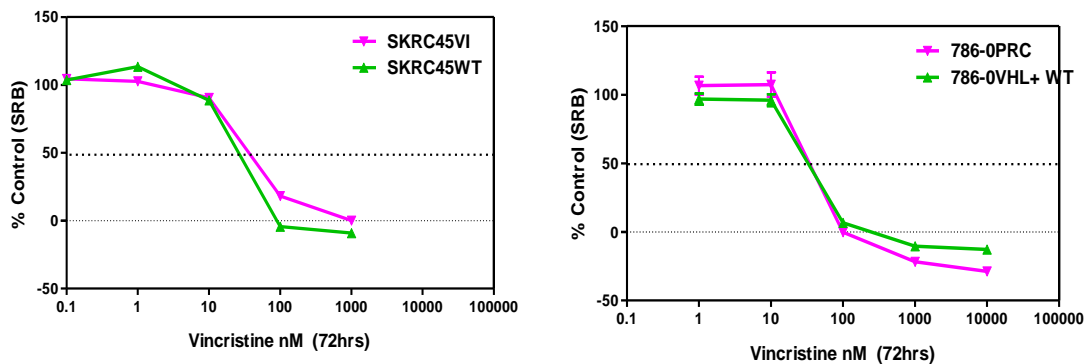


Fig 28: VHL WT+ and VHL- cell growth inhibition in response to exposure of vincristine alone

Little difference in growth inhibition could be seen between the VHL positive and VHL negative cell types when treated with vincristine.

Investigation of the mTOR involvement in vincristine sensitivity in VHL +&- RCCs.

To investigate whether vincristine sensitivity in VHL negative cells and cells with VHL expression could possibly be influenced by changes to the mTOR signalling pathway or have any synergistic effect with rapamycin, once again VHL positive and VHL negative 786-0 cells were incubated overnight, with or without 1nM rapamycin in the medium. Vincristine was then added at a range of concentrations for 72 hours as was done for the previous experiments (with the kind help of Xiaohong Lu in planning and preparation). Growth inhibition curves are shown below in Fig 29 and Fig 30.

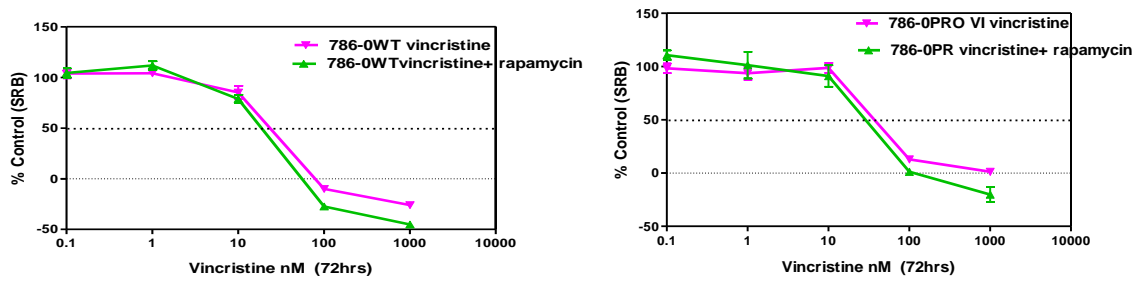


Fig 29: 786-O VHL + and 786-O VHL- cell growth inhibition in response to exposure of vincristine in combination with 1nM rapamycin and with vincristine alone.

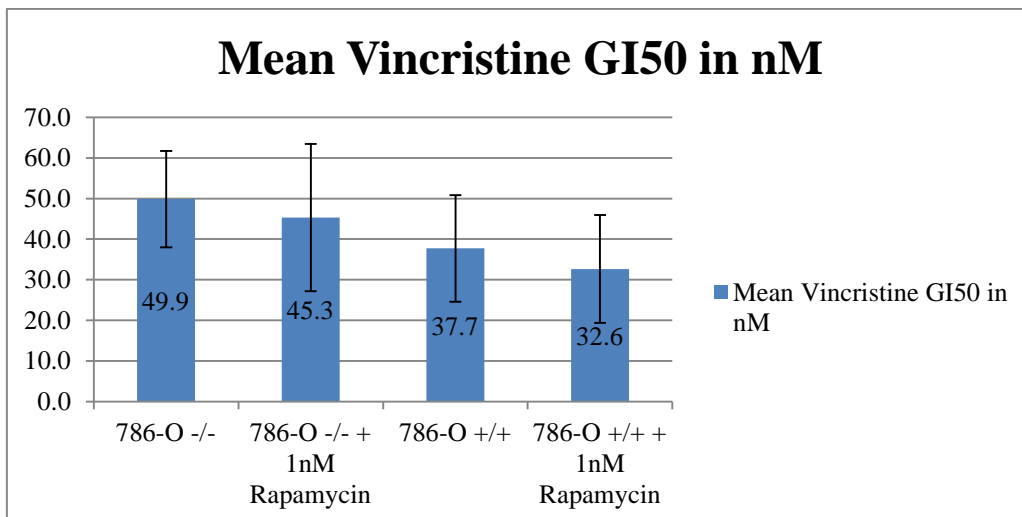


Fig 30: 786-O VHL + and 786-O VHL- cell growth inhibition in response to exposure to vincristine in combination with 1nM rapamycin and vincristine alone.

The trend of the data indicated very small change in the vincristine sensitivity of 786-0 cells, with and without VHL expression, in response to rapamycin treatment. This is not a significant difference but any actual change may possibly be due to the addition of the modest growth inhibitory effects of rapamycin to the cytotoxicity of vincristine.

As the addition of Rapamycin to the vincristine treatment of VHL tumour cells made little to no difference to the efficacy of the growth inhibition, from these data the indications are that the mTOR pathway is unlikely to be greatly involved in these responses.

Chapter 6: Results of Investigations into The Effects of Compound C

Compound C is a known AMPK inhibitor and as such affects the mTOR signalling pathway through this inhibition. For this reason its effects were of interest. SRB growth inhibition assays were carried out to assess the growth inhibitory capability of compound c in UOK257 cells with and without FLCN expression (with the kind help of Xiaohong Lu in planning and preparation).

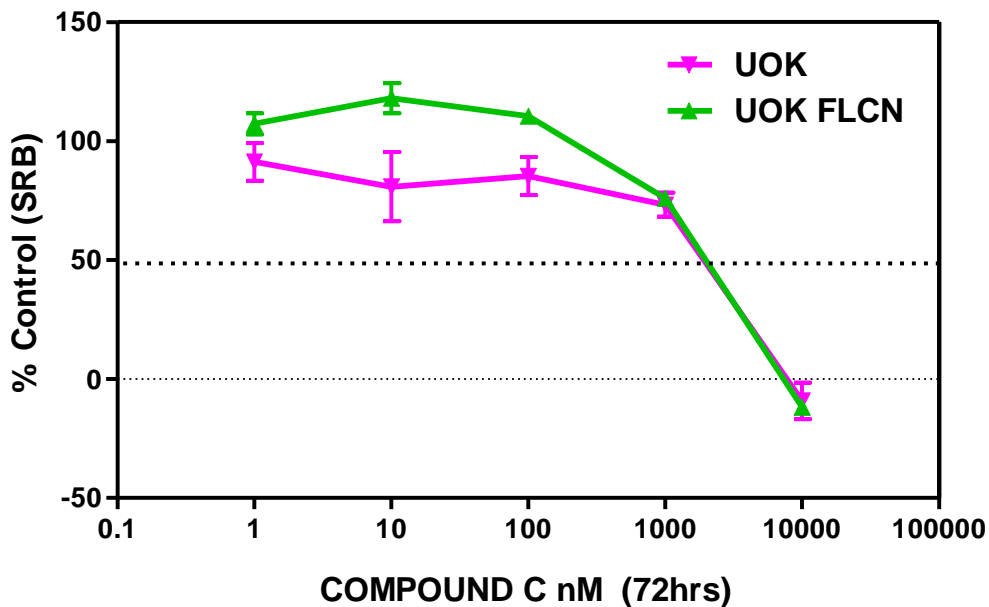


Fig 31: Inhibition of growth, shown by the SRB assay, in UOK-257 cells with and without FLCN expression by Compound C. Cells were continuously exposed to the concentrations to the chemical for 72 hours.

Fig 31 compared SRB growth inhibition assays and did not appear to show any significant difference between FLCN positive and FLCN negative UOK-257 cell lines with regard to

Compound C, which showed an appreciable inhibition only at very high doses the IG_{50} approximately 1 μ M for both cell types tested.

FLCN positive and FLCN negative UOK-257 cells were incubated overnight, with and without 1nM compound C in the medium. Mithramycin was then added at a range of concentrations for 72 hours as was done for the previous experiments. Growth inhibition curves and GI_{50} values were then calculated and are compared (with the kind help of Xiaohong Lu in planning and preparation).

SRB growth inhibition assays did not appear to show any great difference between FLCN positive and FLCN negative UOK257 cell lines with regard to Compound C.

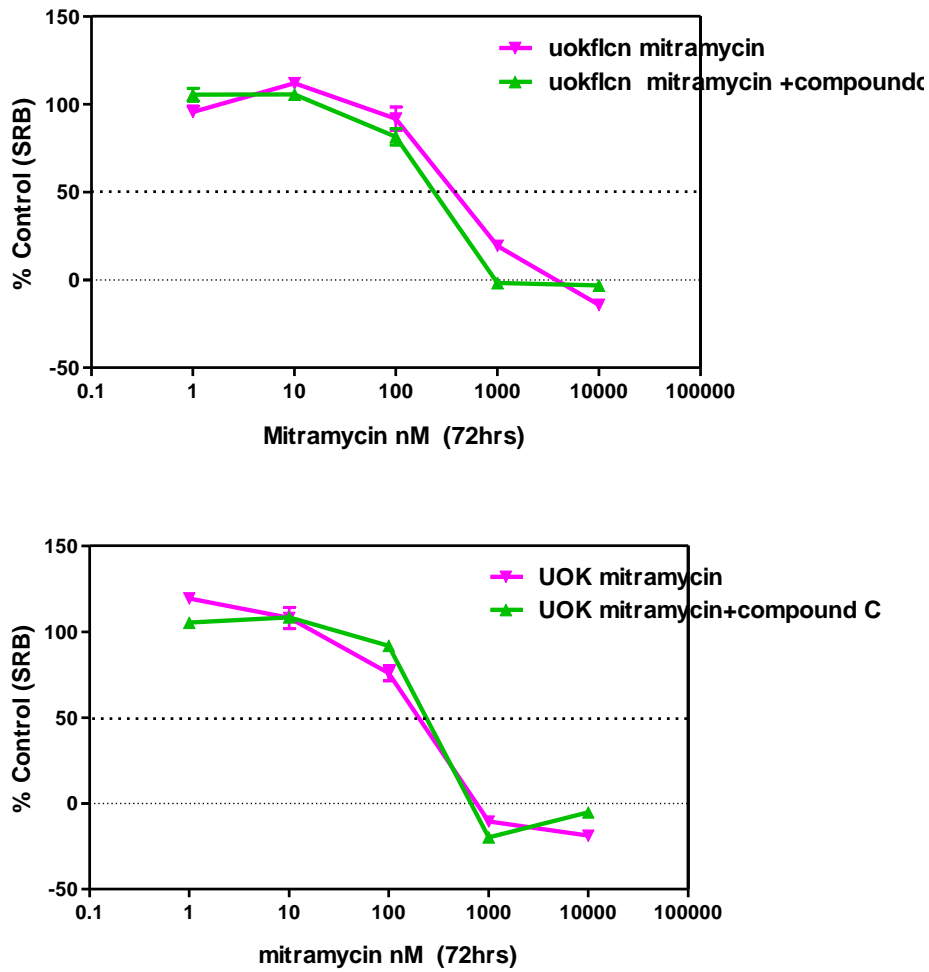


Fig 32: Cell growth inhibition in response to exposure of Mithramycin in combination with 1 nM Compound C and Mithramycin alone, for 72 hours, was determined using the SRB assay

Compound C did not appear to show any sensitising effect on UOK cells, with or without FLCN expression, with regard to inhibition caused by mithramycin treatment (Fig 32).

Chapter 7: Slingshot 2 as a synthetic lethal target of FLCN.

Slingshot (ssh) SiRNA and confocal work,

These experiments were carried out with the kind help of Xiaohong Lu who helped with the transient transfection and gave considerable input into the experimental design.

The synthetic lethal strategy tries to find those genes that are essential to the cancerous cells containing the mutation of interest but not the matched normal cells without the specific cancer gene mutation. Hence loss of these genes (referred to as synthetic lethal genes) in the presence of the given cancer gene mutation will cause the death of the cancerous cells, but not kill normal cells without the mutation. In an attempt to develop new therapeutic treatments for patients suffering from Birt–Hogg–Dubé syndrome, we looked for possible interactions which could cause synthetic-lethality by knocking down a series of phosphatase proteins in cell lines with *FLCN* inactivation (Lu *et al.*, 2013).

Initially, Lu searched for potential targets of a synthetic-lethal for *FLCN* by screening a siRNA library of phosphatases. Knock down of Slingshot serine phosphatases SSH2 and SSH3 met the criteria for potential positive hits with over two-fold increase in Caspase3/7 activity and decrease in cell viability of up to 40% in UOK-257 cells (Lu *et al.*, 2013).

SSH3 is the third phosphatase of Slingshot family of which there are three members. SSH2 is the second. The Slingshot phosphatases have in the past also been shown to have an important role in controlling the Cofilin proteins activity. This in turn mediates actin filament disassembly, assembly and reorganization within the cell (Mizuno, 2012).

I investigated the effects of this SSH2 siRNA knock down by use of clonogenic assays and confocal microscopy in collaboration with Xiaohong Lu. I carried out tissue culture, staining confocal microscopy and colony counting. Data was jointly analysed.

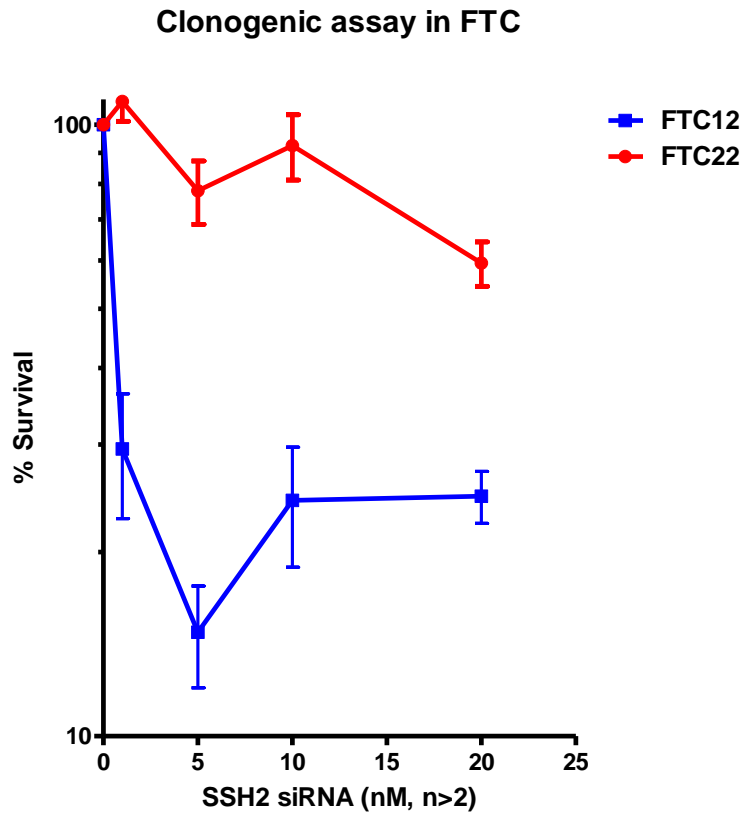


Fig 33: Cell death induced by Sling shot 2 SiRNA treatment of FTC12 cells and FLCN positive FTC22 cells, as measured by the clonogenic assay.

Fig 33 shows that Sling shot 2 SiRNA treatment produced cell death in the FTC12 cells and wild type *FLCN* positive cells FTC22 (FTC12 being a *FLCN* null thyroid cancer cell line and FTC22 being the same cell line in which wild type *FLCN* was re-expressed), as measured by the clonogenic assay and reveals a significant difference between the survival rates of the two cell lines. The absence of *FLCN* combined with the reduction of *SSH2* leads to reduced viability of

the cells, when compared to the absence of either one alone. This data indicated that SSH2 is a synthetic lethal target for FLCN.

In Lu et al. 2013 it is also shown that increased Caspase3/7 activation (associated with apoptotic cell death) after knockdown of SSH2 by siRNA- appears to be a reaction specific to FLCN-negative cells such as FTC133-12 cells and UOK-257 cells. It was believed not to be a feature to be generally associated with knock down Slingshot gene family (though the effects of SSH2 knockdown could be enhanced by knockdown of further SSHs).

p53 mutations are known to be present in both FTC133 cells and UOK-257 cells (Lu *et al.*, 2011) suggesting that SSH2 knockdown induced activation of Caspase3/7 may be mediated by a cell death pathway independent of *p53* (Lu *et al.*, 2013).

Combinations of SSH1 or SSH3 paired with SSH2, and a combination of all three slingshots knockdowns (knockdowns were performed by Xiaohong Lu), showing that the addition of SSH1 or SSH3 siRNA treatments potentiated the effects of SSH2 knockdown indicating that there appeared to be some redundancy between the three slingshot serine phosphatase genes (Lu *et al.* 2013).

The Slingshot proteins have been reported previously to regulate the phosphorylation status of Cofilin working antagonistically with the LIM- kinases (Mizuno, 2013). Testis-specific protein kinases (TESKS) and LIM-kinases (LIMK) bring about the phosphorylation of Cofilin on a specific single serine residue (Ser 3) and this phosphorylated Cofilin (p-Cofilin) is then inactive with regard to binding to filamental-actin (F-actin). This inactivation of filamental-actin binding then results in the stabilization of F-actin. The Slingshot family phosphatases and PDXP (chronophin, pyridoxal phosphate phosphatase) bring about Cofilin reactivation by means of

phosphate removal from this specific residue, ser-3. The F-actin is then bound by this Cofilin which mediates the severing of F-actin and its depolymerization. In UOK-257 cell lines, under normal physiological conditions, knockdown of phosphatases (*SSH/PDXP*) would increase Cofilin phosphorylation, whereas knockdown of kinases (*LIMK/TESK*) would result in the reduction of Cofilin phosphorylation.

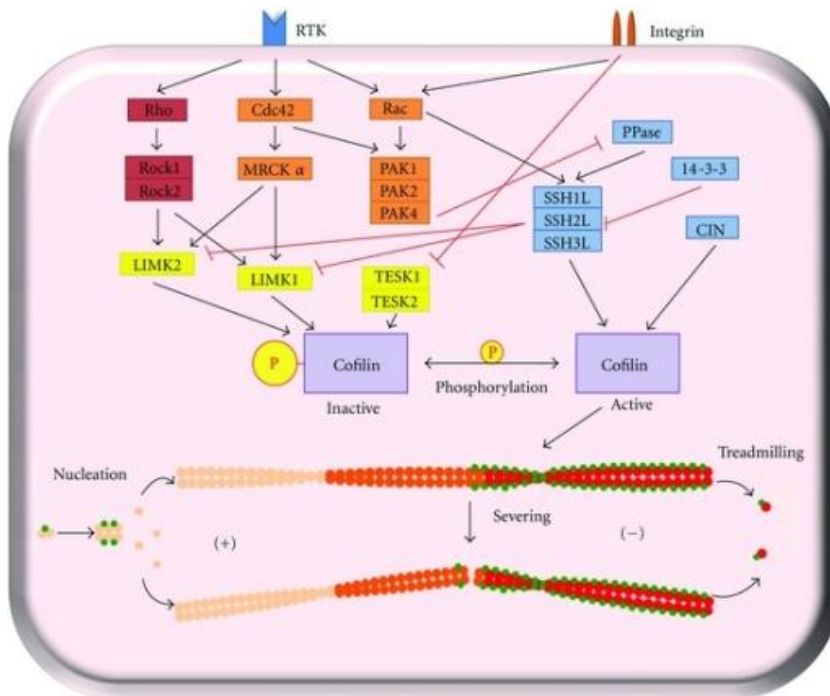


Fig 34: SSH family phosphatase known pathways (Teng *et al.* 2011).

Only a few regulatory pathways resulting in SSH activation have been ever identified. SSH1L's phosphatase activity is negatively regulated through phosphorylation by PAK4 in some cell types, suggesting negative regulation of Rac1 activation on SSH and ADF/cofilin activity. In other cell types, SSH is activated through integrin pathway via Rac1 activation. SSH and filament-actin colocalization has been reported together with the localized activation of SSH1L (Teng *et al.* 2011), indicating that assembly of F-actin can trigger the local activation of SSH1L

and therefore promotes cofilin-mediated actin turnover in protrusive lamellipodia. Scaffolding proteins 14-3-3 can also act in modulation of ADF/cofilin-activity by interaction with SSH isoforms. Phosphorylation of SSH1L on serines 937 and 978 by protein kinase D (PKD) promotes its interaction with 14-3-3 (Teng *et al.*2011). Fig 34 shows SSH in the regulatory pathways modulating cofilin phosphorylation and dephosphorylation. Rho-GTPases are a predominant regulator of cofilin phosphatases and kinases. SSH family phosphatase dephosphorylate cofilin directly or via LIMK inactivation. Phosphorylated cofilin can no longer bind and regulate the F-actin dynamics. Cofilin phosphorylation is mainly regulated by TESK and LIMK (Teng *et al.*2011).

Effects SSH2 knockdown cofilin phosphorylation and actin.

This was investigated further with regard to whether or not there might be effects from SSH2 knockdown, on phosphorylation of Cofilin and its resultant affect on actin organization within the cell in FLCN negative cells. To this end confocal micrographs were taken of cells treated with siRNA to SSH2 or Cofilin and then stained with phalloidine to fluorescently label the filamental actin and DAPI to visualise the nucleus as well as immunofluorescence staining using antibodies to either Cofilin or phosphorylated Cofilin. These where bound by alexa 633 labelled secondary antibodies. These cell staining were then visualised using the confocal microscope. Each of the fluorescent dyes is visualised at a different wave length of light, in one focal plane. This is done using a different combination of excitation laser wavelength and detection parameters to give a separate image for each protein for the same field of view. The results of these experiments are shown in Fig 34 to 43 below.

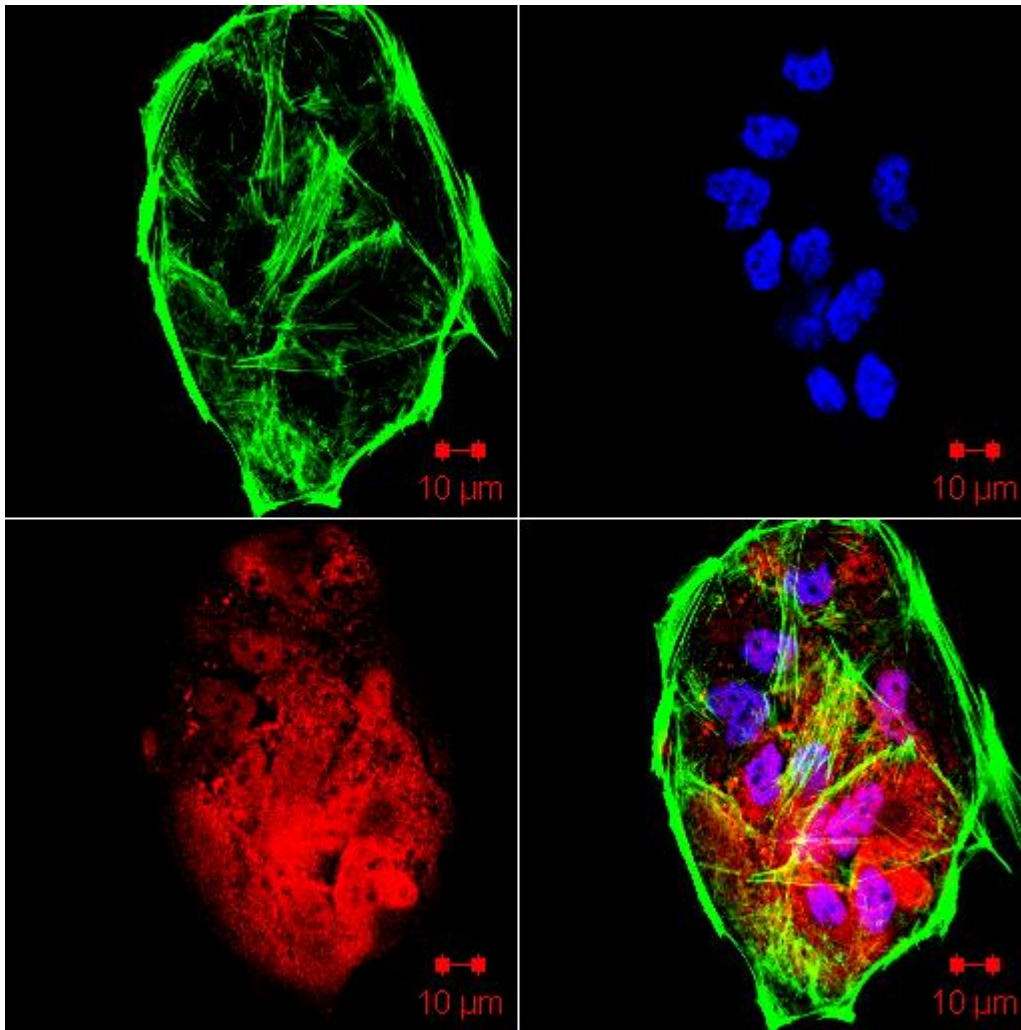


Fig 34: Confocal images showing the effect of treatment with SiRNA to luciferase on Cofilin and F-actin in UOK-257 cells.

Cells labeled with anti-Cofilin alexa 633 in red (bottom left panel and bottom right merged panel), phalloidine F-Actin staining in green (top left panel and bottom right merged panel) and DAPI nuclear staining in blue (top right panel and bottom right merged panel) yellow colour in the merged panel indicates cofilin and actin colocalization. This figure shows the distribution of cofilin across the cytoplasm and nucleus of these FLCN negative cells and filament-actin in the cyto-skeleton.

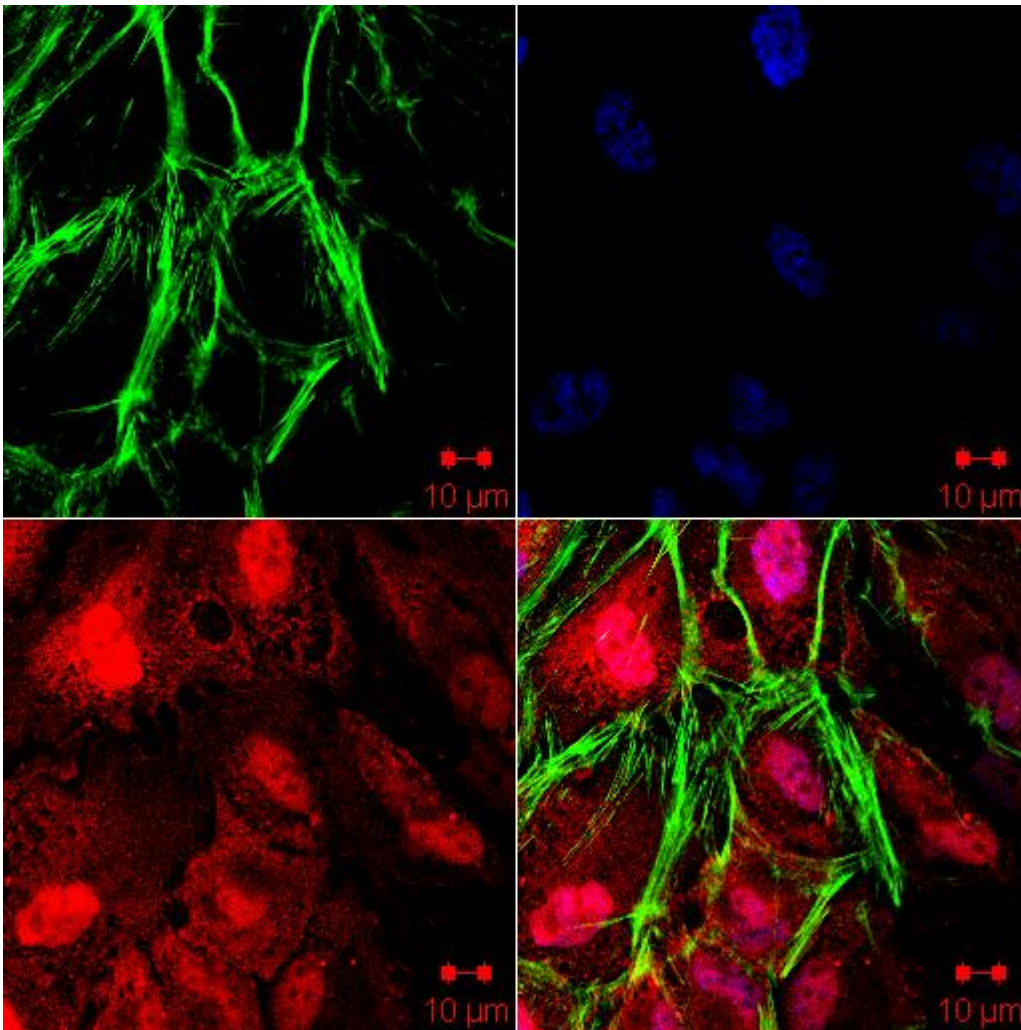


Fig 35: Confocal images showing the effect of treatment with SiRNA to SSH2 on Cofilin and F-actin in UOK-257 cells.

Cells labeled with anti-Cofilin alexa 633 in red (bottom left panel and bottom right merged panel), phalloidine F-Actin staining in green (top left panel and bottom right merged panel) and DAPI nuclear staining in blue (top right panel and bottom right merged panel) yellow colour in the merged panel indicates cofilin and actin colocalization. This figure shows the distribution of cofilin across the cytoplasm and nucleus showing little reduction, compared to the control. The figure also shows filament-actin in the cytoskeleton with little increase compared to the control.

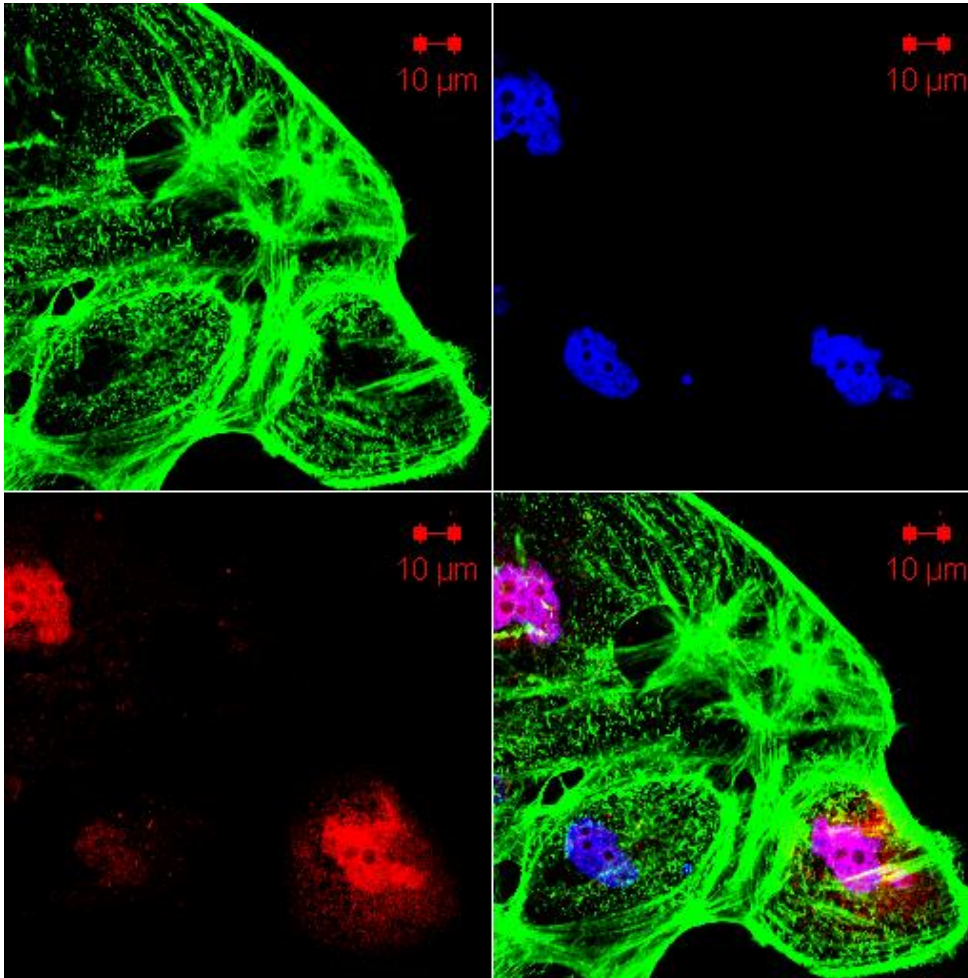


Fig 36: Confocal images showing the effect of treatment with SiRNA to Cofilin on Cofilin and F-actin in UOK-257 cells.

Cells labeled with anti-Cofilin alexa 633 in red (bottom left panel and bottom right merged panel), phalloidine F-Actin staining in green (top left panel and bottom right merged panel) and DAPI nuclear staining in blue (top right panel and bottom right merged panel) yellow colour in the merged panel indicates cofilin and actin colocalization. This figure shows the distribution of cofilin across the cytoplasm and nucleus showing a clear reduction the Cofilin Knock Down was incomplete. The figure also shows that there is some increase in filament-actin in the cytoskeleton, compared to the control.

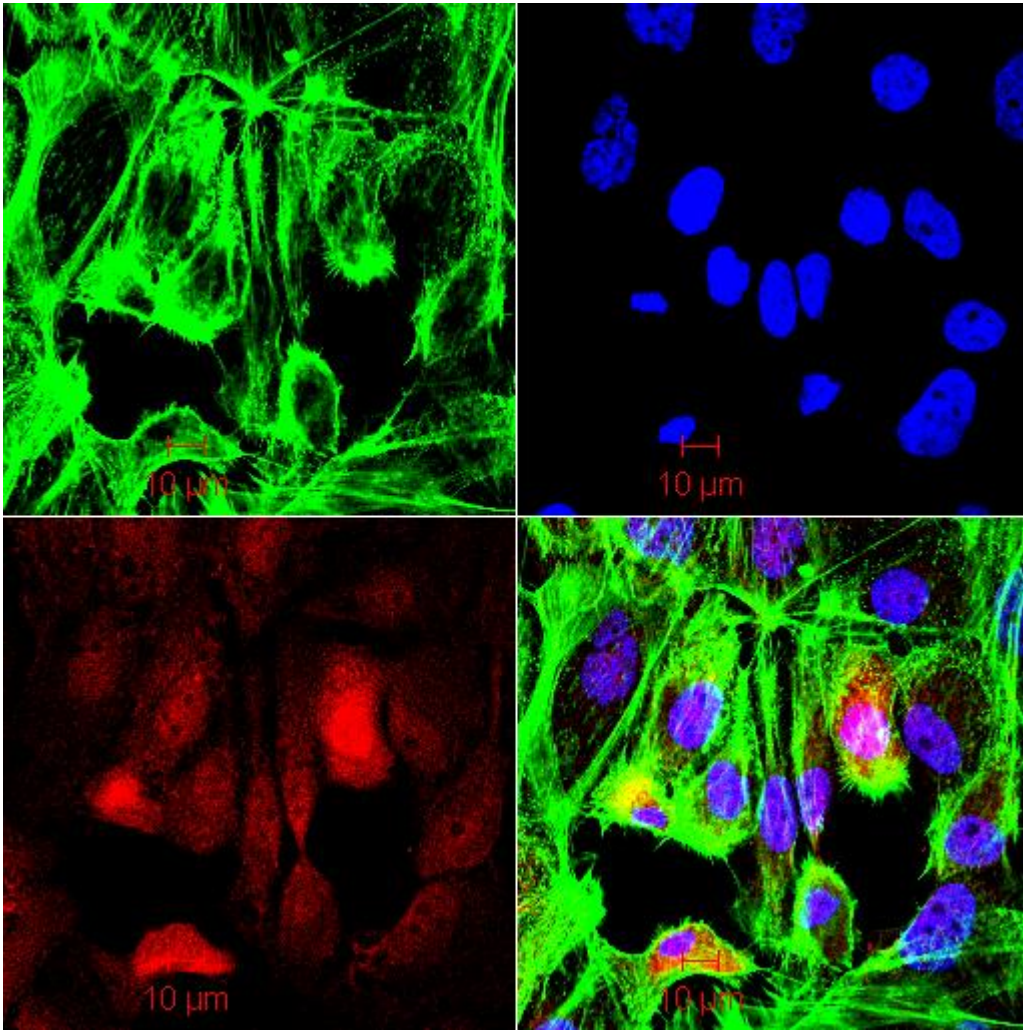


Fig 37: Confocal images showing the effect of treatment with SiRNA to luciferase on P-Cofilin and F-actin in UOK-257 cells.

Cells labeled with anti-P-Cofilin alexa 633 in red (bottom left panel and bottom right merged panel), phalloidin F-Actin staining in green (top left panel and bottom right merged panel) and DAPI nuclear staining in blue (top right panel and bottom right merged panel).

This figure shows the distribution of P-cofilin across the cytoplasm and nucleus of these FLCN negative cells and filament-actin in the cytoskeleton.

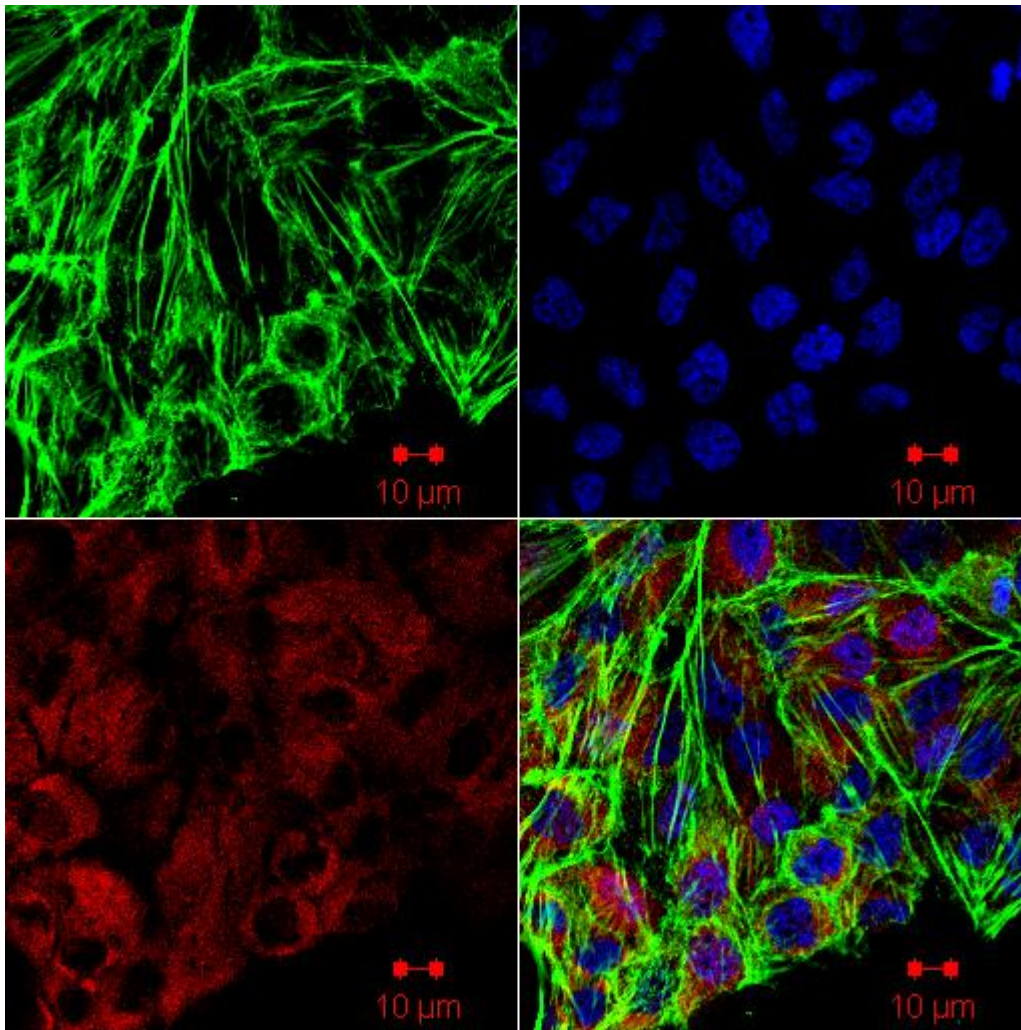


Fig 38: Confocal images showing the effect of treatment with SiRNA to Slingshot 2 on P-Cofilin and F-actin in UOK-257 cells.

Cells labeled with anti-P-Cofilin alexa 633 in red (bottom left panel and bottom right merged panel), phalloidine F-Actin staining in green (top left panel and bottom right merged panel) and DAPI nuclear staining in blue (top right panel and bottom right merged panel).

This figure shows the distribution of P-cofilin across the cytoplasm and nucleus showing little reduction, compared to the control. The figure also shows filament-actin in the cytoskeleton with no increase compared to the control.

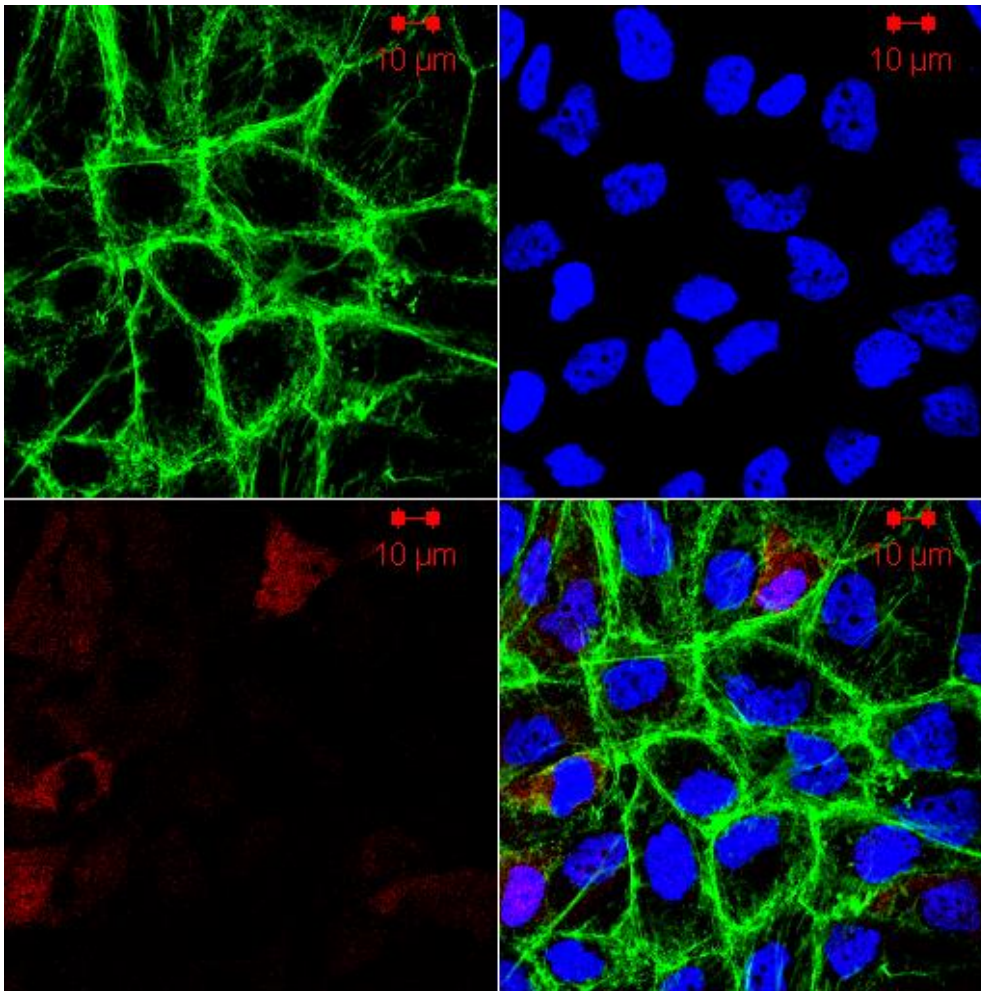


Fig 39: Confocal images showing the effect of treatment with SiRNA to Cofilin on P-Cofilin and F-actin in UOK-257 cells.

Cells labeled with anti-P-Cofilin alexa 633 in red (bottom left panel and bottom right merged panel), phalloidine F-Actin staining in green (top left panel and bottom right merged panel) and DAPI nuclear staining in blue (top right panel and bottom right merged panel).

This figure shows the distribution of P-cofilin across the cytoplasm and nucleus showing a clear reduction, compared to the control. . The figure also shows filament-actin in the cytoskeleton with no increase compared to the control.

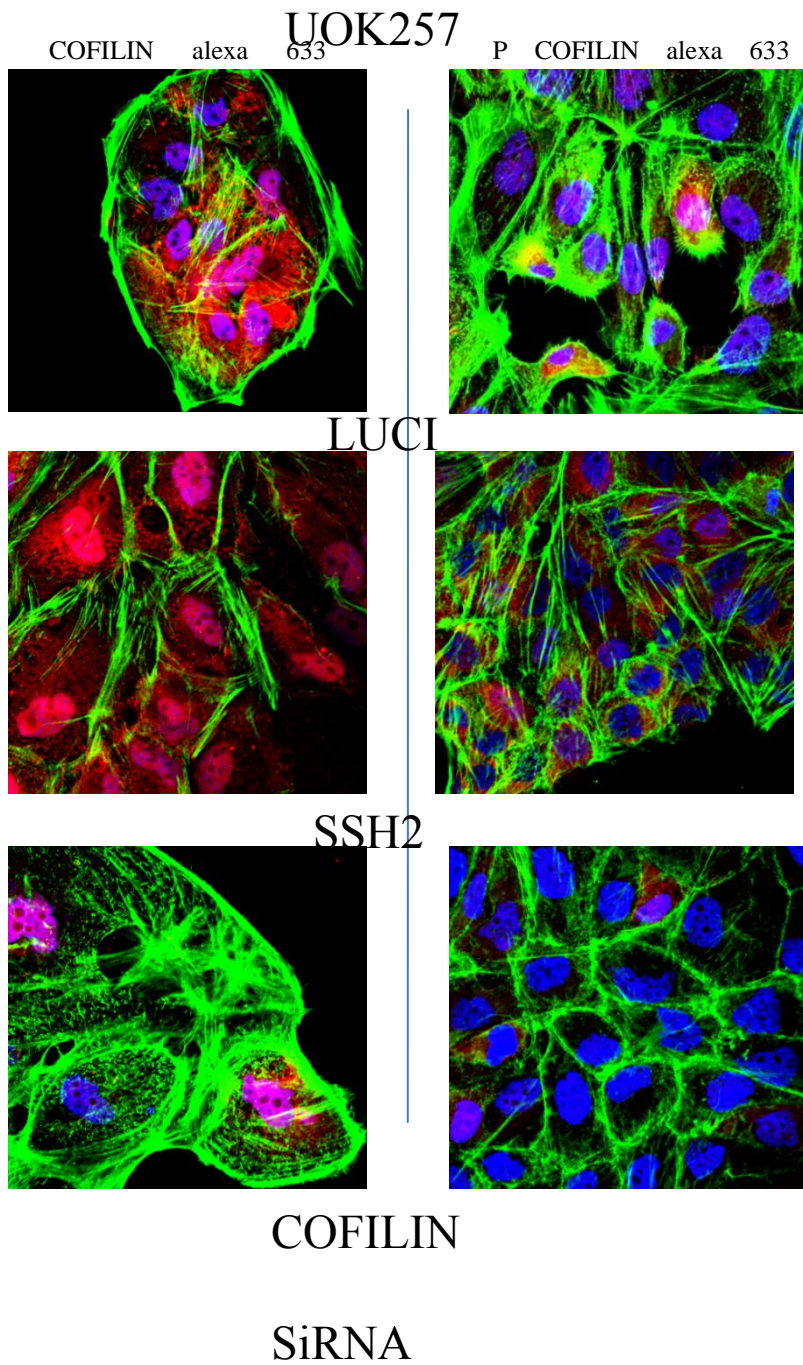


Fig 40: comparison of the effects of SSH2 and Cofilin SiRNA treatment on Cofilin, phospho-Cofilin and actin structure in FLCN negative UOK cells (a compilation of the merged panes of figures 34 to 39 for comparison).

In fig 40 cells are labeled with anti-P-Cofilin alexa 633 in, phalloidine F-Actin staining in green and DAPI nuclear staining in blue, The yellow colour indicates cofilin and actin colocalization (merged panels).

The images in Fig 40 show that these FLCN-null cells did not seem to exhibit a strong Cofilin de/phosphorylation and F-actin regulation response to SSH knockdown and show that these FLCN-null cells exhibited no evidence against Cofilin de/phosphorylation dysregulation.

Figure 41 is a repetition of the SSH2 knock down experiment with slightly different laser settings.

It confirmed the observations made previously. Once again the images in Fig 9 show that these FLCN-null cells did not seem to exhibit a strong Cofilin de/phosphorylation and F-actin regulation response to SSH2 knockdown and show that these FLCN-null cells exhibited no evidence against Cofilin de/phosphorylation dysregulation.

In fig 41 below cells are labeled with anti-P-Cofilin alexa 633 in, phalloidine F-Actin staining in green and DAPI nuclear staining is shown in blue, the yellow colour indicates cofilin and actin colocalization (merged panels). Top left = UOK257cells treated with luciferase control siRNA and stained with anti-Cofilin 633. Top right = UOK257cells treated with luciferase control siRNA and stained with anti-P-Cofilin 633. Bottomleft = UOK257cells treated with SSH2 siRNA and stained with anti-Cofilin 633. Bottom right = UOK257cells treated with SSH2 siRNA and stained with anti-P-Cofilin 633.

UOK257 Comparable laser

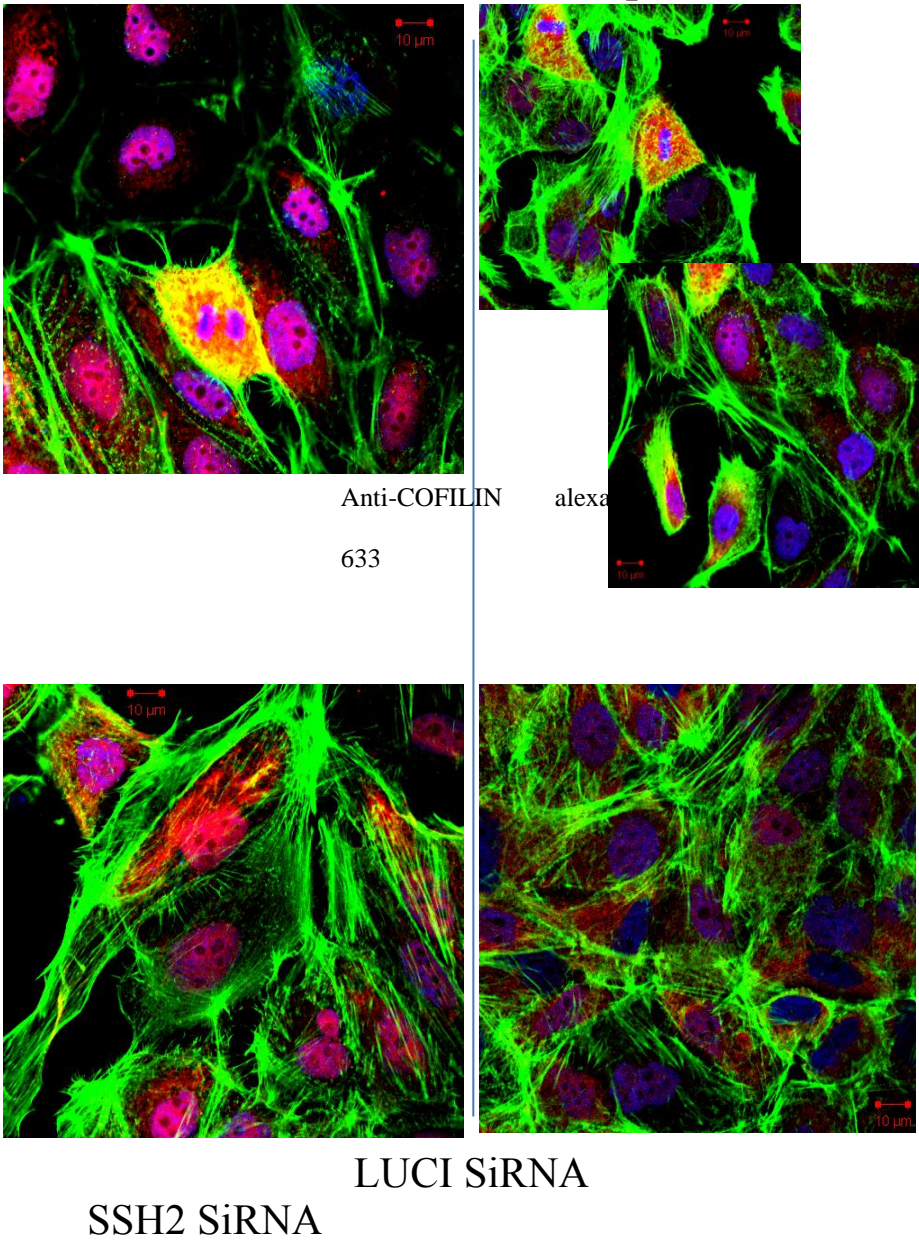


Fig 41: Comparison of the effects of SSH2 treatment on Cofilin, phospho-Cofilin and actin structure in UOK-257 cells.

In theory knocking down the Slingshot genes with siRNAs, under normal physiological conditions, would be expected to give rise to the increase and accumulation of phosphorylated Cofilin. This increase could be seen by western analysis in FLCN positive cell lines (approximately 400% increase in cofilin phosphorylation), but it was seen to be much smaller in the FLCN negative cell line (approximately 150% increase in cofilin phosphorylation), indicating the possibility that FLCN is required for the usual phosphatase activity of Slingshot found in normal cell conditions (Lu *et al.*, 2013).

My findings from the confocal microscopy in UOK-257 cells do not disagree with the findings stated in Lu *et al.* (2013), or the suggestion that the absence of FLCN protein in UOK-257 is associated with the altered regulation of Cofilin de/phosphorylation pathways.

Subtle effects on Cofilin phosphorylation from knockdown of SSH2 phosphatase by siRNA treatment in cell lines may be seen in the figures above. In normal cells, knockdown of SSH phosphatases would increase the phosphorylation of Cofilin, and this increased phospho-Cofilin would lead to increased stabilization of filament-actin. In the stainings carried out in UOK-257 cells without FLCN expression only a slight change in phosphorylation of Cofilin is seen following the knock down of SSH2 by siRNA treatment when compared to the luciferase siRNA control treatment. This suggested that in UOK-257 FLCN negative cells, there appears to be a change to the normal regulation of the phosphorylation and dephosphorylation pathways of cofilin which could be associated with the FLCN proteins absence.

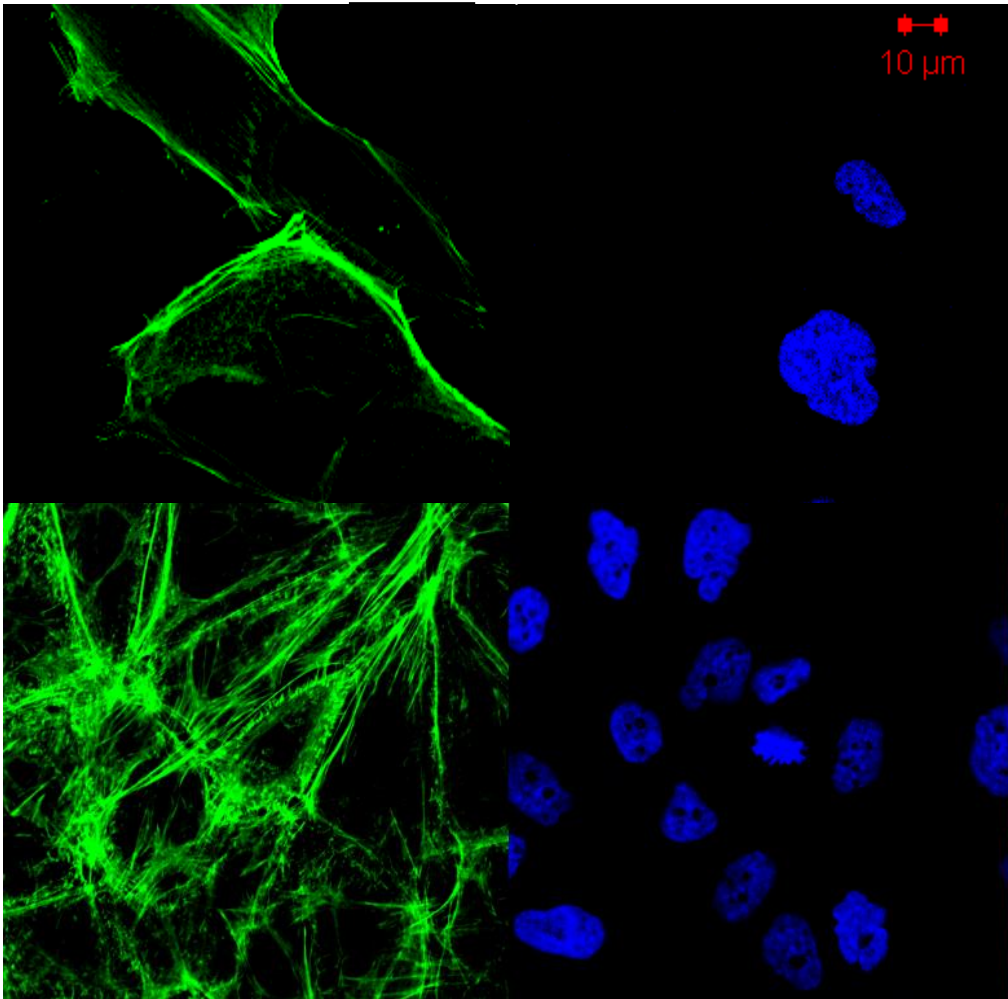


Fig 42: Top UOK-257 treated with SiRNA to luciferase. Bottom UOK-257 treated with SiRNA to SSH2 (phalloidine F-Actin Staining in green and DAPI nuclear staining in blue).

Fig 42 appears to show a small increase in actin accumulation associated with increased Phospho-cofilin, but, while unable to quantify the change per cell, the increase appears more likely to be in the region of up to 150% (reported increase for FLCN-ve cells, Lu et al. 2013) than 400% (reported increase for FLCN+ve cells, Lu et al. 2013).

The changes in Cofilin phosphorylation and filament-actin are small and subtle. Exactly how FLCN may be involved with this is still unknown, as is the possible compensatory regulatory

mechanism among members of SSH family suggested by observations that SSH2 siRNA-induced knockdown was accompanied by increased expression of SSH1 and SSH3, in Lu *et al.* (2013).

It was interesting to note when considering possible future therapeutic options and combinations thereof, that while it was shown by Lu *et al.* (2013) that changes to the cell cycle including S and G2M shortening, as well as G1 arrest, were brought about by siRNA treatment to knock down SSH2 in UOK-257 *FLCN*-negative cells, the results of the other potential therapy for BHD-RCC investigated, mithramycin treatment, showed a pattern change to cell cycle that was quite different. The changes induced by mithramycin included increases in both the population and the elongation time in G2M cell phase (Lu *et al.* 2013).

Chapter 8: Confocal microscopy to show the distribution of Miz 1 and Myc proteins in cells with absent mutated and normal FLCN.

In order to identify potential novel pathways linked to folliculin function, we decided to examine the distribution of FLCN and its putative interactor, the Myc-interacting zinc-finger protein-1 (MIZ-1), within the cells expressing and not expressing FLCN. MIZ-1 was identified by as a putative FLCN-interacting protein by Anne Reiman (unpublished data) working in our lab. After yeast two-hybrid analysis had suggested MIZ-1 as a candidate FLCN-interacting protein and co-immunoprecipitation studies done by Dr. Anne Reiman suggested that this interaction was real (see appendix), therefore it was decided to perform colocalization studies to determine if these were consistent with this conclusion.

The function of FLCN is not very well-defined, but the product of the *FLCN* gene has been linked to the regulation of signalling pathways including the AMPK, Transforming growth factor- β (TGF β), mTOR and hypoxia-responsive genes (see Reiman et al, 2012 and references within).

The cytokine TGF β is known to bring about epithelial cell division arrests by means of switching off the proto-oncogene *c-myc* and further interactions. Its critical cytostatic effects are vital for much of the epithelial tissue homeostasis known to happen. TGF β signal transduction defects have been reported in cancers of the pancreas, colon, breast, oral mucosa and other sites. The responses to the gene that are implicated in this process are complicated and diverse and how the response may be interrelated and mediated remains poorly understood (Seoane *et al.*, 2001).

Myc is a known cell growth mediator and heavily involved in proliferation, as well as repression and activation of transcription, depending on the nature of the factors associated with it. Both Myc messenger RNA and Myc protein are short-lived and *c-myc* transcriptional down-regulation by TGF β causes depletion of the cells' Myc protein and its growth-promoting functions in a short space of time (Seoane *et al.*, 2001). MIZ-1 was identified as a protein that recognizes certain initiator motifs, including core promoters with the sequence 5'-CCCACTCTGC. The amino-terminal BTB/POZ (BR-C, ttk, bab/ Pox virus, Zinc finger) domain near the N-terminus of a fraction of some zinc finger proteins, including in MIZ-1, could possibly mediate oligomerization. The central region of MIZ has twelve zinc-finger motifs that are capable of initiator motif binding for various Myc-repressed genes. The Myc-MIZ-1 complex has been shown to be important in some responses to TGF β , which would be sufficient to bring about rapid changes affecting cell-cycle progression (Seoane *et al.*, 2001).

The mutated *FLCN* constructs, 82 (Cys82Ala) and 85 (Cys85Ala) (where Cys in FLCN potential metal binding domain had been mutated to Ala by site-directed mutagenesis carried out by Uncaar Boora) were transiently transfected into HeLa cells or FTCs to ascertain if, in the presence of the mutation, there is still folliculin interaction with MIZ and other proteins. The constructs which were expressed were flag tagged FLCN 85 TGC >GCC changing a cystine to an alanine, and flag tagged FLCN 82 TGC >GCC changing a cystine to an alanine. We also transiently expressed a Flag tagged full length FLCN construct with no mutations, and an empty vector control.

Experiments carried out with the kind help of Dr. Anne Reiman with design and planning.

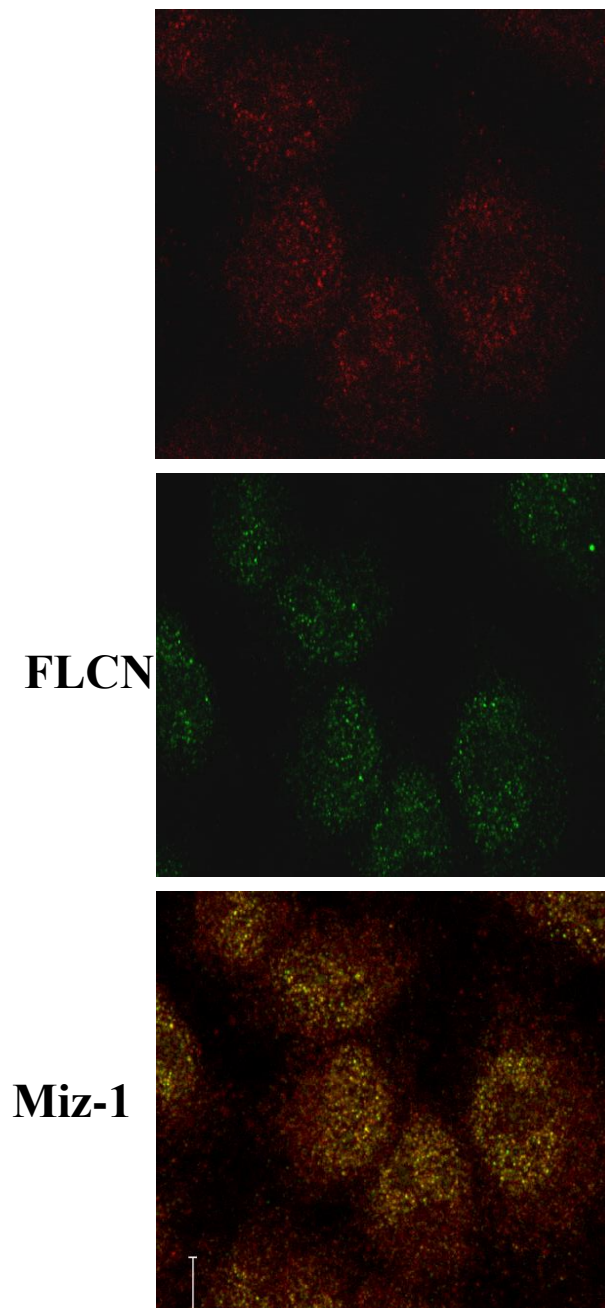


Fig 43: Immunofluorescence staining showing FLCN interaction with MIZ-1

Cells labeled with anti-FLCN alexa 633 in red (top panel and bottom merged panel), anti-MIZ-1 alexa 488 staining in green (middle panel and bottom merged panel). The yellow colour indicates apparent FLCN and Miz1 proximity and possible colocalization (bottom merged panel).

Some evidence of FLCN-MIZ-1 co-localization can be seen in images of immunofluorescence staining using anti FLCN alexa 488 seen in green, and anti MIZ alexa 633 seen in red, in HeLa cells which are wild type for both proteins, as shown in Fig 43. Upon examination of these images, it was decided that the greater resolution of confocal microscopy was needed for the accurate visualization of localization and co-localization within individual cultured cells.

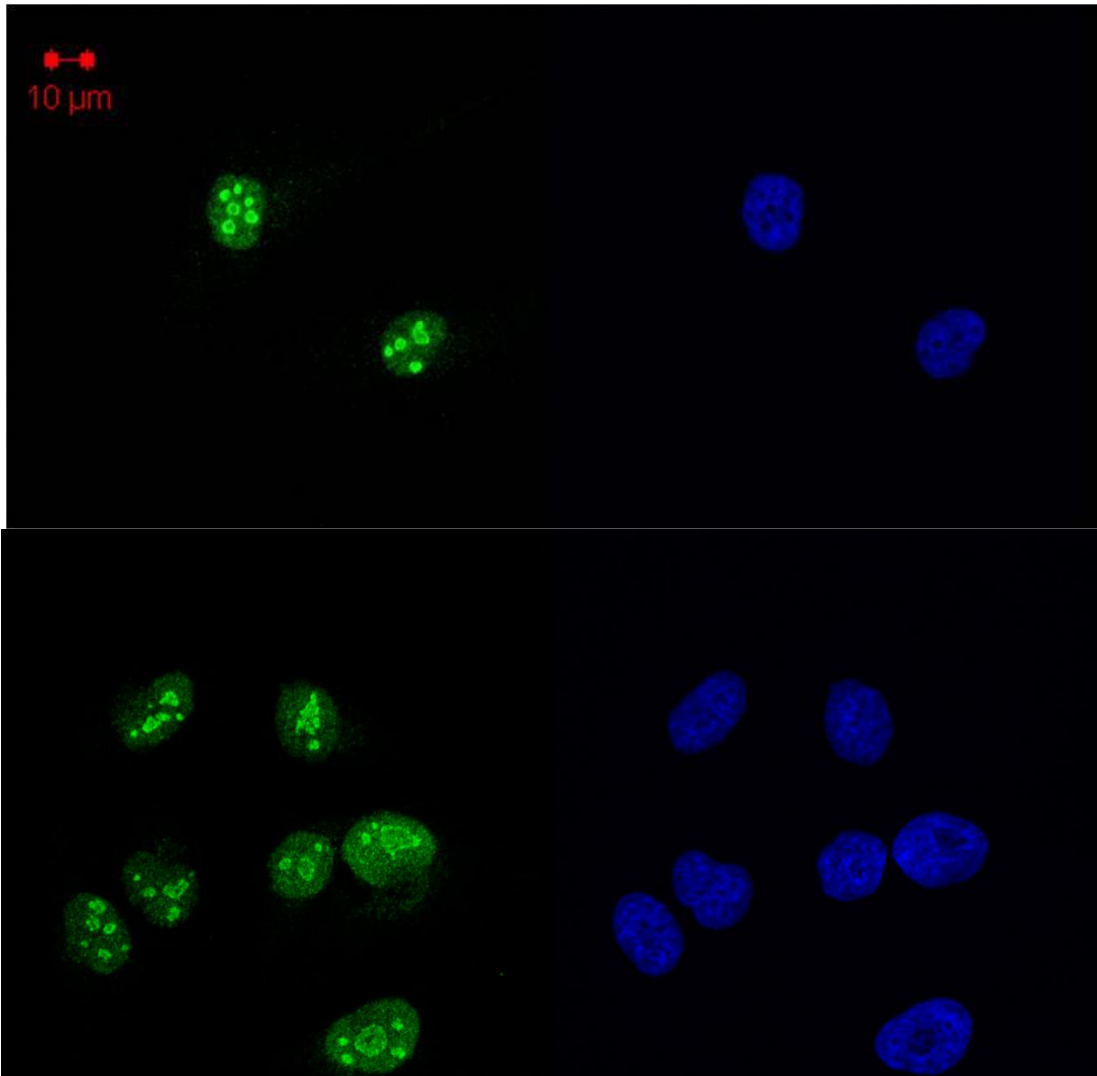


Fig 44: Top: FTC12 cells stained with anti-MIZ alexa 488 in green and DAPI nuclear stain in blue; Bottom: FTC22 cells stained with anti-MIZ alexa 488 in green and DAPI nuclear stain in blue.

Fig 44 shows that in FLCN negative FTC12 cells, MIZ is present in the nucleus and (in small amounts) in the cytoplasm. In the FTC22 cells, this is also the case. However, comparison of the two confocal microscopy images shows that the FLCN positive cells appear to show slightly more MIZ (although the change could not be quantified) in the Cytoplasm than FLCN negative

cells. This could indicate the possibility that interactions with FLCN may have an effect on MIZ distribution. The MIZ protein concentrates in specific areas (nucleoli) within the nucleus.

MIZ FLCN Interaction in ACHN (ATCC® CRL-1611™) cells.

We obtained ACHN renal carcinoma cells and ACHN cells with stable knockdown of FLCN (by shRNA) and a stable, scrambled control that were kindly donated by Professor Arnim Pause (McGill University, Montreal, Canada) and have been described in Hudon et al. (2010). The ACHN cell line was initiated in November 1979 and is derived from a renal cell adenocarcinoma, metastatic site: pleural effusion in a 22 year old male Caucasian patient. ACHN cells are FLCN positive. These cells are used here as a further example of renal cells with wild type FLCN to broaden the study of FLCN. Confocal microscopy of these cells provides clear evidence of a MIZ-FLCN interaction, as illustrated in Fig 45 below.

ACHN3 FLCN positive cells stained with MIZ shown in red and FLCN shown in green and DAPI nuclear stain shown in blue. The yellow areas show colocalization of Miz with folliculin and indicate likely interaction between the 2 proteins.

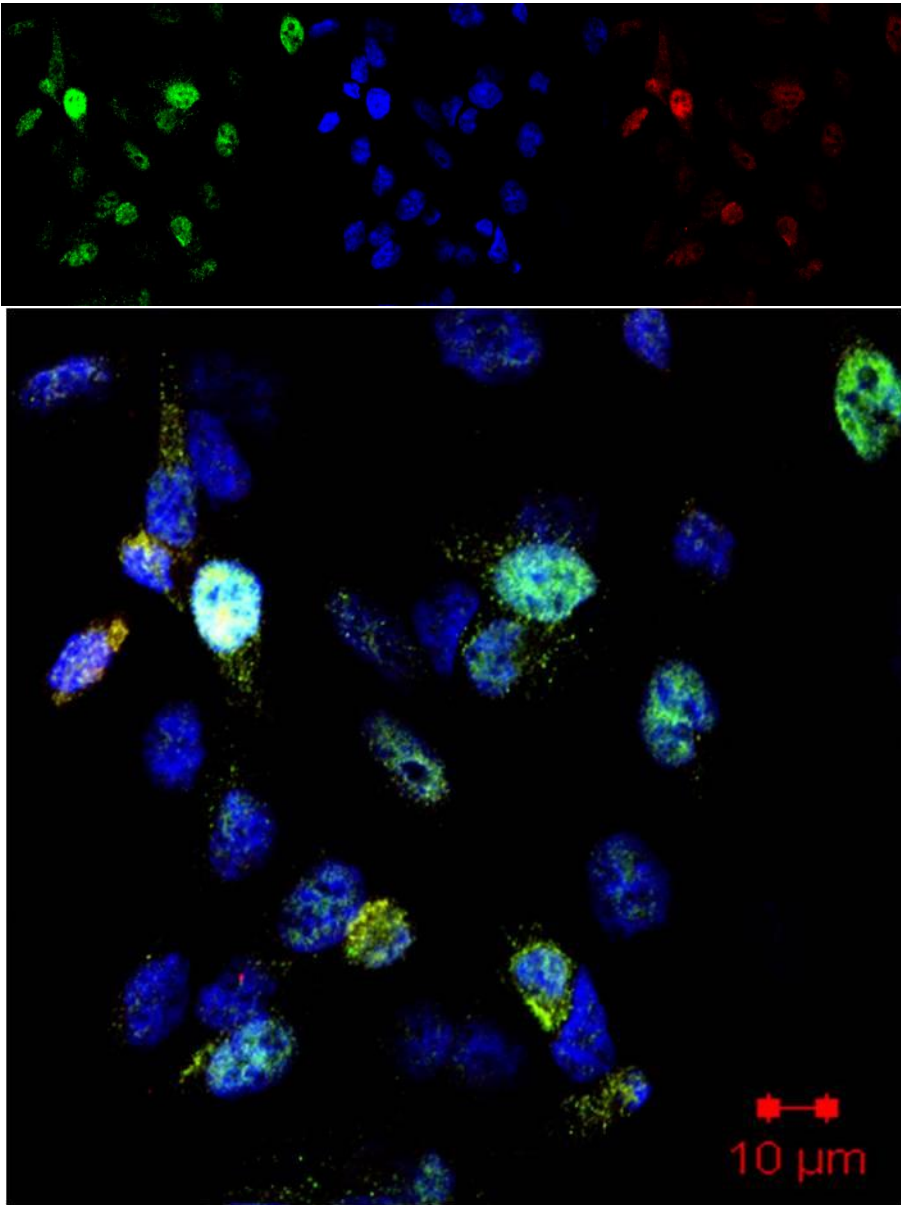
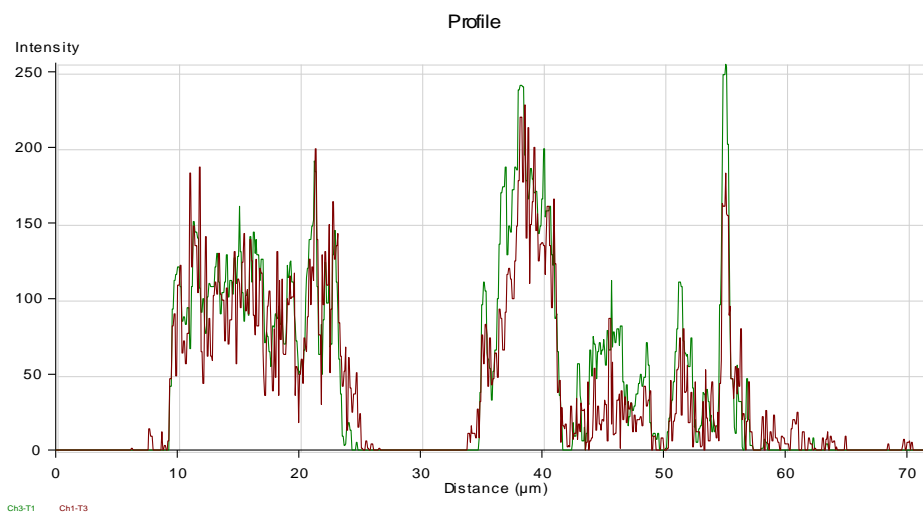
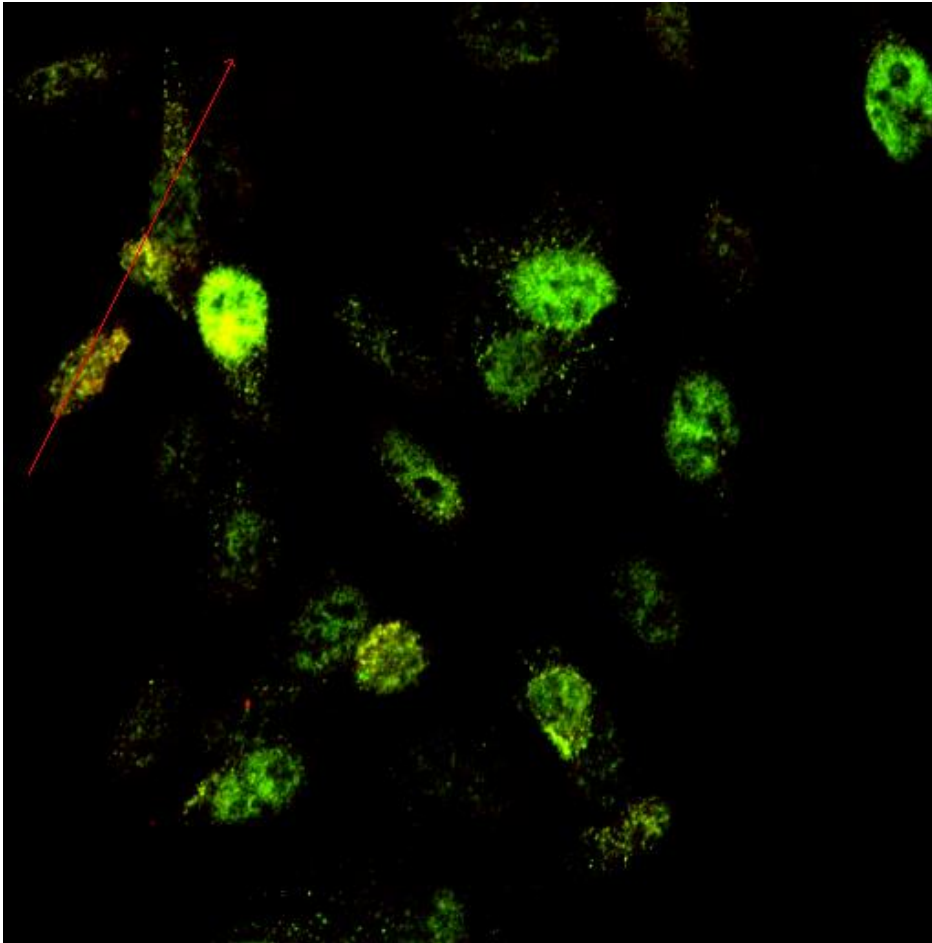


Fig 45: ACHN3 FLCN positive cells stained with anti-MIZ and anti-FLCN to show possible colocalization.

Anti-MIZ alexa 633 staining shown in red (top right) and anti-FLCN alexa488 in green (top left) and DAPI nuclear stain in blue (Top middle). The yellow colour indicates FLCN and Miz1 proximity and probable colocalization (bottom merged panel).



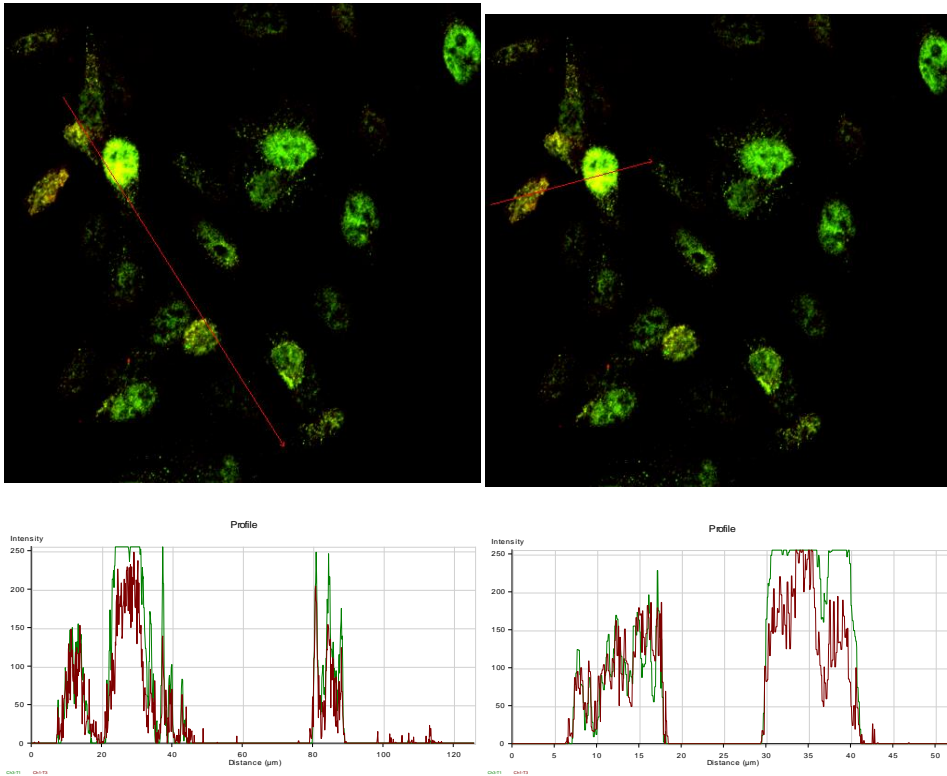


Fig 46 graphical analysis of fig 45 confocal image of ACHN3 FLCN positive cells stained with anti-MIZ and anti-FLCN to show possible colocalization.

Anti-MIZ alexa 633 staining shown in red (graph and merged image) and anti-FLCN alexa488 in green (graph and merged image). The FLCN and Miz1 proximity and probable colocalization indicated by yellow colour in the merged panel and overlapping red and green peaks in the graph.

The graph shows the intensity of each signal/protein at each point in the cell along the line indicated in red in the merged confocal image.

The graphs showing the analysis of the signal intensity of the 2 wavelengths shows that the peaks match closely. While most of the co-localisation occurs within the nucleus it can occur outside the nucleus as seen in the cell on the left of the picture above picture (figure 3 and 4) and the right of the figure below (figure 47 and 48).

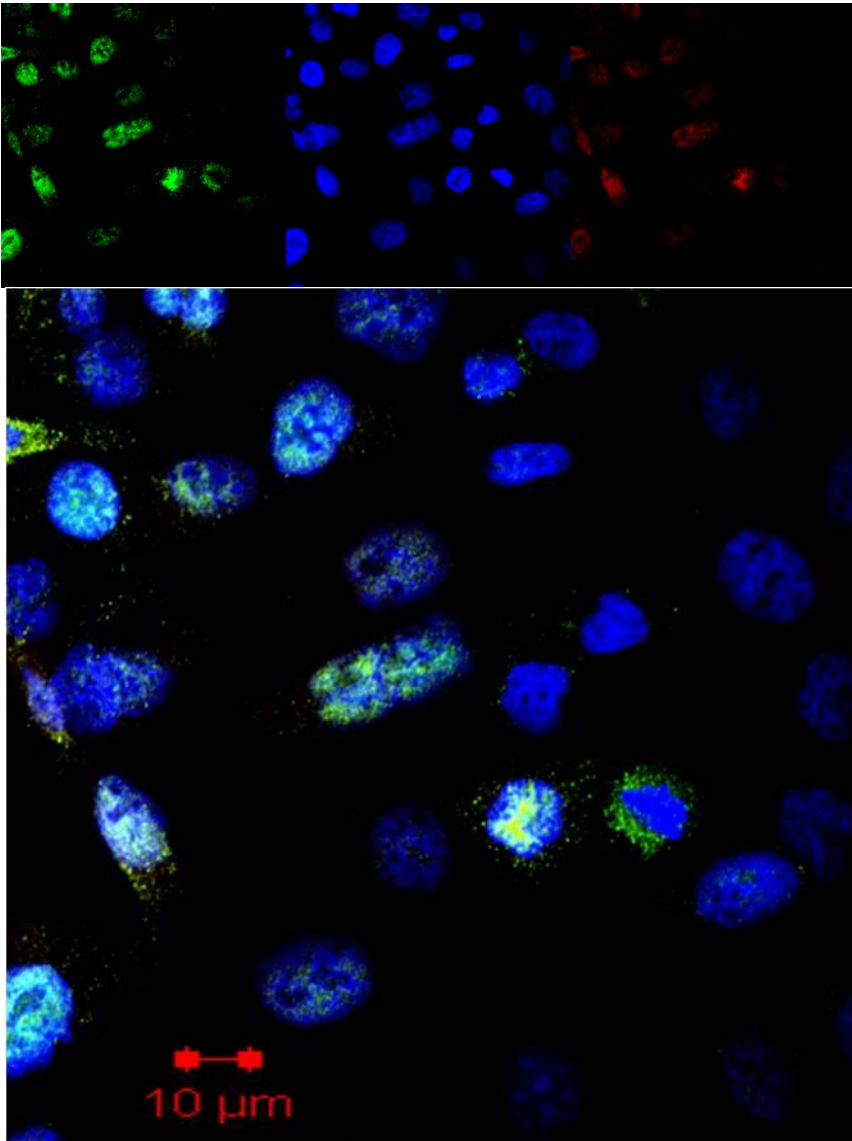


Fig 47: Confocal image of ACHN3 FLCN positive cells were stained with anti-MIZ alexa 633 and anti-FLCN alexa488 as well as DAPI nuclear stain to show possible colocalization.

The anti-MIZ alexa 633 staining is shown in red (top right and merged image). The anti-FLCN alexa488 is seen in green (top left and merged image) and DAPI nuclear stain in blue (top middle and merged image). The FLCN and Miz1 proximity and probable colocalization indicated by yellow colour in the merged panel.

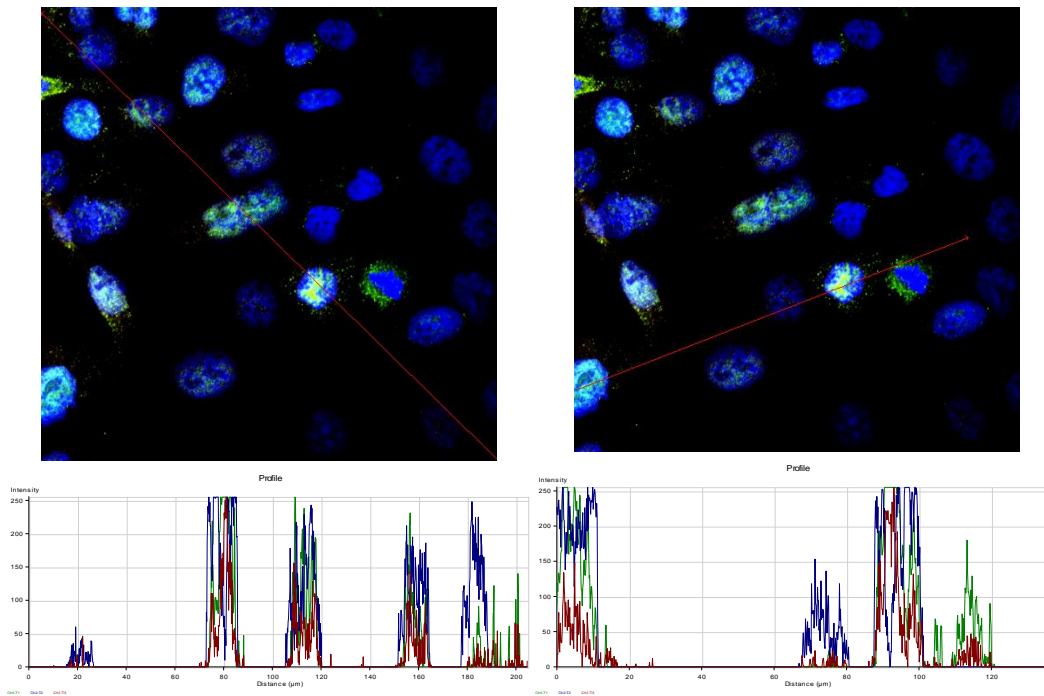


Fig 48: Graphical analysis of the confocal image of ACHN3 FLCN positive cells were stained with anti-MIZ alexa 633 and anti-FLCN alexa488 as well as DAPI nuclear stain to show possible colocalization.

Anti-MIZ alexa 633 staining shown in red (graph and merged image), anti-FLCN alexa488 in green (graph and merged image) and DAPI nuclear stain in blue (graph and merged image). The FLCN and Miz1 proximity and probable colocalization indicated by yellow colour in the merged panel and overlapping red and green peaks in the graph. The graph shows the intensity of each signal/protein at each point in the cell along the line indicated in red in the merged confocal image.

Clear evidence of MIZ – FLCN interaction can be seen in Fig 48. The MIZ is mostly in the nucleus and the mutant FLCN is in the nucleus and in the cytoplasm. The graphs showing the

analysis of the signal intensity of the 2 wavelengths shows that the peaks match closely. The inclusion of the DAPI stain in this analysis shows more clearly that while most of the co-localisation occurs within the nucleus, it can also occur outside the nucleus as seen in the cell towards the right which appears as if it may be undergoing cell division.

We continued our investigation of FLCN and MIZ protein localization with the transient transfection of different constructs into FTC12 FLCN negative cells and comparison of the different states.

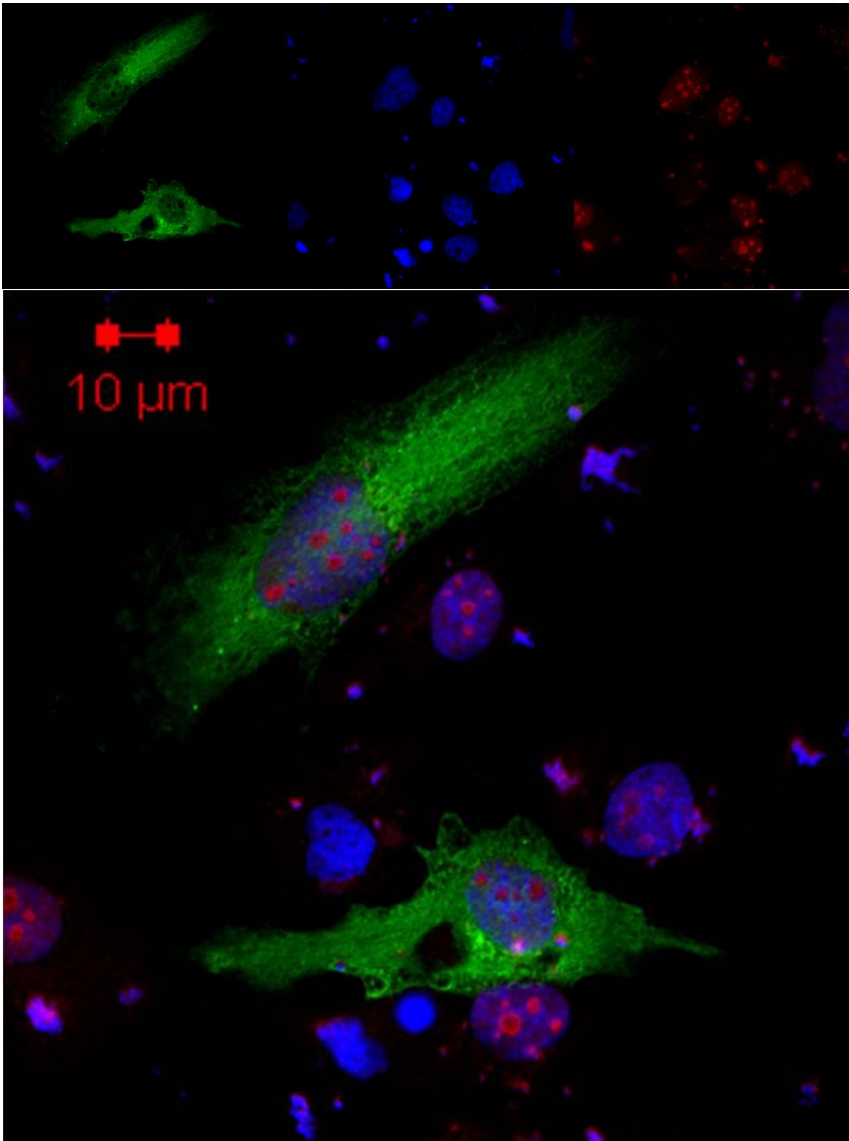


Fig 49: FTC 12 cells transiently transfected with construct 82. The cells were later stained with anti-Flag alexa 488 and anti-MIZ alexa633 as well as DAPI nuclear stain.

The anti-MIZ alexa 633 staining is shown in red (top right and merged image). The anti-Flag alexa488 is seen in green (top left and merged image) and DAPI nuclear stain in blue (top middle and merged image).

Fig 49 shows that in FTC12 cells transiently transfected with construct 82 (full length FLCN with a Cys82Ala mutation), the mutant FLCN and the MIZ don't appear to interact in this instance. The MIZ is seen as a red punctuate staining and in the corresponding locations there is a lack of green alexa 488. The images show no interaction happening in the cell at the time of fixation.

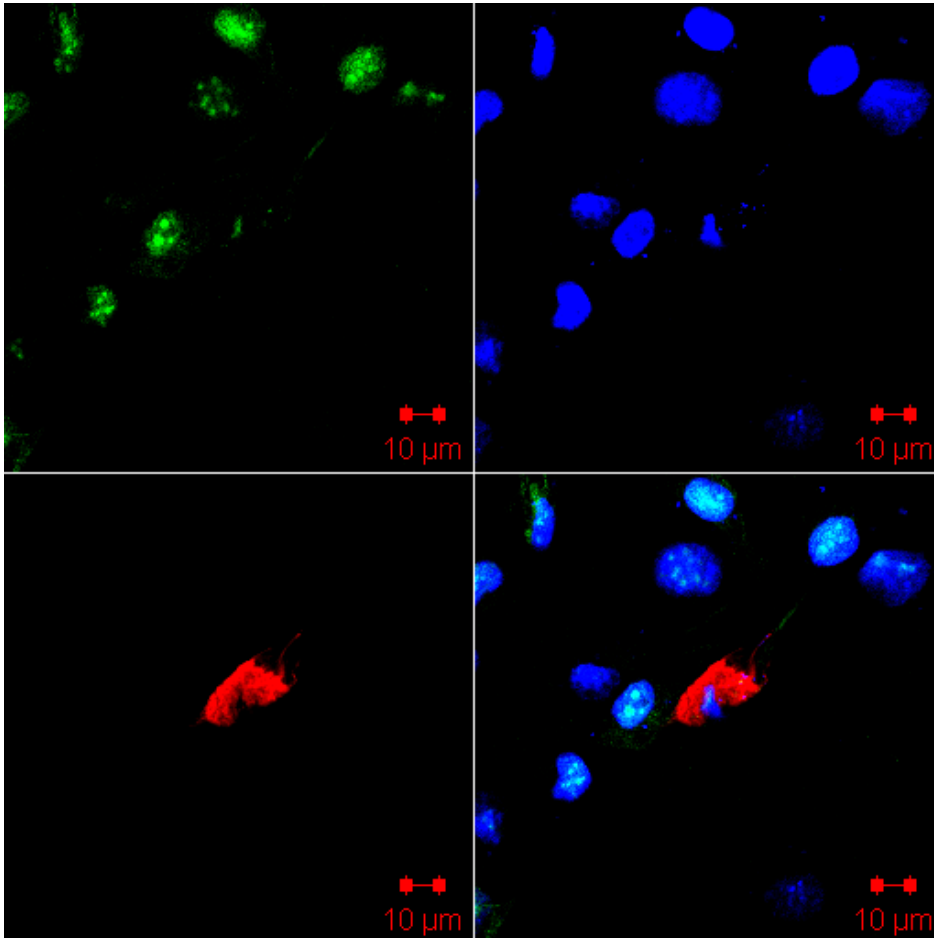


Fig 50: FTC 12 cells transiently transfected with constructs 82. The cells were later stained with anti-Flag alexa 633 and anti-MIZ alexa488 as well as DAPI nuclear stain.

The anti-Flag alexa 633 staining is shown in red (bottom left and bottom right merged image). The anti-MIZ alexa488 is seen in green (top left and merged image) and DAPI nuclear stain in blue (top right and merged image).

In agreement with Fig49 no evidence of MIZ – FLCN interaction can be seen in Fig 50. The MIZ is mostly in the nucleus and the mutant FLCN is mostly in the cytoplasm.

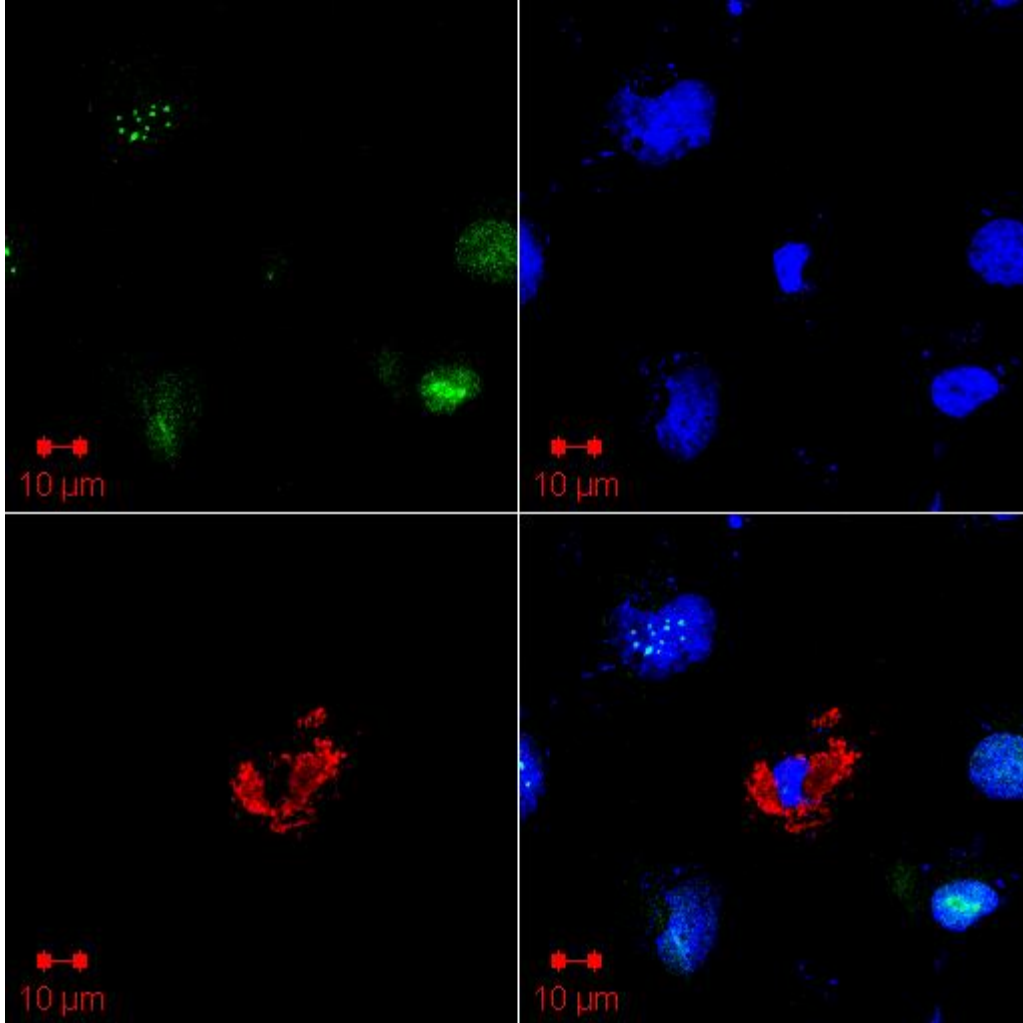


Fig 51: FTC 12 cells which were transiently transfected with constructs 82. The cells were later stained with anti-Flag alexa 633 and anti-MIZ alexa488 as well as DAPI nuclear stain.

The anti-Flag alexa 633 staining is shown in red (bottom left and bottom right merged image). The anti-MIZ alexa488 is seen in green (top left and merged image) and DAPI nuclear stain in blue (top right and merged image).

No evidence of MIZ – FLCN interaction can be seen in this case. The MIZ is mostly in the nucleus and the mutant FLCN is mostly in the cytoplasm.

Figures 49, 50 and 51 demonstrate that there is no evidence of FLCN 82 co-localization with MIZ. This does not rule out the possibility of such interaction, but my results suggest that the Cys82Ala mutation may affect FLCN/Miz-1 interaction.

Fig 52: Top: FTC12 cells stained with anti -MYC alexa 594 in red and DAPI nuclear stain in blue.

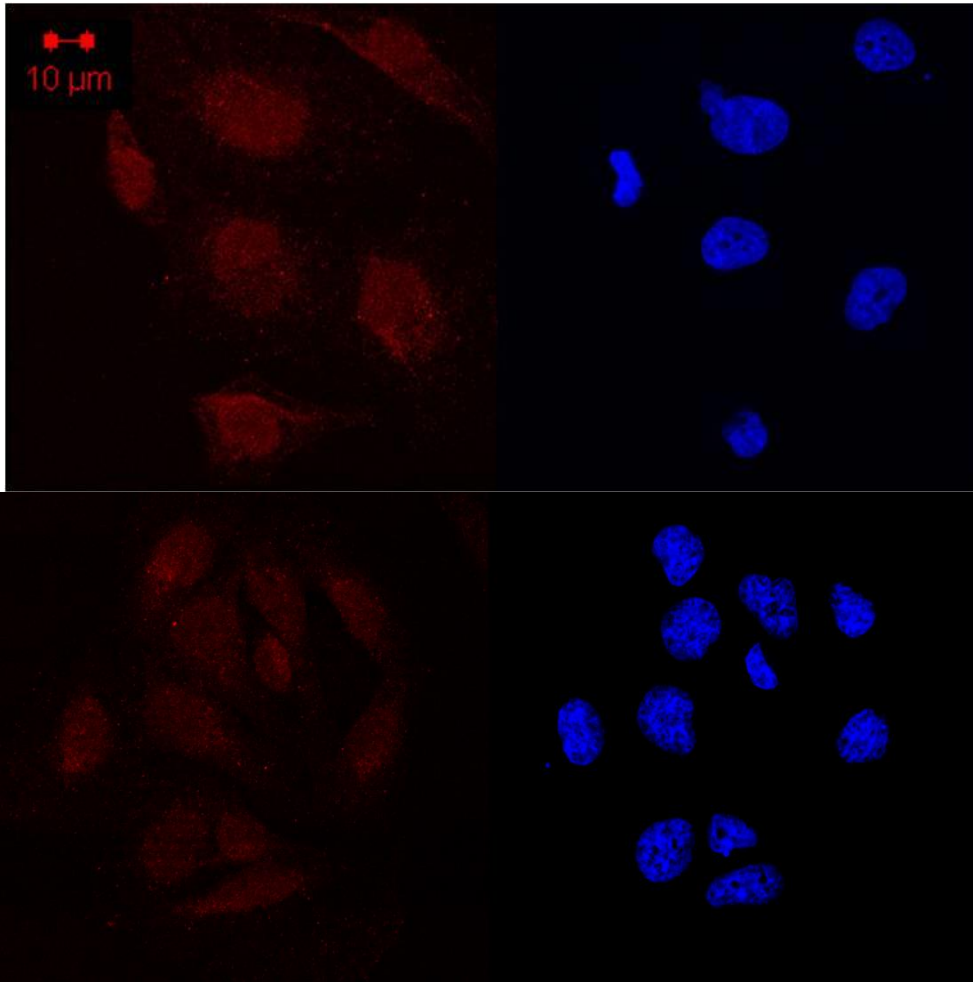


Fig 52: Bottom: FTC22 cells stained with anti -MYC alexa 594 in red and DAPI nuclear stain in blue. Myc is present in the nucleus and in small amounts in the cytoplasm in both FLCN positive and negative FTC cells with little difference to be seen between the two states.

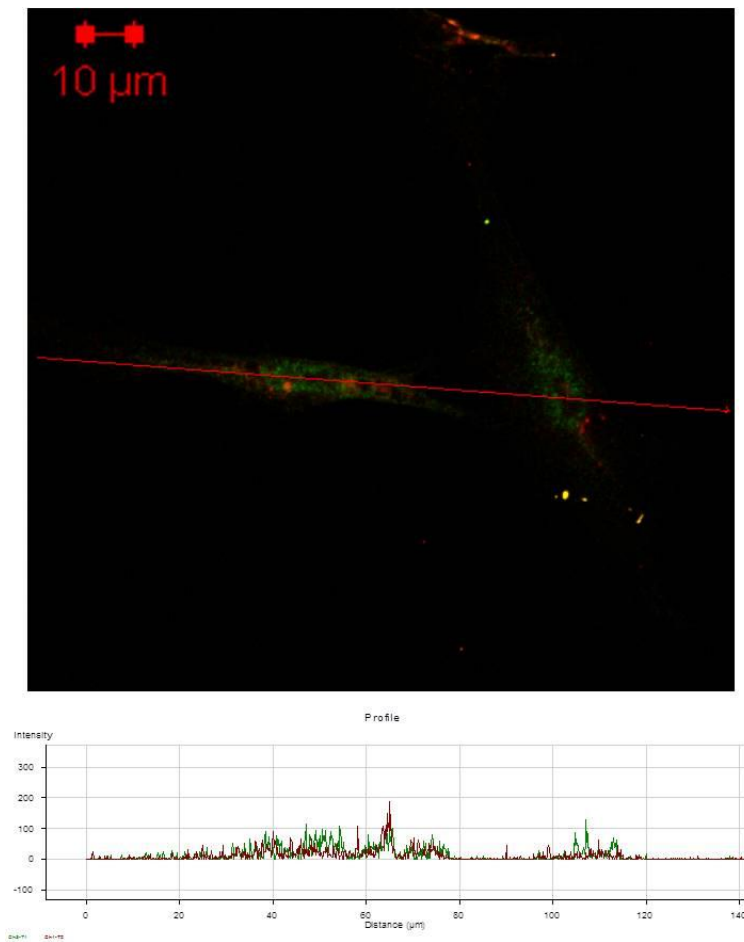


Fig 53: Merged image of FLCN positive cells stained with anti-FLCN alexa 488 and anti-MYC alexa 594

The anti-MYC alexa 594 staining is shown in red (graph and merged image). The anti-FLCN alexa488 is seen in green (graph and merged image) and DAPI nuclear stain in blue (graph and merged image).

The graph shows the intensity of each signal/protein at each point in the cell along the line indicated in red in the merged confocal image.

In Fig 53 the graph shows the relative intensities of green and red signal along the line through the image. Green and red peaks at the same point indicate probable proximity of the proteins in the cell. This suggests that the proteins are in the same location within the cell and that they may interact or possibly be functionally related.

Chapter 9: Discussion

Xiaohong Lu and Wenbin Wei used the COMPARE algorithm to find candidate anticancer compounds, tested on the NCI-60 cell line panel, that show preferential cytotoxicity to cell lines expressing low levels of active FLCN protein. Fifteen chemicals were selected for their differential sensitivity being more effective in cells with low FLCN expression than in cells with high FLCN expression. From these compounds, various techniques were used to identify those which might impair the viability of a RCC folliculin negative cell line more severely than a wild type.

The main screening method chosen for the screening of the compounds was the SRB growth inhibition assay, as it had been used by members of the lab for a substantial period of time and had been believed by them to be a robust and cost-effective method of obtaining the information needed.

Initially the choice of cells to be experimented on was difficult, and many of the experiments were carried out in systems that were less than ideal. Comparable lines were needed with positive and negative *FLCN* status. These were eventually obtained in the form of the UOK257 cell lines, but prior to that, attempts were made to use siRNA knock-downs in FLCN positive RCC cell lines.

We detected differential sensitivity of FLCN negative UOK257 cells over FLCN positive UOK257-2 cells for 7 chemicals. Mithramycin was the most notable drug as it showed about a 10-fold change in the value of the GI_{50} between FLCN negative UOK257 cells and FLCN positive

UOK257-2 cells. The compound also produced an increase in cytotoxicity (nearly 10-fold more) in FLCN negative UOK257 cells when compared to FLCN positive UOK257-2 cells (clonogenic survival assay, 200 nmol/L), as well as inducing the activity of caspase 3/7 in FLCN negative UOK257 cells preferentially in a manner that was dose-dependent. Preliminary tests of compounds were made in other cell lines, but these systems were not ideal. In the absence of any other FLCN negative RCC cell lines, attempts were made to knock down FLCN in FLCN-containing cells. Each of the lines available at the time in the lab were tested in turn to identify the best system. They all offered some insight into the differences in response of different cancer cells to drug treatments, but none were satisfactory as the method of transient siRNA knockdown was unsuitable for producing a uniform population of FLCN null cells. FTC133 cells were obtained which were useful but at the time of the first experiment had no comparable FLCN positive line. This problem was later solved by the stable transfection of *FLCN* into FTC133 clones for use in the later experiments, which were useful for comparison and gave insight into FLCN in non-renal cancers.

The only RCC cell line that is derived from a patient with BHD available to date is UOK-257, and no homozygous FLCN negative sporadic RCC cell lines could be found during the time of this study. In wild-type FLCN containing sporadic RCCs (SKRC47 cells and CaKi cells, RCC Cell lines with wild type FLCN) knockdown of the expression of FLCN by siRNA, in our hands, was not 100% effective, making these models unsuitable for producing comparable findings or supporting the work in FLCN negative UOK257 cells and FLCN positive UOK257-2 cells. The results were hard to interpret and not very robust. Furthermore, this approach did not replicate the

situation in BHD syndrome in which inactivation of folliculin is the event which initiates tumorigenesis.

While FTC133 cells are FLCN negative, the fact that they derive from a thyroid metastasis gives rise to different properties and behavior. Sensitivity to mithramycin was not seen to correspond to the cells' expression levels for FLCN. Several explanations for this are possible.

Firstly, co-existing epimutations or mutations in oncogenes or other tumour-suppressor genes may alter the response of a cell line which is *FLCN*-negative to treatment by Mithramycin. Also in the thyroid carcinoma FTC-133 cell line *FLCN*, inactivation may have occurred at a late stage of tumorigenesis and as such lead to different functional consequences compared to UOK257 cells (BHD RCC), in which *FLCN* inactivation is an initiating step.

Thirdly, the cell tissue type may affect the functional consequences of inactivating a tumour suppressor gene (e.g. in RCC cell lines, hypoxic induction of HIF-2 expression or *VHL* inactivation induces oncogenic *CCND1* expression but in cancer cell lines other than RCCs *CCND1* expression is not hypoxia-inducible.) The very specific nature of the inherited cancer syndrome-associated cancer-susceptibility phenotypes, such as BHD syndrome and VHL disease, may possibly be explained in this way.

Thus, ideally, the experiments in UOK-257 cells would be replicated in additional FLCN-null RCC cell lines from BHD patients if they were to become available.

It must be noted that, using a strategy for differentially acting drug candidate identification similar to that used by myself and Lu et al. , Sutphin *et al.* identified 10 chemicals using the

COMPARE algorithm that showed differential activity against NCI60 cell lines expressing VHL at low and high levels. Of these compounds, four were tested against paired RCC cell lines of VHL positive and VHL negative types and it was seen that differential toxicity was shown in clonogenic survival studies by Chromomycin A3 (ChA3), to VHL-negative cell lines compared to VHL-wild type RCC cell lines.

ChA3 inhibits transcription when it binds in the minor groove of DNA. It is an aureolic acid compound, but unlike Mithramycin (also an aureolic acid), no differences between the growth inhibitions of ChA3 in UOK-257 FLCN negative cell lines were found when compared to FLCN positive cells. GC-rich regions of DNA are bound by Mithramycin which inhibits the gene transcription if promoters are rich in GC- residues, and several types of cancer, including leukaemia and testicular carcinoma have been treated using Mithramycin (Yuan P *et al*). Low doses of rapamycin (1nM) increased Mithramycin's selective inhibition of FLCN negative cell proliferation. It has been noticed that the presence or absence of wild type p53 in a cell may play an important part in Mithramycin-induced cell polyploidy modulation of the death of cells in colon carcinoma (Bataller *et al*). A novel analogue of Mithramycin, Mithramycin SK (MSK), in HCT116 cells with wt p53 results in polyploidization and mitotic catastrophe and death by necrosis in the majority of cell populations, but early p53-independent apoptosis from G2M block was the primary cause of death in HCT-116 (p53^{-/-})cells. Therefore it may be worth considering the possibility that UOK-257 (with p53 gene inactivation) cells' response to exposure to Mithramycin, could also be death by apoptosis when arrested in G2M block involving a p53-independent pathway. This is supported by Xiaohong Lu's cell cycle analysis results, which

reported that UOK257-FLCN⁻ cells showed an S and G2M phase arrest of the cell cycle in response to exposure to Mithramycin. Rapamycin at a low dose (1nM) potentiated Mithramycin sensitivity strongly by increasing the tendency to arrest in G2M. In *FLCN* positive cells, Mithramycin induced little G2M cell cycle arrest.

Caspase 3 (cysteine-aspartic acid protease 3) is the protein which is encoded by the gene *CASP3*. Caspase3 exists in an inactive pro-enzyme form that is processed by proteolytic enzymes to form the active Caspase3, which was detected by the antibodies in the blot of the FLCN positive cells. Activation of Caspase3 plays a crucial role in bringing about and controlling cell death by apoptosis.

Though the FLCN has been linked to the regulation of a variety of signalling pathways (e.g. the hypoxia-responsive genes, mTOR, TGFbeta and AMPK), the function of the FLCN protein is still far from fully defined. In order to improve the understanding of its function, other members of the lab tested UOK257, FTC 12 and FTC22 cells in gene expression and protein (Kinexus) arrays (Reiman *et al.* 2012). This revealed 5 targets that were expressed differently in all data sets dependant on FLCN status. Among these was CASP1 (Caspase 1), which was reduced in FLCN negative cells

Taking into account the importance of CASP1 in apoptosis and our labs data, which showed a markedly higher level of active Caspase3 in FLCN⁺ - compared to UOK257-FLCN⁻ - cells(Lu et al.2013), other apoptosis related proteins were investigated, with regard to FLCN expression effects. This found increased levels of SMAC/Diablo and HtrA2 in FLCN positive cells (Reiman et al 2012).The figure below shows pathways involving SMAC/Diablo and HtrA2 by which

further effects may occur.

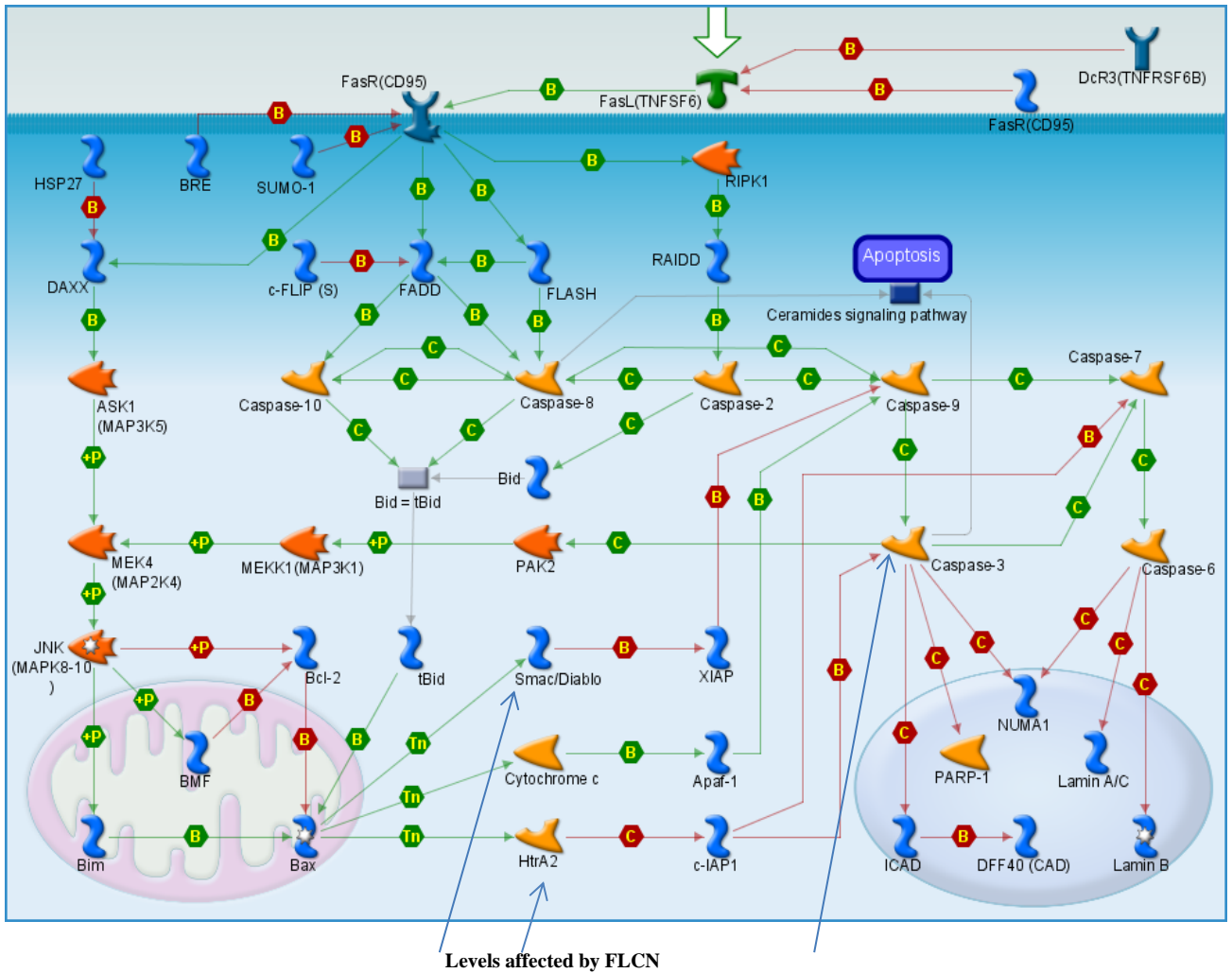


Fig 54: Apoptosis and survival_FAS signaling cascades

(Main diagram found from <http://pathwaymaps.com/maps/418/> © 2013 Thomson Reuters)

In both sporadic and familial cases it is difficult to treat metastatic kidney cancers. Patients may still only be diagnosed after presentation with advanced RCC even though renal imaging is offered on an annual basis to enable early RCC detection for patients with BHD syndrome

(Menko et al 2009). Some patients may respond to immunotherapy with the cytokines interleukin-2 and interferon but this is not frequent. Recently the most frequent management strategy has emerged as treatment with therapies (e.g. Sunitinib, Sorafenib, Bevacizumab, etc) to targeted HIF downstream targets and the mTOR pathway (e.g. Everolimus Temsirolimus,). These agents however are not cytotoxic: while they do prolong life, the identification of targeted cytotoxic agents would be a significant advance. Therefore the investigation of Mithramycin as a potential treatment for FLCN deficient RCC is of considerable interest.

After the phosphatase siRNA library screen by Xiaohong Lu in *FLCN*-null UOK257 cells, Slingshot 2 serine phosphatase (*SSH2*) was identified as a possible synthetic lethal candidate gene for FLCN. *SSH2* knockdown preferentially induced activation of Caspase3/7 in the *FLCN*-null FTC133-12 thyroid carcinoma cell line and the *FLCN*-null BHD syndrome UOK257 cell line compared with the relevant isogenic FLCN-expressing counterpart line FTC133-22 and UOK257-2 respectively.

By contrast, the other two Slingshot family members *SSH1* and *SSH3* did not show similar patterns as seen with *SSH2* when knocked down, although a compensatory regulation mechanism in transcripts and proteins was indicated among members of *SSH* family. Multiple knockdown of *SSH1* and / or *SSH3* potentiated *SSH2* siRNA activity in both cell cycle kinetics and induction of Caspase3/7 in *FLCN*-null cells, thus providing indications that Caspase3/7 activation brought about by *SSH2* knockdown induced siRNA- treatment is not a general Slingshot gene family feature, but is an event specific to *FLCN*-null FTC133-12 and UOK257 cells. (Lu et al 2013)

Having already found Caspase3/7 activity to be induced preferentially in FLCN-deficient UOK257 cells following mithramycin treatment it is worth noting that in contrast to *SSH2*

knockdown, no preferential effect was apparent in FLCN-deficient FTC133. It is thought that *SSH2*-knockdown induction of Caspase3/7 activation by is mediated by a cell death pathway that is p53-independent, as *p53* mutations have been identified in UOK257 and FTC133 cells. (UOK257: C.153C>T mutation resulted in an early truncation of P53 protein. FTC133: point mutation of P53 gene led to inactivation of P53 function by accumulation of the protein.)

In Lu *et al* 2013, evidence of cofilin phosphorylation and de-phosphorylation dysregulation, or differences in folliculin deficient cells, was shown, but this dysregulation could be partly recovered in FTC133 cells, or fully in UOK257 cells, by folliculin replacement as seen in their folliculin-expressing counterparts FTC133-22 and UOK257-2. Here I have shown immunofluorescent images of these effects in the UOK257 cells, and also evidence of the cytotoxic effects as demonstrated by the effect on colony forming ability in FTC133 cells.

The involvement of LIM-kinases and phosphatases of the Slingshot family in filament-actin stabilization / activation by cofilin phosphorylation and de/phosphorylation is interesting. Links between the function of actin in the cytoskeleton and the function of folliculin had not been seen before (Lu *et al* 2013), where we note that siRNA knockdown *SSH1/2* and *PDXP* phosphatases, known regulators for phosphorylation of cofilin, can be associated with reduction in FLCN protein expression and transcript of FLCN in the cells examined (data not shown). Inverse expression patterns between FLCN and SSH3 proteins and transcripts in UOK257 and ACHN cells have been seen (data not shown) which are interesting to note. *SSH2* siRNA knockdown (and the knock down of other Slingshots) was seen to be accompanied by a reduction in expression of FLCN protein, even though no clear relationship was found between basal levels of *FLCN* and *SSH2* in the examined cells. The preferential sensitivity to *SSH2* knock down by

siRNA treatment in folliculin-deficient cells could occur because of the abnormal functioning of actin as well as slingshot family dysregulation. There is a possibility that the functional relationship between SSH2, folliculin and cell death could relate to functions of SSH2 that are independent of cofilin. The diverse functions reported for cofilin have included cytochrome c release and Bax translocation to mitochondria during excitotoxic neuronal death as well as modulation of actin dynamics (Bernstein *et al* 2010, Posadas I *et al* 2012).

The heterogeneous groups of disorders that are represented in human cancers are associated with tumour suppressor gene inactivation and oncogene activation. The development of targeted cancer therapies by targeting the activation of an oncogene is more straightforward, in general, than correcting the inactivation of a tumour suppressor gene. A practical approach for novel targeted therapy development to improve the management of kidney cancers could be provided by this route of synthetic lethal interaction identification (Reinhardt *et al* 2009, Kaelin *et al* 2009, Kaelin *et al* 2005), as was shown by the developments for p53 and *BRCA1/2* (Reinhardt *et al* 2007, Fong *et al* 2009).

Finding a synthetic lethal target candidate (*SSH2*) for cells that lack folliculin suggests that a possible option for developing new drugs for BHD syndrome targeted molecularly, and possibly for some RCCs of a sporadic nature, could be small molecular weight compounds developed to target the activity of SSH2 phosphatase in the future.

Investigation of the evolutionary conservation patterns of the *FLCN* sequence have shown them to be consistent with the slow evolution of folliculin protein under a purifying selection which is stronger than most genes (Nahorski, *et al.*, 2011). The early part of the gene (the first 230 codons approximately) showed the purifying selection and slower evolution more strongly. Non-

synonymous mutations throughout the protein sequence have been predicted to be potentially pathogenic. To date, of the mutations described in *FLCN*, more than half have been predicted to truncate the protein prematurely (Lim, *et al.*, 2010), but putative pathogenic missense mutations were not restricted to specific folliculin protein domains. The pathogenicity of missense mutations analyzed seemed to be by means of folliculin stability disruption. These observations could be consistent with the hypothesis that folliculin has multiple functions and mutations that will compromise multiple aspects of folliculin function result in BHD syndrome. Folliculin functions are not well characterized to date. FNIP1 and FNIP2, the two folliculin interacting proteins reported, bind to folliculin carboxy-portion (a region beyond codons 516 and 362 respectively) (Takagi *et al.*, 2008; Baba, *et al.*, 2006). A domain between codons 100 to 230 is apparently highly conserved, and this domain might contain folliculin interacting proteins binding sites for as-yet unidentified interactors, or could be of great importance for the proteins' structural integrity.

Using bioinformatic software, an extensive search was performed (Nahorski, *et al.*), with the aim of identifying the folliculin proteins' structural homologues. A KOG3715 domain was seen to be carried in the N-terminus of the folliculin protein which spanned the amino acids around 100-230. No domain super-family is assigned to the KOG3715 domain and the domain structure has not been found to date. Although sequences of distant homologues have been found, the LST7 (Lethal with Sec thirteen protein 7) protein in *Saccharomyces cerevisiae* is the only one with an annotation. This yeast protein is required for the nitrogen-regulated transport of some amino acid permeases from the Golgi to the cell surface (Roberg, *et al.*, 1997). At a size of only 242 amino

acids, the LST7 protein is the smallest evolutionarily-functional folliculin protein and is smaller than the human folliculin by a large margin.

A range of missense/IFD (in frame deletion) mutations (p.Phe157del, p.His255Pro, p.Arg239Cys, p.Glu510del p.Lys508del and Arg362Cys), were reported to be scattered across the whole folliculin protein, with the potential to impair the protein stability in mutated folliculin protein. In medical genetics, identifying whether an IFD or missense variant is an unusual polymorphic variant or a pathogenic mutation is a recurring obstacle to be overcome. The majority of the missense/IFD variants examined in Nahorski, et al., 2011, caused impaired protein stability. In unpublished experiments, I investigated the effects of a missense substitution in the amino-terminal region of folliculin (Cys82Ala), on the ability of folliculin to co-localize with a selection of proteins. I showed co-localization with wild type folliculin and Miz and found some indications that the Cys82Ala substitution might interfere with the colocalisation of folliculin and a candidate interacting protein. This observation is consistent with the hypothesis that amino acid residues in the amino-terminal region of folliculin are implicated in folliculin function.

FLCN is a tumour suppressor gene (Vocke, *et al.*, 2005), and reintroducing the wild-type protein into null cells has been shown to bring about tumour inhibition in nude mice xenografts (Hong, *et al.*, 2010).

To date the function of the FLCN protein has not been fully defined. If FLCN is shown to exert tumour suppressor activity via a single function then modulation of the relevant pathway might represent a promising therapeutic strategy for BHD-related tumours. However, the experiments

described here which involve a more unbiased screening approach also provide a strategy to developing novel treatments for the disorder.

References

Alnemri ES, Livingston DJ, Nicholson DW, Salvesen G, Thornberry NA, Wong WW, Yuan J (October 1996). "Human ICE/CED-3 protease nomenclature". *Cell* 87 (2): 171. doi:10.1016/S0092-8674(00)81334-3. PMID 8861900.

Baba M, Hong SB, Sharma N, Warren MB, Nickerson ML, Iwamatsu A, Esposito D, Gillette WK, Hopkins RF 3rd, Hartley JL, Furihata M, Oishi S, Zhen W, Burke TR Jr, Linehan WM, Schmidt LS, Zbar B. 2006, Folliculin encoded by the BHD gene interacts with a binding protein, FNIP1, and AMPK, and is involved in AMPK and mTOR signaling. *Proc Natl Acad Sci U S A.* 2006;103:15552-7

Masaya Baba , Mutsuo Furihata , Seung-Beom Hong , Lino Tessarollo , Diana C Haines , Eileen Southon, Vishal Patel, Peter Igarashi, W. Gregory Alvord, Robert Leighty, Masahiro Yao, Marcelino Bernardo, Lilia Ileva, Peter Choyke, Michelle B. Warren, Berton Zbar, W. Marston Linehan, Laura S. Schmidt Kidney -Targeted Birt-Hogg-Dubé Gene Inactivation in a Mouse Model: Erk1/2 and Akt-mTOR Activation, Cell Hyperproliferation, and Polycystic Kidneys jnci.oxfordjournals.org JNCI Vol. 100, Issue 2 | January 16, 2008

Baba M, Keller JR, Sun HW, Resch W, Kuchen S, Suh HC, Hasumi H, Hasumi Y, Kieffer-Kwon KR, Gonzalez CG, Hughes RM, Klein ME, Oh HF, Bible P, Southon E, Tessarollo L, Schmidt

LS, Linehan WM, Casellas R. *Blood*. 2012 Aug 9;120(6):1254-61. doi: 10.1182/blood-2012-02-410407. The folliculin-FNIP1 pathway deleted in human Birt-Hogg-Dubé syndrome is required for murine B-cell development.

Bataller, M., et al., Mitramycin SK modulates polyploidy and cell death in colon carcinoma cells. *Mol Cancer Ther*, 2008. 7(9): p. 2988-97.

Bernstein BW, Bamburg JR. ADF/cofilin: a functional node in cell biology. *Trends Cell Biol* 2010; 20: 187–195.

Birt AR, Hogg GR, Dube WJ. 1977, Hereditary multiple fibrofolliculomas with trichodiscomas and acrochordons. *Arch Dermatol*;113:1674-1677.

Elizabeth Cartwright Pfaffenroth, M.D. and W. Marston Linehan, M.D. 2003. Genetic Basis for Kidney Cancer Opportunity for Disease-Specific Approaches to Therapy

Coppin C, Porzsolt F, Awa A, Kumpf J, Coldman A, Wilt T.

Cochrane Database Syst Rev. 2005 Jan 25;(1):CD001425. Immunotherapy for advanced renal cell cancer.

Cohen HT, McGovern FJ. Renal-cell carcinoma. *N Engl J Med* 2005;353:2477–2490.

Escudier B, Eisen T, Stadler WM, Szczylik C, Oudard S, Siebels M, Negrier S, Chevreau C, Solska E, Desai AA, Rolland F, Demkow T, Hutson TE, Gore M, Freeman S, Schwartz B, Shan M, Simantov R, Bukowski RM; TARGET Study Group. Sorafenib in advanced clear-cell renal-cell carcinoma. *N Engl J Med*. 2007 Jan 11;356(2):125-34.

Escudier B, Pluzanska A, Koralewski P, Ravaud A, Bracarda S, Szczylik C, Chevreau C, Filipek M, Melichar B, Bajetta E, Gorbunova V, Bay JO, Bodrogi I, Jagiello-Gruszczyk A, Moore N; AVOREN Bevacizumab plus interferon alfa-2a for treatment of metastatic renal cell carcinoma: a randomised, double-blind phase III trial. *Lancet*. 2007 Dec 22;370(9605):2103-11.

Feldman DR, Motzer RJ. 2006 Novel targets and therapies for metastatic renal cell carcinoma. *Oncology* 2006;20:1745-53

Fogh, J., and Trempe, G. New Human Tumor Cell Lines. In: J. Fogh (ed.),

Human Tumor Cells In Vitro, pp. 115-160. New York: Plenum Press, 1975.

Fong PC, Boss DS, Yap TA, Tutt A, Wu P, Mergui-Roelvink M et al. Inhibition of poly(ADP-ribose) polymerase in tumors from BRCA mutation carriers. *N Engl J Med* 2009; 361: 123–134.

Foster K, Prowse A, van den BA, Fleming S, Hulsbeek MM, Crossey PA, Richards FM, Cairns P, Affara NA, Ferguson-Smith MA, 1994. Somatic mutations of the von Hippel-Lindau disease tumour suppressor gene in non-familial clear cell renal carcinoma. *Hum Mol Genet*;3:2169-2173.

Fyfe G, Fisher RI, Rosenberg SA, et al. Results of treatment of 255 patients with metastatic renal cell carcinoma who received high-dose recombinant interleukin-2 therapy. *Journal of Clinical Oncology*. 1995;13(3):688-696.

RM Gemmill, M Zhou, L Costa, C Korch, RM Bukowski and HA Drabkin. Synergistic growth inhibition by Iressa and Rapamycin is modulated by VHL mutations in renal cell carcinoma. *British Journal of Cancer* (2005) 92, 2266 – 2277

Gnarra JR, Tory K, Weng Y, Schmidt L, Wei MH, Li H, Latif F, Liu S, Chen F, Duh FM, 1994. Mutations of the VHL tumour suppressor gene in renal carcinoma. *Nat Genet* 1994;7:85-90.

Hasumi H, Baba M, Hong SB, Hasumi Y, Huang Y, Yao M et al.(2008). Identification and characterization of a novel folliculininteracting protein FNIP2. *Gene* 2008 415: 60–67.#

Hong SB, Oh H, Valera VA, Stull J, Ngo DT, Baba M, Merino MJ, Linehan WM, Schmidt LS. Tumor suppressor FLCN inhibits tumorigenesis of a FLCN-null renal cancer cell line and regulates expression of key molecules in TGF-beta signaling. *Mol Cancer*. 2010 Jun 23;9:160. doi: 10.1186/1476-4598-9-160.

Hudes G, Carducci M, Tomczak P, Dutcher J, Figlin R, Kapoor A, Staroslawska E, Sosman J, McDermott D, Bodrogi I, Kovacevic Z, Lesovoy V, Schmidt-Wolf IG, Barbarash O, Gokmen E, O'Toole T, Lustgarten S, Moore L, Motzer RJ; Global.2007 ARCC Trial. Temsirolimus, interferon alfa, or both for advanced renal-cell carcinoma. *N Engl J Med.*; 2007 356:2271-81

Hudon V., Sabourin S., Dydensborg A.B., Kottis V., Ghazi A., Paquet M., Crosby K., Pomerleau V., Uetani N., Pause A. Renal tumour suppressor function of the Birt-Hogg-Dube syndrome gene product folliculin. *J. Med. Gene* 2010

Mariam Jafri, Xiaohong Lu, Mark Morris, Dean Gentle, Eamonn Maher.B32

Identifying new molecular targets in Renal Cell Carcinoma Using a Synthetic Lethality Screen.

<http://conference.ncri.org.uk/abstracts/2012/abstracts/B32.html> Copyright NCRI 2006-2012,

ISSN 1756-3038

JEMAL A, SIEGEL R, WARD E, MURRAY T, XU J, SMIGAL C, et al. Cancer statistics, 2006. *CA Cancer J Clin.* 2006;56:106–130

Kaelin WG. The von Hippel-Lindau tumor suppressor protein: roles in cancer and oxygen sensing. *Cold Spring Harb Symp Quant Biol* 2005; 70: 159–166.

Kaelin WG. Treatment of kidney cancer: insights provided by the VHL tumor-suppressor protein. *Cancer* 2009; 115(10 Suppl): 2262–2272.

R. J. B. King, 2000 *Cancer Biology*

Kovacs G, Akhtar M, Beckwith BJ, Bugert P, Cooper CS, Delahunt B, et al. The Heidelberg classification of renal cell tumours. *J Pathol* 1997;183:131–133.

Latif F, Tory K, Gnarr J, Yao M, Duh F-M, Orcutt ML, Stackhouse T, Kuzmin I, Modi W, Geil L, Schmidt L, Zhou F, Li H, Wei MH, Chen F, Glenn G, Choyke P, Walther MM, Weng Y, Duan DR, Dean M, Glavac D, Richards FM, Crossey PA, Ferguson-Smith MA, Le Paslier D, Chumakov I, Cohen D, Chinault CA, Maher ER, Linehan WM, Zbar B, Lerman MI (1993). Identification of the von Hippel-Lindau disease tumour suppressor gene. *Science* 1993;260:1317-1320

LINEHAN WM, WALTHER MM, ZBAR B. The genetic basis of cancer of the kidney. *J Urol.*;170: (6 Pt 1):2163–2172 2003

W.M. linehan, J.Vasselli, R Srinivasan, M. M Walther, M. Merino, P. Choyke, C. Vocke, L. Schmidt, J. S. Isaacs, G. Glenn, J. Toro, B Zbar, D. Bottaro, and L. Neckers. 2004 Genetic basis of cancer of the kidney: Disease specific approaches to therapy. *Clinical cancer research*.

W. Marston Linehan, Ramaprasad Srinivasan & Laura S. Schmidt

Nature Reviews Urology 7, 277-285 (May 2010)

doi:10.1038/nrurol.2010.47

Lingaas F, Comstock KE, Kirkness EF, Sorensen A, Aarskaug T, Hitte C et al. (2003). A mutation in the canine BHD gene is associated with hereditary multifocal renal cystadenocarcinoma and nodular dermatofibrosis in the German shepherd dog. *Hum Mol Genet* 12: 3043–3053.

Xiaohong Lu, Wenbin Wei, Janine Fenton, Michael S Nahorski, Erzsebet Rabai, Anne Reiman, Laurence Seabra, Zsuzsanna Nagy, Farida Latif, Eamonn R Maher *Molecular Cancer Therapeutics* 01/2011; 10(1):80-9. Therapeutic targeting the loss of the birt-hogg-dube suppressor gene.

Lu X, Boora U, Seabra L, Rabai EM, Fenton J, Reiman A, Nagy Z, Maher ER. Knockdown of Slingshot 2 (SSH2) serine phosphatase induces Caspase3 activation in human carcinoma cell lines with the loss of the Birt-Hogg-Dubé tumour suppressor gene (FLCN). *Oncogene*. 2013 Feb 18. doi: 10.1038/onc.2013.27.

Maxwell P, Wiesener M, Chang G-W, Clifford SC, Vaux E, Cockman M, Wykoff C, Pugh C, Maher ER, Ratcliffe PJ. The tumour suppressor protein VHL targets hypoxia-inducible factors for oxygen-dependent proteolysis. *Nature* 1999;399:271-5

Menko, F.H., et al., Birt-Hogg-Dube syndrome: diagnosis and management. *Lancet Oncol*, 2009. 10(12): p. 1199-206.

Mizuno K. Signaling mechanisms and functional roles of cofilin phosphorylation and dephosphorylation. *Cell Signal*. 2013 Feb;25(2):457-69. doi: 10.1016/j.cellsig.2012.11.001. Epub 2012 Nov 12.

Motzer RJ, Bander NH, Nanus DM. Renal-cell carcinoma. *N Engl J Med* 1996;335:865–875.

Motzer RJ, Mazumdar M, Bacik J, Berg W, Amsterdam A, Ferrara J.

J Clin Oncol. 1999 Aug;17(8):2530-40. Survival and prognostic stratification of 670 patients with advanced renal cell carcinoma.

Motzer RJ, Michaelson MD, Redman BG, Hudes GR, Wilding G, Figlin RA, Ginsberg MS, Kim ST, Baum CM, DePrimo SE, Li JZ, Bello CL, Theuer CP, George DJ, Rini BI. J Clin Oncol. 2006 Jan 1;24(1):16-24. Epub 2005 Dec 5. Activity of SU11248, a multitargeted inhibitor of vascular endothelial growth factor receptor and platelet-derived growth factor receptor, in patients with metastatic renal cell carcinoma.

T Murakami, F Sano, Y Huang, A Komiya, M Baba, Y Osada, Y Nagashima, K Kondo, N Nakaigawa, T Miura, Y Kubota, M Yao and T Kishida 2007 J Pathol; 211: 524–531. Identification and characterization of Birt–Hogg–Dubé associated renal carcinoma

Nickerson ML, Warren MB, Toro JR, Matrosova V, Glenn G, Turner ML, Duray P, Merino M, Choyke P, Pavlovich CP, Sharma N, Walther M, Munroe D, Hill R, Maher E, Greenberg C, Lerman MI, Linehan WM, Zbar B, Schmidt LS. 2002, Mutations in a novel gene lead to kidney tumors, lung wall defects, and benign tumors of the hair follicle in patients with the Birt-Hogg-Dube syndrome. Cancer Cell; 2002 2:157-164.

Noriyuki Misago, Keiichiro Joh, Hitomi Yatsuki, Hidenobu Soejima and Yutaka Narisawa 2008. A BHD Germline Mutation Identified in an Asian Family with Birt-Hogg-Dubé Syndrome *Acta Dermato-Venereologica*.

Okimoto K, Kouchi M, Matsumoto I, Sakurai J, Kobayashi T, Hino O. (2004a). Natural history of the Nihon rat model of BHD. *Curr Mol Med* 4: 887–893.

Okimoto K, Sakurai J, Kobayashi T, Mitani H, Hirayama Y, Nickerson ML et al. (2004b). A germ-line insertion in the Birt-Hogg-Dubé (BHD) gene gives rise to the Nihon rat model of inherited renal cancer. *Proc Natl Acad Sci USA* 101: 2023–2027

Pavlovich CP, Walther MM, Eyer RA, Hewitt SM, Zbar B, Linehan WM, Merino MJ. 2002, Renal tumors in the Birt-Hogg-Dubé syndrome. *Am J Surg Pathol*. 2002;26:1542–1552.

Pham TM, Fujino Y, Matsuda S, Yoshimura T. 2010 Premature mortality due to cancer in Japan, 1995 and 2005. *Int J Cancer*. Jul 1 2010; 127(1):190-4.

Posadas I, Perez-Martinez FC, Guerra J, Sanchez-Verdu P, Cena V. Cofilin activation mediates Bax translocation to mitochondria during excitotoxic neuronal death. *J Neurochem* 2012; 120: 515–527.

Ravi K. Nookala, Lars Langemeyer, Angela Pacitto, Bernardo Ochoa-Montaña, Jane C. Donaldson, Beata K. Blaszczyk, Dimitri Y. Chirgadze, Francis A. Barr, J. Fernando Bazan and

Tom L. Blundell. Crystal structure of folliculin reveals a hidden function in genetically inherited renal cancer. *Open Biol* 2012 2, 120071, published 8 August 2012

Reiman A, Lu X, Seabra L, Boora U, Nahorski MS, Wei W, Maher ER. *Anticancer Res.* 2012 Nov;32(11):4663-70. Gene expression and protein array studies of folliculin-regulated pathways. *Anticancer research* 11/2012; 32(11):4663-70.

Reinhardt HC, Aslanian AS, Lees JA, Yaffe MB. p53-deficient cells rely on ATM- and ATR-mediated checkpoint signaling through the p38MAPK/MK2 pathway for survival after DNA damage. *Cancer Cell* 2007; 11: 175–189.

Reinhardt HC, Jiang H, Hemann MT, Yaffe MB. Exploiting synthetic lethal interactions for targeted cancer therapy. *Cell Cycle (Georgetown, Tex)* 2009; 8: 3112–3119

Robb VA, Karbowiczek M, Klein-Szanto AJ, Henske EP. 2007, Activation of the mTOR signaling pathway in renal clear cell carcinoma. *J Urol.*;177:346-52.

Rongioletti F, Hazini R, Gianotti G, Rebora A. 1989, Fibrofolliculomas, trichodiscomas and acrochordons (Birt-Hogg-Dube) associated with intestinal polyposis. *Clin Exp Dermatol*; 1989.14:72-74.

ROTH JS, RABINOWITZ AD, BENSON M, GROSSMAN ME. Bilateral renal cell carcinoma in the Birt-Hogg-Dube syndrome. *J Am Acad Dermatol*. 1993;29:1055–1056.

Sabourin LA, Tamai K, Seale P, Wagner J, Rudnicki MA. *Mol Cell Biol*. 2000 Jan;20(2):684-96. Caspase 3 cleavage of the Ste20-related kinase SLK releases and activates an apoptosis-inducing kinase domain and an actin-disassembling region.

SCHMIDT LS, NICKERSON ML, WARREN MB, GLENN GM, TORO JR, MERINO MJ, et al. Germline BHD-mutation spectrum and phenotype analysis of a large cohort of families with Birt-Hogg-Dube syndrome. *Am J Hum Genet*. 2005;76:1023–1033.

Joan Seoane, Celio Pouponnot, Peter Staller, Manuela Schader, Martin Eilers & Joan Massagué TGF β influences Myc, MIZ-1 and Smad to control the CDK inhibitor p15INK4b *Nature Cell Biology* 3, 400 - 408 (2001)

Shin J-H, Shin Y-K, Ku J-L, Jeong S-Y, Hong S-H, Park S-Y, Kim W-H and Park J-G: Mutations of the Birt Hogg Dubé (BHD) gene in sporadic colorectal carcinomas and colorectal carcinoma cell lines with microsatellite instability. *J Med Genet* 40: 364-367, 2003.

da Silva NF, Gentle D, Hesson LB, Morton DG, Latif F, Maher ER. Analysis of the Birt–Hogg–Dubé (BHD) tumor suppressor gene in sporadic renal cell carcinoma and colorectal cancer. *J Med Genet* 2003;40:820–824.

Skehan P, Storeng R, Scudiero D, Monks A, McMahon J, Vistica D, Warren JT, Bokesch H, Kenney S, Boyd MR. New colorimetric cytotoxicity assay for anticancer-drug screening.

J Natl Cancer Inst. 1990 Jul 4;82(13):1107-12.

Sternberg CN, Davis ID, Mardiak J et al. Pazopanib in locally advanced or metastatic renal cell carcinoma: results of a randomized phase III trial. *Journal of Clinical Oncology.* 2010;28:1061-1068

Sutphin PD, Chan DA, Li JM, Turcotte S, Krieg AJ, Giaccia AJ. 2007, Targeting the loss of the von Hippel-Lindau tumor suppressor gene in renal cell carcinoma cells. *Cancer Res.* 2007;67:5896-905

Y Takagi, T Kobayashi, M Shiono, L Wang, X Piao, G Sun, D Zhang, M Abe, Y Hagiwara K Takahashi and O Hino.(2008) Interaction of folliculin (Birt-Hogg-Dube' gene product)with a novel Fnip1-like (FnipL/Fnip2)protein Oncogene 27, 5339–5347

Teng B, Lukasz A, Schiffer M The ADF/Cofilin-Pathway and Actin Dynamics in Podocyte Injury- Int J Cell Biol 2011

Togashi Y, Kobayashi T, Momose S, Ueda M, Okimoto K, Hino O.(2006). Transgenic rescue from embryonic lethality and renal carcinogenesis in the Nihon rat model by introduction of a wildtype Bhd gene. Oncogene 25: 2885–2889.

TORO JR, GLENN G, DURAY P et al.: Birt-Hogg-Dubé syndrome: a novel marker of kidney neoplasia. Archives of dermatology (1999);135:1195–1202.

TORO JR, PAUTLER SE, STEWART L, GLENN GM, WEINREICH M, TOURE O, et al. Lung Cysts, Spontaneous Pneumothrorax and Genetic Associations in 89 Families with Birt-Hogg-Dube Syndrome. Am J Respir Crit Care Med. 2007;175:1044–1053.

Vocke CD, Yang Y, Pavlovich CP, Schmidt LS, Nickerson ML, Torres-Cabala CA, Merino MJ, Walther MM, Zbar B, Linehan WM. High frequency of somatic frameshift BHD gene mutations in Birt-Hogg-Dubé-associated renal tumors. *J Natl Cancer Inst.* 2005 Jun 15;97(12):931-5.

Hiroyoshi Wada, Edward T. H. Yeh and Tetsu Kamitani. The von Hippel-Lindau Tumor Suppressor Gene Product Promotes, but Is Not Essential for, NEDD8 Conjugation to Cullin-2*. *The Journal of Biological Chemistry* 1999, 274, 36025-36029.

YANG JC, SHERRY RM, STEINBERG SM, TOPALIAN SL, SCHWARTZENTRUBER DJ, HWU P, et al. Randomized study of high-dose and low-dose interleukin-2 in patients with metastatic renal cancer. *Journal of Clinical Oncology.* 2003;21:3127–3132.

Yang Y, Padilla-Nash HM, Vira MA, Abu-Asab MS, Val D, Worrell R, Tsokos M, Merino MJ, Pavlovich CP, Ried T, Linehan WM, Vocke CD. The UOK 257 cell line: a novel model for studies of the human Birt-Hogg-Dubé gene pathway. *Cancer Genet Cytogenet.* 2008 Jan 15;180(2):100-9. doi: 10.1016/j.cancergencyto.2007.10.010.

Yuan, P., et al., Therapeutic inhibition of Sp1 expression in growing tumors by Mitramycin a correlates directly with potent antiangiogenic effects on human pancreatic cancer. *Cancer*, 2007. 110(12): p. 2682-90.

Zbar B, Alvord WG, Glenn G, Turner M, Pavlovich CP, Schmidt L, Walther M, Choyke P, Weirich G, Hewitt SM, Duray P, Gabriel F, Greenberg C, Merino MJ, Toro J, Linehan WM. 2002, Risk of renal and colonic neoplasms and spontaneous pneumothorax in the Birt-Hogg-Dube syndrome. *Cancer Epidemiol Biomarkers Prev*; 2002.11:393–400.

On line resources referenced:

http://www.cbioportal.org/public-portal/cross_cancer.do?cancer_study_id=all&data_priority=0&case_ids=&gene_set_choice=user-defined-list&gene_list=FLCN&clinical_param_selection=null&tab_index=tab_visualize&Action=Submit#crosscancer/overview/0/FLCN

02/05/2014

<http://www.medogene.com/My%20Researches/Kidney%20cell%20lines.html>

02/05/2014

http://www.polyplus-transfection.com/wp-content/uploads/2009/08/PF_INTERFERin_vF.pdf

29/08/2013

<http://pathwaymaps.com/maps/418/> © 2013 Thomson Reuters Date accessed 25/08/2013

http://www.cell-lines-service.de/content/e3969/e4049/e4076/index_eng.html 17/08/2013

<http://www.lgcstandards-atcc.org>

http://www.lgcstandards-atcc.org/products/all/HTB-46.aspx?geo_country=gb 17/08/2013

("Entrez Gene: CDKN1A cyclin-dependent kinase inhibitor 1A (p21, Cip1)"). Date accessed 25/08/2013

("Entrez Gene: CDKN2B cyclin-dependent kinase inhibitor 2B (p15, inhibits CDK4)") Date accessed 25/08/2013

<http://www.cancerresearchuk.org/cancer-info/cancerstats/types/kidney/incidence/uk-kidney-cancer-incidence-statistics> (Quoted material collected on 27/07/2013)

<http://news.cancerconnect.com/stage-iv-renal-cancer> Date accessed 25/08/2013

<http://dtp.nci.nih.gov/compare/>

APENDIX 1**NCI60 compounds' FLCN expression Data**

APENDIX 2

FNIP3: Evidence that the Folliculin tumour suppressor interacts with Miz-1

Extract from a Summary of Work by Eamonn Maher and Work undertaken by Anne Reiman at University of Birmingham, UK.

Folliculin interacts with, and co-localises with, the c-Myc interacting protein Miz-1

Miz-1 (c-Myc interacting protein) was detected as a potential interacting partner of folliculin in a yeast two-hybrid screen using full-length folliculin as a bait against human fetal brain cDNA library. Two independent clones mapping to exons 8-9 of Miz-1 were identified and Miz-1 was one of seven potential interactors detected more than once (data not shown). In order to refute or confirm this potential interaction *FLCN* cDNA was amplified from neuroblastoma cell lines and cloned into pFLAG-CMV-3 vector. Following immunoprecipitation in HeLa cells transiently over-expressing both Flag-*FLCN* and pCDNA-Miz-1, *FLCN* was shown to co-immunoprecipitate with Miz-1 in a reciprocal manner. Then HEK293 cells were transiently or stably transfected with FLAG-*FLCN* construct and empty FLAG vector and FLAG beads were used for immunoprecipitation. Following immunoprecipitation of FLAG-*FLCN* and probing with anti-Miz-1 antibody, Miz-1 was found to co-immunoprecipitate with folliculin (Figure 1). In addition, overexpressed Flag-Folliculin coimmunoprecipitated with endogenous Miz-1. In addition pulldown of endogenous folliculin in HEK293 cells coimmunoprecipitated Miz-1. The co-immunoprecipitation data were supported by immunofluorescence staining studies that demonstrated that Miz-1 and folliculin demonstrated partial and predominately nuclear co-localisation.

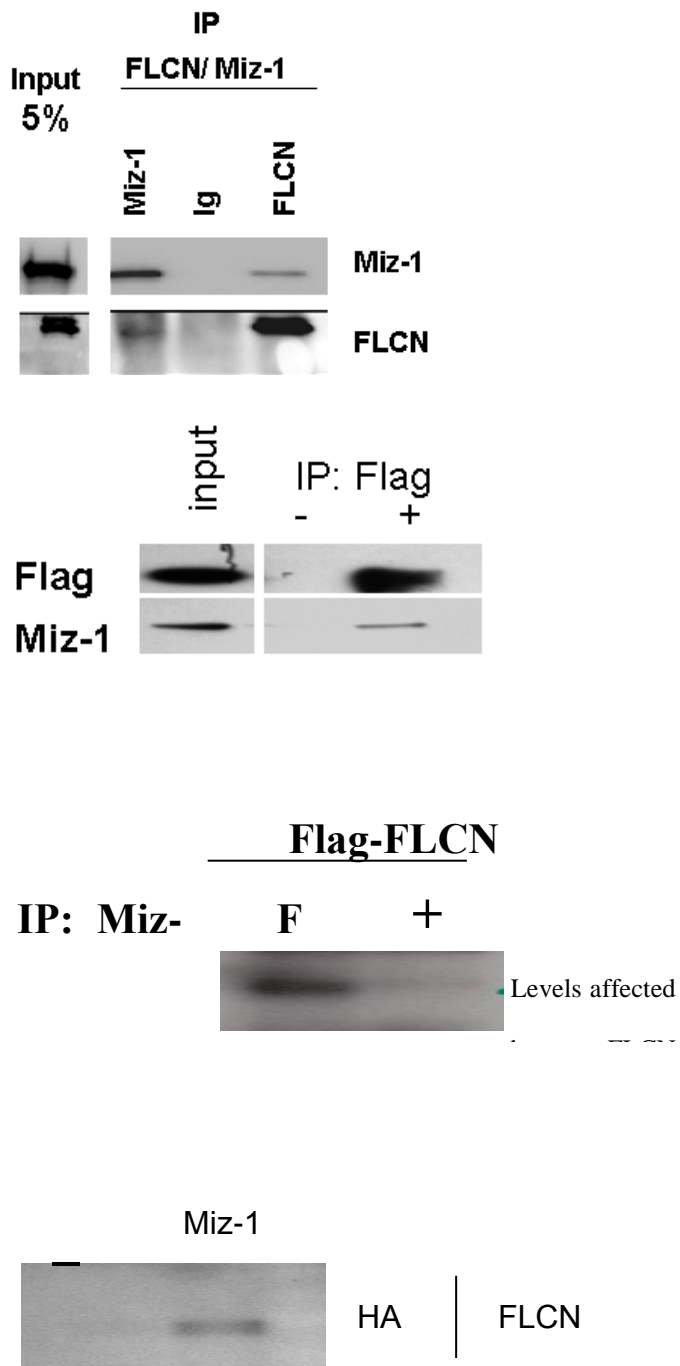


Fig.A FLCN interacts with Miz-1 in vitro and in vivo.

APENDIX 3

Publications

Publications on this project:

Knockdown of Slingshot 2 (SSH2) serine phosphatase induces Caspase3 activation in human carcinoma cell lines with the loss of the Birt-Hogg-Dubé tumour suppressor gene (FLCN). X Lu, U Boora, L Seabra, E M Rabai, J Fenton, A Reiman, Z Nagy, E R Maher 18 February 2013; doi:10.1038/onc.2013.27.

Birt Hogg-Dubé syndrome-associated FLCN mutations disrupt protein stability. Michael S Nahorski, Anne Reiman, Derek H K Lim, Ravi K Nookala, Laurence Seabra, Xiaohong Lu, Janine Fenton, Uncaar Boora, Magnus Nordenskjöld, Farida Latif, Laurence D Hurst, Eamonn R Maher Human Mutation 04/2011; 32(8):921-9.

Therapeutic targeting the loss of the birt-hogg-dube suppressor gene. Xiaohong Lu, Wenbin Wei, Janine Fenton, Michael S Nahorski, Erzsebet Rabai, Anne Reiman, Laurence Seabra, Zsuzsanna Nagy, Farida Latif, Eamonn R Maher Molecular Cancer Therapeutics 01/2011; 10(1):80-9.

Publications on other projects published during the period of study:

Toll-6 and Toll-7 function as neurotrophin receptors in the Drosophila melanogaster CNS. Graham McIlroy, Istvan Foldi, Jukka Aurikko, Jill S Wentzell, Mei Ann Lim, Janine C Fenton, Nicholas J Gay, Alicia Hidalgo Nature Neuroscience 07/2013

Vacuolar-type H⁺-ATPase V1A subunit is a molecular partner of Wolfram syndrome 1 (WFS1) protein, which regulates its expression and stability. Seley Gharanei, Malgorzata Zatyka, Dewi Astuti, Janine Fenton, Attila Sik, Zsuzsanna Nagy, Timothy G Barrett Human Molecular Genetics 10/2012

The glial regenerative response to central nervous system injury is enabled by pros-notch and pros-NFκB feedback. Kentaro Kato, Manuel G Forero, Janine C Fenton, Alicia Hidalgo PLoS Biology 08/2011; 9(8):e1001133.

Previous publications:

19-P007 A gene regulatory network involving prospero, Notch, TNF and NFκB underlies a glial-repair-response to CNS injury Kentaro Kato, Manuel Forero, Janine Fenton, Alicia Hidalgo Mechanisms of Development - MECH DEVELOP. 01/2009; 126.

Drosophila neurotrophins reveal a common mechanism for nervous system formation. Bangfu Zhu, Jenny A Pennack, Peter McQuilton, Manuel G Forero, Kenji Mizuguchi, Ben Sutcliffe, Chun-Jing Gu, Janine C Fenton, Alicia Hidalgo PLoS Biology 12/2008; 6(11):e284

Two distinct mechanisms segregate Prospero in the longitudinal glia underlying the timing of interactions with axons. Rachel C Griffiths, Jonathan Benito-Sipos, Janine C Fenton, Laura Torroja, Alicia Hidalgo Neuron Glia Biology 02/2007; 3(1):75-88

Novel D-ring modified steroid derivatives as potent, non-estrogenic, steroid sulfatase inhibitors with in vivo activity. Delphine S Fischer, Surinder K Chander, L W Lawrence Woo, Janine C Fenton, Atul Purohit, Michael J Reed, Barry V L Potter The Journal of Steroid Biochemistry and Molecular Biology 03/2003; 84(2-3):343-9.